From the Institute for Pharmacology

at Heinrich Heine University Düsseldorf

The acute inhibition of lipolysis using DREADD system does not reverse MI-induced changes in subcutaneous white adipose tissue, but improves cardiac systolic function

Dissertation

To obtain the academic title of Doctor of Philosophy (Ph.D.) in Medical Sciences

from the Faculty of Medicine at Heinrich Heine University Düsseldorf

submitted by

Luzhou Wang

(2024)

As an inaugural dissertation printed by permission of the Faculty of Medicine at Heinrich Heine University Düsseldorf

signed:

Dean: Prof. Dr. med. Nikolaj Klöcker

Examiners: Prof. Dr. Jens W. Fischer, Prof. Dr. Martina Krüger

Parts of this work have been published:

Wang, Luzhou; Zabri, Heba; Gorressen, Simone; Semmler, Dominik; Hundhausen, Christian; Fischer, Jens W.; Bottermann, Katharina (2022): Cardiac ischemia modulates white adipose tissue in a depot-specific manner. In: *Frontiers in physiology* 13, S. 1036945. DOI: 10.3389/fphys.2022.1036945.

Zusammenfassung

Ein Myokardinfarkt (MI) stellt eine der häufigsten Todesursachen weltweit dar und betrifft nicht nur das Herz, sondern hat systemische Auswirkungen auf den gesamten Organismus und viele verschiedenen Organe. Ein erhöhter β-adrenerger Tonus aufgrund unter anderem einer verringerten Herzleistung ist eine der stärksten Stimulationen der Lipolyse im weißen Fettgewebe. Wie das weiße Fettgewebe nach einem MI beeinträchtigt wird, ist noch unklar. In dieser Doktorarbeit wurden daher die Veränderungen des subkutanen und viszeralen weißen Fettgewebes während der Reperfusionsphase nach einer kardialen Ischämie im Mausmodell analysiert. Die Analysen ergaben, dass der MI das weiße Fettgewebe depotspezifisch moduliert, wobei das subkutane Depot deutlich stärker betroffen ist. Die histologische Analyse ergab eine geringere Adipozytengröße nach MI im subkutanen Depot wahrscheinlich aufgrund einer erhöhten Lipolyse. Dieser Effekt war in der späten Reperfusionsphase stärker ausgeprägt was darauf hindeutete, dass die Lipolyse ein chronischer Prozess während der Reperfusion ist. Der MI führte ebenfalls zu einer verringerten Lipogenese auf der Ebene der Genexpression. Die langanhaltend verminderte Genexpression von *Lpl* bestätigte den chronischen Effekt. Darüber hinaus deutete die H&E-Färbung auch auf ein *"browning"* und Immunzellinfiltration im subkutanen Depot hin, welche durch Analyse der UCP1-Proteinexpression in der Immunhistochemie und Western Blot Analyse sowie durch Immunhistochemie von Anti-MAC-2 validiert wurde. Darüber hinaus reduzierte MI auch die Adipokin-Genexpression im subkutanen Depot. Da die gezielte Behandlung des Fettgewebes als vielversprechende Therapiestrategie zur Verbesserung der Herzfunktion angesehen wird, wurde in dieser Doktorarbeit ein induzierbares Adipozyten-spezifisches inhibitorisches DREADD-System verwendeten, um die Lipolyse gezielt während und nach der kardialen Ischämie im Fettgewebe zu hemmen. Die Hemmung wurde durch einen akuten Rückgang der zirkulierenden freien Fettsäure-Spiegel validiert, was ebenfalls mit einer Verringerung des Insulinspiegels einherging. Die akute Hemmung konnte jedoch keine durch den MI verursachten Veränderungen im subkutanen weißen Fettgewebe modifizieren. Es konnte jedoch nach 7 Tagen Reperfusion eine verbesserte kardiale systolische Funktion festgestellt werden. Diese ging einher mit einer erhöhten PKA-Aktivität in Kardiomyozyten nach 30 Minuten Reperfusion, vermutlich aufgrund reduzierter NEFA- und Insulinspiegel. Passend dazu war die Expression von GLUT4 auf Ebene der Genexpression unterdrückte, und die Phosphorylierung von PLN und TnI erhöht. Dies verbessert direkt die kardiale Relaxation und damit indirekt auch die kontraktile Funktion. Es wird vermutet, dass dieser Mechanismus zu der beobachten verbesserten kontraktile Funktion nach 7 Tagen Reperfusion beträgt.

Summary

Myocardial infarction (MI), which impacts the whole body and triggers responses in several other organs, is still one of the leading causes of death worldwide. The increased β-adrenergic stimulation mainly due to reduced cardiac output is one of the strongest stimuli of lipolysis in white adipose tissue. How white adipose tissue gets affected after MI is still unclear, therefore, in this study the changes of subcutaneous and visceral white adipose tissue during the reperfusion phase were analyzed in a mouse model of cardiac ischemia. The analyses revealed that MI modulates white adipose tissue in a depot-specific manner, as the subcutaneous depot was much more affected. Histological analysis showed smaller adipocyte size after MI in subcutaneous depot possibly due to increased lipolysis. The effect was stronger at later reperfusion timepoints which indicated that lipolysis occurred chronically. This went along with a reduced lipogenesis at gene expression level and the long-lasting reduced gene expression of *Lpl* validated the chronical effect. In addition, histological analysis also indicated browning and immune cell infiltration in the subcutaneous depot, which was verified by positive UCP1-expression and anti-Mac2-staining. Furthermore, gene expression of several adipokines was also reduced after MI.

Targeting adipose tissue has been regarded as a promising therapeutic strategy to improve cardiac function. Therefore, in this study, an inducible adipocyte-specific inhibitory DREADD system was used to spatio-temporally inhibit lipolysis. A successful inhibition was validated by acutely reduced circulating NEFA levels, which went along with reduced circulating insulin levels. The acute inhibition of lipolysis did not reverse any MI-induced changes in subcutaneous white adipose tissue. However, an improved systolic function was found after 7 d of reperfusion. At the timepoint of reduced circulating NEFA and insulin levels (30 min of reperfusion) an increased PKA activity in cardiomyocytes could be observed. In line with this suppressed GLUT4 at gene expression level, as well as an increased phosphorylation of PLN and TnI was observed, that directly increases relaxation and thereby also indirectly improves cardiomyocyte contractile function. It was speculated that this mechanism adds to the improved systolic function after 7 d of reperfusion.

List of abbreviations

AC	Adenylyl cyclase
ACC1	Acetyl-CoA carboxylase 1
ACLY	ATP-citrate lyase
AKT	Protein kinase B
ALT	Alanine transaminase
AST	Aspartate transaminase
ATGL	Adipose triglyceride lipase
ATP	Adenosine triphosphate
BAT	Brown adipose tissue
BCA	Bicinchoninic acid
BSA	Bovine serum albumin
BW	Bodyweight
°C	Grad Celsius
cAMP	Cyclic adenosine monophosphate
CCL2	Chemokine (C-C motif) ligand 2
CD36	Cluster of differentiation 36
cDNA	Complementary deoxyribonucleic acid
CGI-58	Comparative gene identification-58
cGMP	Cyclic guanosine monophosphate
ChREBP	Carbohydrate-responsive element-binding protein
ChoRE	Carbohydrate response element
Cidea	Cell death activator
CLS	Crown-like structure
CNO	Clozapine N-oxide
CO	Cardiac output
Cox8b	Cytochrome C oxidase subunit 8B
d	Day
DAB	3,3’-Diaminobenzidine
DAMP	Danger-associated molecular pattern
DAPI	4’,6-diamino-2-phenylindole
DG	Diglyceride

Dgat2	Diacylglycerol O-acyltransferase 2
DNA	Deoxyribonucleic acid
dNTP	Deoxy-ribonucleoside triphosphate
DPBS	Dulbecco’s phosphate-buffered saline
DREADD	Designer receptor exclusively activated by designer drugs
DTT	1,4-Dithiothreitol
ECG	Electrocardiogram
EDTA	Ethylenediaminetetraacetic acid
EDV	End diastolic volume
EF	Ejection fraction
ESV	End systolic volume
ELISA	Enzyme-linked immunosorbent assay
FA	Fatty acid
FAC	Fractional area change
FAO	Fatty acid oxidation
FASN	Fatty acid synthase
FCS	Fetal calf serum
FFA	Free fatty acid
FoxO1	Forkhead box protein O1
FS	Fractional shortening
g	Gram
G0S2	G0/G1 switch gene 2
GAPDH	Glyceraldehyde 3-phosphate dehydrogenase
GFP	Green fluorescent protein
GIP	Gastric inhibitory peptide
GLP-1	Glucagon-like peptide 1
GLUT4	Glucose transporter type 4
GPCR	G protein-coupled receptor
GSK2	Glycogen synthase kinase 2
GSK3	Glycogen synthase kinase 3
gWAT	Gonadal white adipose tissue
h	Hour
HA	Hemagglutinin epitope

HCl	Hydrogen chloride
H&E	Hematoxylin and eosin
hM3Dq	Human M3 G_{α} protein-coupled receptor
hM4Di	Human M4 G_{i} protein-coupled receptor
HSL	Hormone-sensitive lipase
IGF1R	Insulin-like growth factor 1 receptor
IHC	Immunohistochemistry
IL-6	Interleukin 6
IR	Insulin receptor
IRS	Insulin receptor substrate
iWAT	Inguinal white adipose tissue
KCl	Potassium chloride
kg	Kilogram
KH_2PO_4	Monopotassium phosphate
LAC	Left ascending artery
mA	Milliampere
MCP1	Monocyte chemotactic protein 1
µg	Microgram
mg	Milligram
MG	Monoglyceride
MGL	Monoacylglycerol lipase
MI	Myocardial infarction
MIF1	Macrophage migration inhibitory factor 1
min	Minute
µL	Microliter
mL	Milliliter
MLX	Max-like protein X
µm	Micrometer
mM	Millimolar
mTORC1	Mammalian target of rapamycin complex s1
Na_2HPO_4	Disodium phosphate
NaCl	Sodium chloride
NAFLD	Nonalcoholic fatty liver disease

NEFA	Non-esterified fatty acids
ng	Nanogram
NGS	Normal goat serum
nm	Nanometer
P2A	Self-cleaving peptides
PAI-1	Plasminogen activator inhibitor-1
PBS	Phosphate-buffered saline
PCR	Polymerase chain reaction
PDE3B	Phosphodiesterase 3
PDH	Pyruvate dehydrogenase
PI3K	Phosphoinositide 3-kinase
PKA	Protein kinase A
PKB	Protein kinase B
PKG	Protein kinase G
PLIN1	Perilipin 1
PLN	Phospholamban
PPARγ	Peroxisome proliferator-activated receptor gamma
PRDM16	PR domain containing 16
PSLA	Parasternal long axis
RASSL	Receptor activated solely by a synthetic ligand
rM3Ds	Rat M3 G_s protein-coupled receptor
RNA	Ribonucleic acid
ROS	Reactive oxygen species
rpm	Revolutions per minute
s	Second
SAT	Subcutaneous adipose tissue
SCD1	Stearoyl-CoA desaturase-1
SDS	Sodium dodecyl sulfate
SDS PAGE	Sodium dodecyl sulfate polyacrylamide gel electrophoresis
SEM	Standard error mean
SREBP1	Sterol regulatory element-binding protein-1
SV	Stroke volume
SVF	Stromal vascular fraction

TEMED	Tetramethylethylenediamine
TBS	Tris-buffered saline
TBS-T	Tris-buffered saline with Tween 20
TCA	Tricarboxylic acid
TG	Triglyceride
TIMP1	Metallopeptidase inhibitor 1
TLR	Toll-like receptor
TnI	Troponin I
TNF-α	Tumor necrosis factor alpha
TSC1/2	Tuberous sclerosis protein 1/2
UCP1	Uncoupling protein 1
V	Volt
VAT	Visceral adipose tissue
WAT	White adipose tissue
WGA	Wheat germ agglutinin

Table of Contents

1 Introduction

1.1 Adipose tissue

Adipose tissue is a loose connective tissue, which is mainly composed of adipocytes, but also contains the stromal vascular fraction (SVF), a heterogeneous collection of cells including pre-adipocytes, immune cells, fibroblasts and vascular endothelial cells (Nguyen et al. 2016). The main function of adipose tissue is storing energy in the form of triglycerides, each gram of fat yields 9 calories, which are more than as twice as many calories yielded by carbohydrates and proteins. Energy intake and consumption keep together the energy balance, excess calories obtained from food in any form are either digested, absorbed and stored as triglycerides in adipose tissue, or digested, absorbed, synthesized and stored in the form of triglycerides in the liver. The triglycerides stored in the liver serve together with those in adipose tissue as the energy source when body requires energy (Swett 1975).

Unlike the other organs, adipose tissue is distributed throughout the whole body and compartmentalized into different depots. Some of these depots show risk associations with metabolic syndrome (Schoettl et al. 2018). Adipose tissue is generally divided into white adipose tissue and brown adipose tissue, which are morphologically and functionally different. White adipose tissue is characterized by adipocytes with large unilocular lipid droplets, which are mainly responsible for storing energy in the form of triglycerides and protecting organs from mechanical damage (Frayn et al. 2003; Luong and Lee 2018). Adipocytes in brown adipose tissue on the other hand, contain multilocular lipid droplets and a large number of mitochondria, which are, together with the high capillary density, responsible for the characteristic brown color (Kwok et al. 2016). The main function of brown adipose tissue is to dissipate energy in the form of heat through mitochondrial uncoupling due to the presence of uncoupling proteion-1 (UCP1) (Enerbäck et al. 1997; Feldmann et al. 2009). White adipose tissue can be further roughly subdivided into different depots as visceral white adipose tissue and subcutaneous white adipose tissue (Pond 1992). In humans, adipocytes from subcutaneous depots are larger in size than in visceral depots, while this relation is reversed in mice, which have larger adipocytes in visceral depots (Sackmann-Sala et al. 2012; Pellegrinelli et al. 2016). Murine subcutaneous white adipose tissue is divided into anterior depots including inguinal, dorsolumbal and gluteal, and posterior depots including cervical, axillary, interscapular and subscapular (Cinti 2012). Visceral white adipose tissue is mainly composed of mesenteric, retroperitoneal, perirenal

and perigonadal depots (Fantuzzi and Mazzone 2007; Tran and Kahn 2010). In this study, inguinal and perigonadal depots are respectively used as subcutaneous and visceral white adipose tissue for analyses. Previous studies demonstrated that increased visceral white adipose tissue is associated with increased risk of metabolic syndrome, whereas subcutaneous white adipose tissue might even be protective against metabolic disorders (Kissebah et al. 1982; Gastaldelli et al. 2002; Zhang et al. 2015).

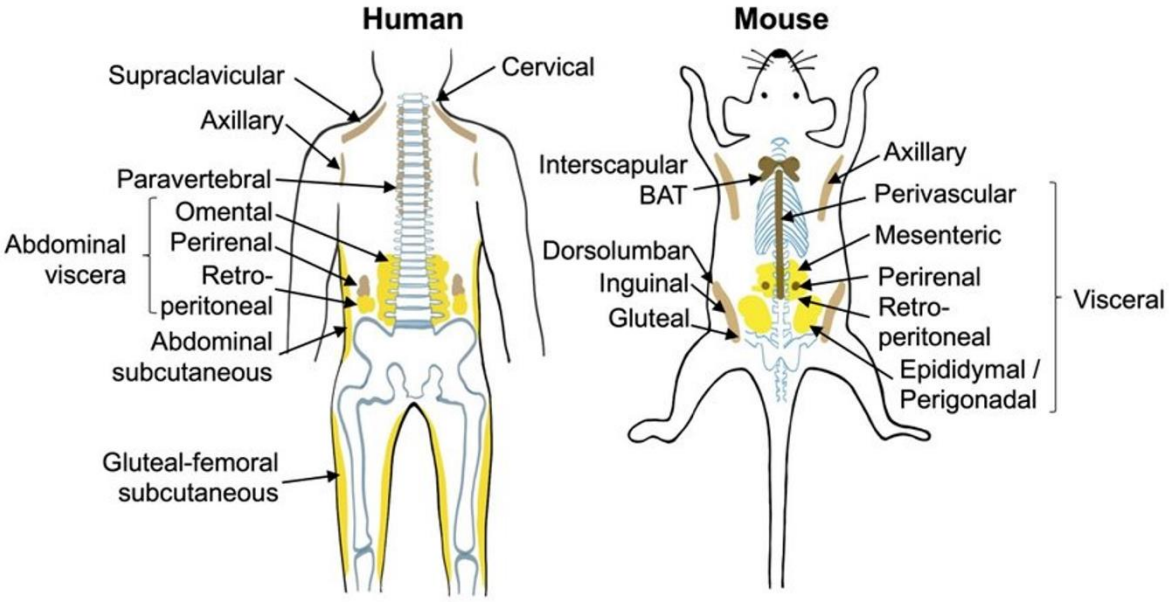

Fig. 1: Adipose tissue distribution. Distribution of subcutaneous and visceral depots of white adipose tissue and brown adipose tissue in human and mouse. BAT: Brown adipose tissue. (Cheong and Xu 2021).

1.1.1 Lipolysis

Lipolysis describes the metabolic process of triglyceride hydrolysis occurring mainly in adipocytes, into glycerol and free fatty acids (FFAs) (Schweiger et al. 2014). Lipolysis is extremely important in times of nutrient deprivation and during fasting states, and when blood glucose levels are low. Released FFAs and glycerol via breakdown of triglycerides from white adipose tissue serve as the major energy supplier for non-adipose tissues (Schweiger et al. 2014). The hydrolysis of triglycerides into a glycerol and FFAs is performed in turn by adipose triglyceride lipase (ATGL), which is the rate-limiting enzyme (Zimmermann et al. 2004), hormone-sensitive lipase (HSL) and monoacylglycerol lipase (MGL) (VAUGHAN et al. 1964). Peripheral adipose tissue lipolysis is initiated via stimulation of G_s protein-coupled receptors mainly, β_3-adrenergic receptors, but also β_1- and β_2-adrenergic receptors (Malfacini and Pfeifer 2023). The binding of catecholamines to G protein-coupled receptors on the cell membrane of adipocytes leads to the activation of G_s alpha subunit and its binding and activation of adenylyl cyclase (AC). AC converts ATP into cAMP, the increased cAMP productions results in the activation of protein kinase A (PKA). PKA plays an important role in regulating lipolysis since it directly phosphorylates HSL and perilipin-1 (PLIN1). The phosphorylation of HSL leads to its translocation from the cytosol to the lipid droplet (Egan et al. 1992; Clifford et al. 2000). Under basal conditions, PLIN1 is bound to CGI-58 and occupies the binding site of ATGL. After PKA phosphorylation, PLIN1 releases CGI-58 and makes it available for ATGL-binding and its translocation from the cytosol to the lipid droplet surface (Granneman et al. 2007; Schweiger et al. 2014). A negative regulator of lipolysis is G0/G1 switch gene 2 (G0S2), as it acts as a competitive inhibitor by blocking the CGI-58-binding site of ATGL (Zhang et al. 2014b). Many hormones can affect lipolysis, such as insulin, glucagon, adrenaline, noradrenaline and atrial natriuretic peptide, among which, insulin is the most important inhibitory regulatory hormone (Grabner et al. 2021). After insulin binding, the insulin receptors located on the cell membrane of adipocytes activate insulin receptor substrate, which in turn activates phosphoinositide 3-kinase (PI3K). Activated PI3K phosphorylates the serine-threonine kinase Akt, which subsequently phosphorylates phosphodiesterase 3B (PDE3B) (Kitamura et al. 1999). Phosphorylated PDE3B leads to the degradation of cAMP in adipocytes and the reduction of cAMP-levels results in a decreased lipolysis (Duncan et al. 2007; Jocken and Blaak 2008).

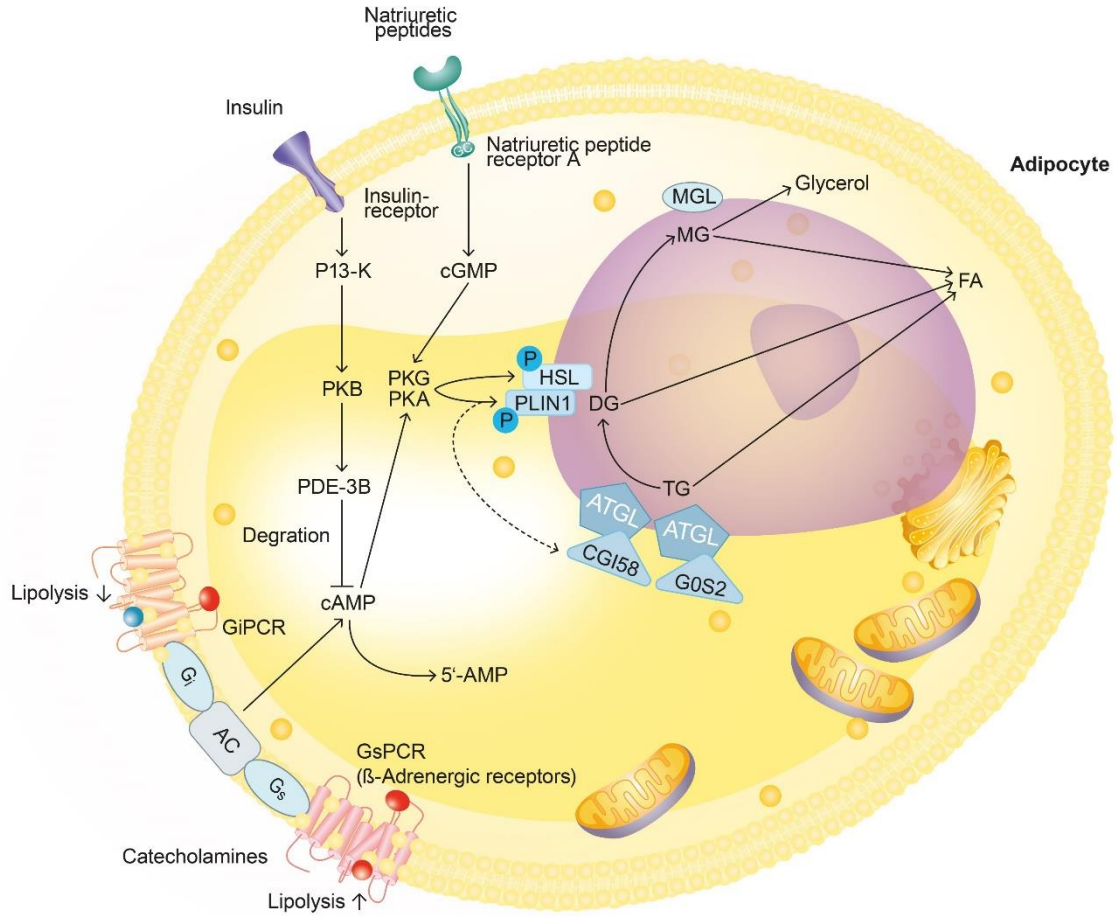

Fig. 2: The main regulation of lipolysis in adipocytes. The binding of catecholamines to Gs protein-coupled receptors activates AC, which drives the conversion from ATP into cAMP, the accumulation of cAMP activates PKA and PKG. PKA and PKG phosphorylate target proteins HSL and PLIN1. PLIN1 phosphorylation is essential for the sequential triglyceride hydrolysis. The binding of natriuretic peptides to natriuretic peptide receptor A stimulates lipolysis via the promotion of cGMP accumulation, which activates PKA and PKG. Insulin, after binding to insulin receptors, activates insulin-like receptor substrates and PI3K, through activation of PDE3B, it inhibits lipolysis via the degradation of cAMP. AC: Adenylyl cyclase. ATGL: Adipose triglyceride lipase. ATP: Adenosine triphosphate. cAMP: Cyclic adenosine monophosphate. cGMP: Cyclic guanosine monophosphate. CGI58: Comparative gene identification-58. DG: Diglyceride. FA: Fatty acid. G0S2: G0/G1 switch gene 2. GiPCR: Gi protein-coupled receptor. GsPCR: Gs protein-coupled receptor. HSL: Hormone-sensitive lipase. MG: Monoglyceride. MGL: Monoacylglycerol lipase. PDE3B: Phosphodiesterase 3. PI3K: Phosphoinositide 3-kinase. PKA: Protein kinase A. PKB: Protein kinase B. PKG: Protein kinase G. PLIN1: Perilipin 1. TG: Triglyceride. (Arner and Langin 2014)

1.1.2 Lipogenesis

The balance between lipolysis and lipogenesis maintains adipose tissue homeostasis and regulates body composition. Being the opposite of lipolysis, lipogenesis refers to the synthesis of FAs and subsequent conversion of FAs and glycerol into triglycerides in the liver and adipose tissue (Kersten 2001). Both FA synthesis and triglyceride synthesis mainly occur in the liver and adipose tissue. The synthesis of FA takes place in the cytoplasm, where two carbon units are repeatedly added to acetyl-CoA by a multienzyme complex called fatty acid synthase (FASN). The synthesis of triglycerides carries out in the endoplasmic reticulum membrane, where three FAs and a glycerol molecule are converted to a triglyceride. High carbohydrate diet elevates plasma glucose level and stimulates lipogenesis, since glucose serves as a substrate for lipogenesis, induces the lipogenic gene expression and stimulates the release of insulin, which is the most important hormone regulating lipogenesis (Kersten 2001) via its binding to the insulin receptor. After activating tyrosine kinase, the phosphorylation of tyrosines (Tyr1148, Tyr1152, Tyr1153) induces many downstream effects (Lane et al. 1990; Nakae and Accili 1999). Previous studies reported that insulin stimulates the expression of lipogenic genes via the transcription factor SREBP1 (Assimacopoulos-Jeannet et al. 1995). Insulin mediated increased lipogenesis via SREBP1 mainly occurs in the liver, since increased synthesis of triglycerides and expression of lipogenic genes were proved in mice overexpressing SREBP1a or SREBP1c in the liver (Horton and Shimomura 1999). In white adipose tissue, only cholesterol metabolism was demonstrated to be significantly increased in mice overexpressing SREBP1c, while this was not altering lipogenic gene expression (Shimomura et al. 1998). Interestingly, SREBP1 was demonstrated hereafter as target of leptin mediating the inhibitory effect of leptin on lipogenic gene expression (Kakuma et al. 2000; Soukas et al. 2000). Leptin, which is an important hormone produced from white adipose tissue, downregulates the expression of genes regarding fatty acid and triglyceride synthesis (Soukas et al. 2000). Besides SREBP1, PPARγ, which induces adipogenesis, namely the differentiation of pre-adipocytes to mature adipocytes, is another transcription factor regulating lipogenesis. Previous studies demonstrated the activation of PPARγ in white adipose tissue via insulin and SREBP1, furthermore, elevated triglyceride accumulation in the liver is closely linked with increased PPARγ expression, which revealed the lipogenic effect of PPARγ in both white adipose tissue and liver (Vidal-Puig et al. 1997; Fajas et al. 1999; Chao et al. 2000).

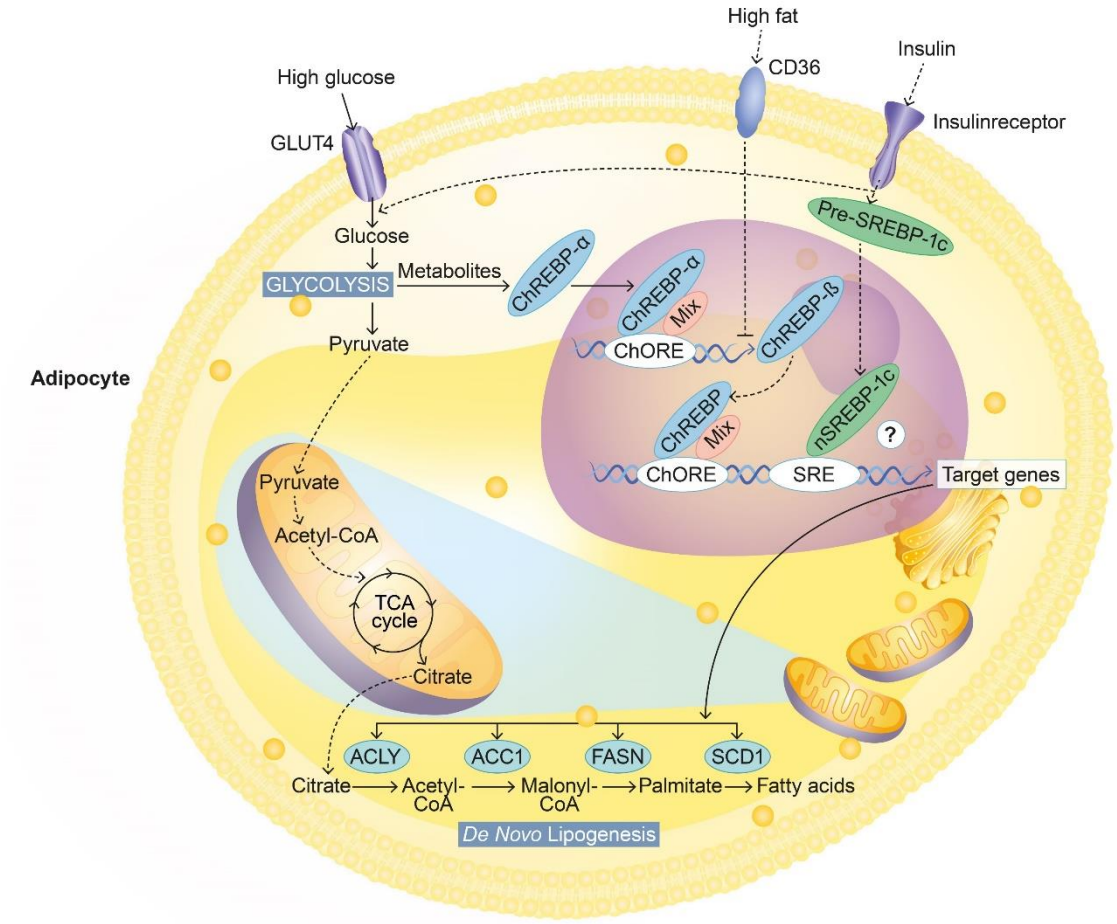

Fig. 3: Transcriptional activation of *de novo* lipogenesis in adipocytes. Glucose in the circulation is partly taken up by adipocytes through GLUT4, and then converted into pyruvate via glycolysis, which further enters TCA cycle in mitochondria. Citrate from TCA cycle is used as a substrate for *de novo* lipogenesis. Metabolites generated during glycolysis activate ChREBP-α, which binds to ChoRE together with MLX in the promoters of target genes including ACLY, ACC1, FASN, and SCD1. Insulin stimulates lipogenesis via the lipogenic transcription factor SREBP1c. ACC1: Acetyl-CoA carboxylase 1. ACLY1: ATP-citrate lyase. CD36: Cluster of differentiation 36. ChoRE: Carbohydrate response element. ChREBP: Carbohydrate-responsive element-binding protein. FASN: Fatty acid synthase. GLUT4: Glucose transporter type 4. MLX: Max-like protein X. SCD1: Stearoy-CoA desaturase-1. SREBP1c: Sterol regulatory element-binding protein-1c. TCA: Tricarboxylic acid. (Song et al. 2018)

1.1.3 Browning of white adipose tissue

Browning describes a process, in which white adipocytes are transformed into brown-fat like adipocytes which are multilocular and have a large number of mitochondria (Betz and Enerbäck 2015; Bargut et al. 2016; Bargut et al. 2017). The conversion from white adipocytes to brite (brown-in-white) adipocytes leads to increased thermogenesis and is demonstrated to be beneficial in metabolism regarding fatty acid anabolic and catabolic pathways (Wu et al. 2012; Barquissau et al. 2016). As described above, white and brown adipocytes are morphologically and functionally different, and they differentiate from distinct progenitor cells (Bargut et al. 2017). Of great significance, a previous study has revealed that in both human and mice, after stimulation, a subset of white adipocytes in white adipose tissue are able to acquire a brown fat-like phenotype (Wu et al. 2012). However, these brite adipocytes do not share the genetic markers with either white or brown adipocytes, but have a unique gene expression pattern (Wu et al. 2012; Petrovic et al. 2010). UCP1, which is a mitochondrial carrier protein and performs thermogenesis, serves as a marker to identify browning of white adipose tissue (Shabalina et al. 2013). Besides, PR domain containing 16 (PRDM16) is usually expressed together with UCP1 to identify the presence of browning, and it is demonstrated to be responsible for the maintenance of browning (Seale et al. 2008). Previous studies revealed browning as a reversible process, brite adipocytes could not be seen anymore with a low expression of PRDM16 (Cohen et al. 2014; Harms et al. 2014). Browning has been reported to be triggered by sustained adrenergic stimulation, β_3-adrenergic receptors are suggested to be mainly responsible for it by inducing PGC1-α, which further activates PPARs and mitochondrial biogenesis (Mirbolooki et al. 2014; Cypess et al. 2015; Piantadosi and Suliman 2006; Robidoux et al. 2005; Hondares et al. 2011). From the different white adipose tissue depots, the white adipocytes in subcutaneous WAT have a higher potential to transform into brite adipocytes (Gustafson and Smith 2015).

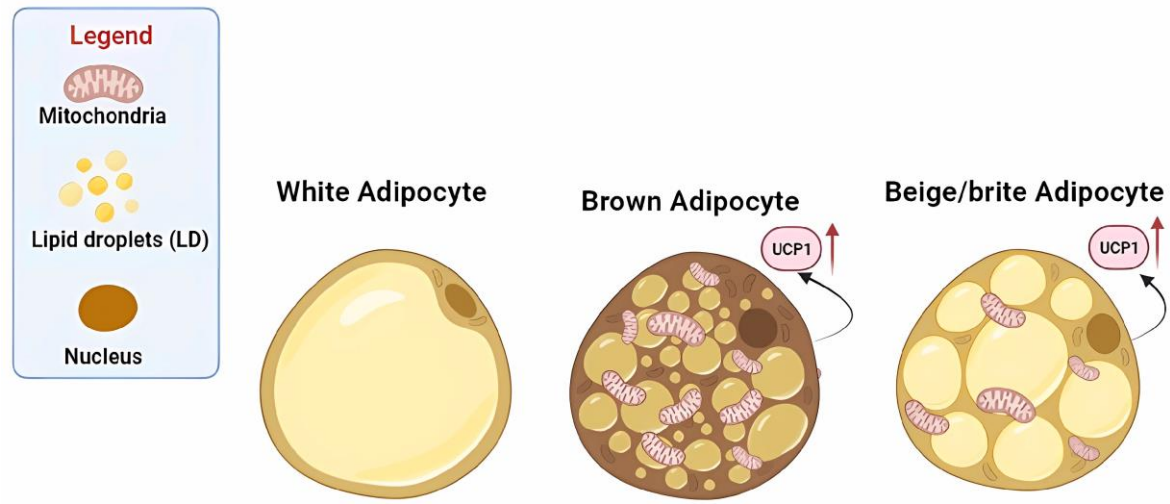

	White Adipocyte	Brown Adipocyte	Beige/Brite Adipocyte
LD morphology	Unilocular	Multilocular	Multilocular
Mitochondrial density	Low	High	Medium
UCP1 expression	Negative	Positive	Positive

Fig. 4: Characteristics of three types of adipocytes. LD: Lipid droplets. UCP1: Uncoupling protein 1. (Lange et al. 2023)

1.1.4 Inflammation of white adipose tissue

The expansion of adipose tissue in obese conditions results from adipocyte hypertrophy and hyperplasia, which is often accompanied by the occurrence of inflammation in adipose tissue (Schoettl et al. 2018). A character of inflammation of white adipose tissue is the infiltration of inflammatory cells such as monocytes and macrophages, which are recruited in response to chemokines like monocyte chemotactic protein 1 (MCP1) (Weisberg et al. 2003; Han et al. 2007). Macrophages are the most important immune cells that infiltrate adipose tissue during inflammation. Under lean state, M2 macrophages are resident in adipose tissue and maintain the homeostasis (Bourlier et al. 2008). During inflammation, the recruitment induces a phenotypic change from anti-inflammatory to pro-inflammatory turning M2 macrophages into M1 macrophages (Lumeng et al. 2007). During obesity-induced adipose tissue inflammation, macrophages are prone to accumulate in visceral depots rather than in subcutaneous depots, and some of the macrophages surround dying or dead adipocytes forming crown-like structures (CLSs) (Harman-Boehm et al. 2007; Murano et al. 2008). Besides macrophages, mast cells, B-cells and T-cells are also increased during inflammation (Winer et al. 2011; Liu et al. 2009). The obesity-induced inflammation can also induce a phenotypic change of T-cells turning TH2 T-cells to TH1 T-cells and cytotoxic T cells (Winer et al. 2009). During adipose tissue inflammation, the circulating levels of several cytokines and adipokines are elevated. First of all, MCP1 which is secreted by adipocytes and induces the recruitment of monocytes and macrophages, is getting increased during tissue injury, the infiltrated macrophages secrete MCP1 as well and leads to further infiltration (Yeop Han et al. 2010; Wellen and Hotamisligil 2003). In addition to MCP1, IL-6 and TNF-α are two important cytokines which are increased during tissue injury. Previous studies demonstrated that the increased circulating levels of IL-6 was due to increased FFA levels from lipolysis during obesity, and increased circulating levels of IL-6 promotes insulin resistance in the liver (Matsubara et al. 2012; Zhang et al. 2014a). TNF-α is an adipokine secreted from adipocytes but mainly from macrophages, during obesity, and circulating levels of TNF-α closely correlate to the infiltration of pro-inflammatory macrophages (Weisberg et al. 2003). TNF-α promotes as well insulin resistance by increasing the activity of HSL and thereby FFA levels (Zahorska-Markiewicz 2006).

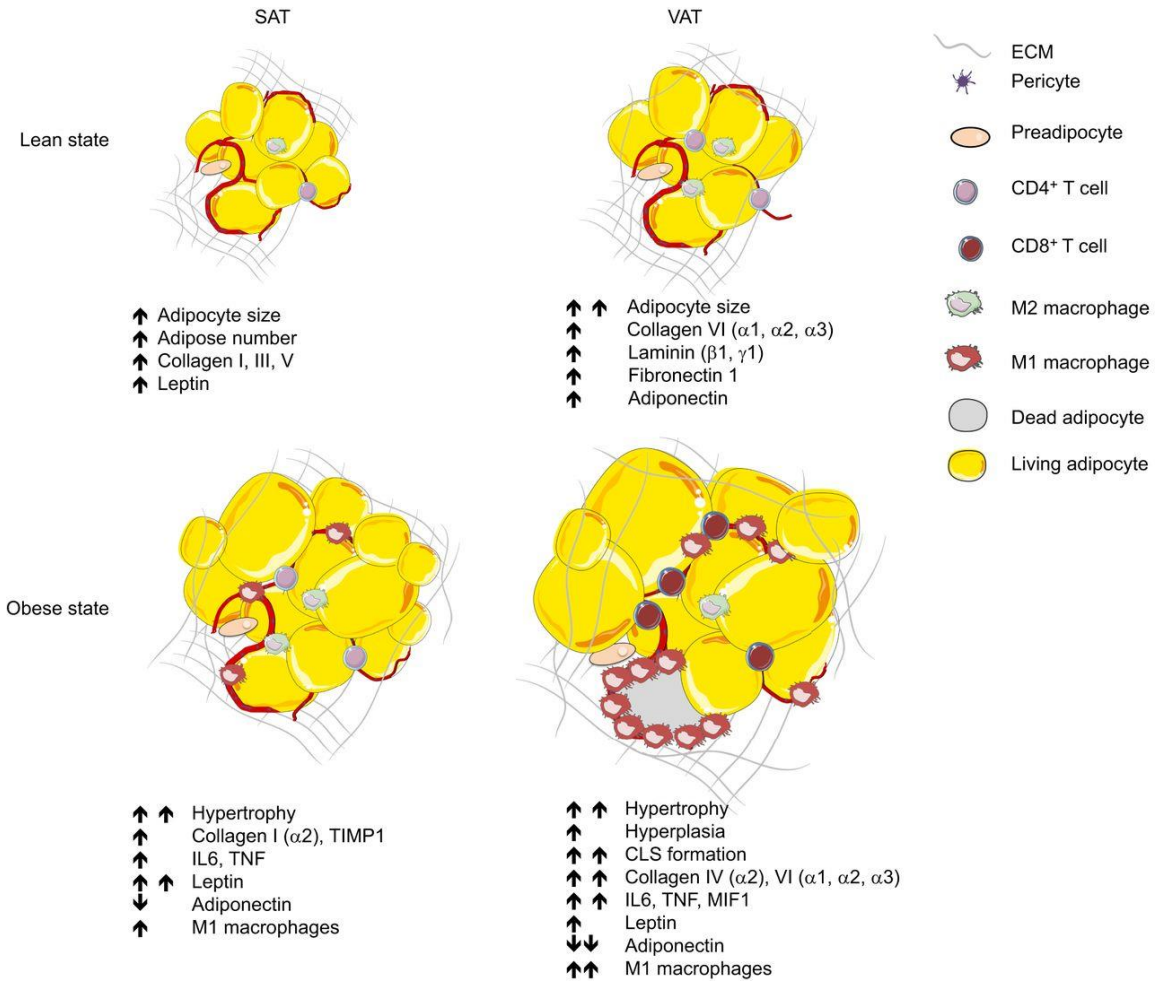

Fig. 5: SAT and VAT under lean state and obese state. Obesity triggers hypertrophy of white adipocytes with a more rapid expansion in visceral depots. Obesity triggers as well ECM remodeling and an inflammatory profile. The obese adipose tissue is accompanied by change of collagen types, increased cytokine secretion such as IL-6 and TNF, as well as phenotypic change of macrophages from M2 to M1, which can surround dead or dying adipocytes forming CLSs in VAT. CLS: Crown-like structure. ECM: Extracellular matrix. IL-6: Interleukin 6. MIF1: Macrophage migration inhibitory factor 1. SAT: Subcutaneous white adipose tissue. TIMP1: Metallopeptide inhibitor 1. TNF: Tumor necrosis factor. VAT: Visceral white adipose tissue. (Schoettl et al. 2018)

1.1.5 Endocrine function of white adipose tissue

Adipose tissue is not only an organ storing energy in the form of triglycerides, but also an important endocrine organ which secretes plenty of cytokines and adipokines. Adipokines regulate different metabolic processes and they have different expression patterns in different adipose tissue depots (Ahima and Lazar 2008). Leptin is a hormone secreted exclusively by adipocytes and shows effects on other target organs (Zhang et al. 1994; Chait and Hartigh 2020). Leptin does not only suppress appetite by binding to leptin receptors in the central nervous system, but is also demonstrated to reduce insulin resistance and be cardioprotective (Taleb et al. 2007; Farooqi and O'Rahilly 2014; Friedman 2016). Adiponectin is a protein hormone secreted by adipose tissue and was first discovered in 1995 (Scherer et al. 1995). Opposite from leptin, and even it is secreted from adipose tissue, its levels are inversely proportional to adiposity (Ukkola and Santaniemi 2002). Adiponectin functions on several organs and improves the metabolic disorders by binding to adiponectin receptors through the mediation of transcription factor PPARα (Fang and Judd 2018). Adiponectin was demonstrated to be an anti-inflammatory adipokine (Fang und Judd 2018). Unlike leptin and adiponectin, resistin is considered as a pro-inflammatory adipokine and recently suggested to be secreted mainly from adipocytes in mouse and from macrophages of inflamed adipose tissue in humans (Savage et al. 2001; Jamaluddin et al. 2012). Resistin promotes inflammation not only by directly promoting insulin resistance, but also by upregulating the expression of several inflammatory cytokines such as IL-6 and TNF-α, which can further promote inflammation in adipose tissue and metabolic disorders in other organs (Bokarewa et al. 2005). As already described, adipose tissue is the largest organ, therefore, hundreds of adipokines pronouncedly affect the whole body by being released into circulation and modulating target organs, thereby playing an important role in the maintenance of metabolic homeostasis.

1.2 DREADD system

Designer receptor exclusively activated by designer drugs (DREADD) are a class of engineered G protein-coupled receptors, which can solely be activated by synthetic ligands but not endogenous ligands (Armbruster et al. 2007). Together with receptors activated solely by a synthetic ligand (RASSL), these engineered receptors enable to control cellular signaling pathways in a remote manner. The advantage of DREADD over RASSL is its two-way selectivity of the receptor-ligand pair, synthetic ligands used for RASSL activate other receptors as well, however, ligands used for DREADD can only activate DREADD (Rogan and Roth 2011; Farrell and Roth 2013). DREADD were first designed in 2007 in Roth's lab (Armbruster et al. 2007). They generated DREADD by mutating two amino acids Y149C and A239G on human muscarinic receptors which are G protein-coupled receptors, and yielded receptors insensitive to endogenous ligand acetylcholine but only sensitive to clozapine N-oxide (CNO), which is an agonist being inert at endogenous targets (Weiner et al. 2004; Armbruster et al. 2007). According to the classification of GPCRs, three types of DREADD were designed and are currently in use: human M3 $G_{\alpha q}$ protein-coupled receptor (hM3Dq) activates $G_{\alpha q}$ signaling pathway, human M4 $G_{\alpha i}$ protein-coupled receptor (hM4Di) activates $G_{\alpha i}$ signaling pathway and rat M3 $G_{\alpha s}$ protein-coupled receptor (rM3Ds) activates $G_{\alpha s}$ signaling pathway (Farrell and Roth 2013). All these three types of DREADD share the same point mutations, but since $G_{\alpha s}$ does not couple to any native muscarinic receptors, to generate rM3Ds, the intracellular loops 2 and 3 of rat M3 receptor sequence was replaced by β_1-adrenergic receptor sequence from turkey (Guettier et al. 2009).

Mostly, Cre-loxP technique is used for DREADD systems to enable an inducible receptor expression. DREADD system allows for a controlling of cellular signaling pathways in a spatial and temporal specific manner, particular cell type or anatomical region-specific and only after administration of particular ligands (Rogan and Roth 2011). By using Cre-loxP technique, also the receptor expression can be precisely modulated. In our study, it is also not feasible to use viral vectors to express the construct since the efficacy of viral infection in adipose tissue is very low (Bates et al. 2020). Here, the DREADD system is therefore applied also by using Cre-loxP technique. To drive spatially restricted activity of Cre-recombinase, which excises DNA flanked by loxP sites, a tissue-specific promotor is required. In our study, we want the receptors to express solely in adipose tissue, the adipocyte specific promotor AdipoQ was therefore used. The peripheral lipolysis is expected to be inhibited, when hM4Di receptors activate $G_{\alpha i}$ signaling. The constructs were generated by

placing a loxP-flanked STOP codon between hM4Di and a strong ubiquitous CAG promotor, the constructs were then cloned into on ROSA26 DREADD vector to replace tdTomato sequence (Zhu et al. 2016b). To visualize the expression of hM4Di, each hM4Di is tagged by a hemagglutinin (HA) and followed by a P2A sequence and a fluorescent reporter mCitrine. P2A is a self-cleaving peptide, therefore, after translation, the fused protein splits into two parts: mCitrine enters the cytoplasm and allows for the visualization of receptor expression, HA-tagged hM4Di locates on the cell membrane and allows for the determination of detailed spatial localization of hM4Di in adipocyte. To cut STOP codon and realize hM4Di expression, the mice need to be mated with an adipocyte-specific Cre-driver line as described.

To modulate DREADD activity, synthetic ligands which are bioavailable and drug-like such as CNO are needed. Due to the good bioavailability, the ligands can be administered using simple methods such as food, drinking water, subcutaneous injection and intraperitoneal injection (Farrell and Roth 2013). CNO is initially considered as biolo$_{gi}$cally inert, however, recent findings suggested that CNO can be back converted to clozapine which activates not only DREADD but also serotonin and dopamine receptors in humans but not in mice (Chang et al. 1998; Guettier et al. 2009). Consequently, DREADD agonist 21 also named as Compound 21 was used in this study for muscarinic-based DREADD system. DREADD agonist 21 is reported to be effective both *in vitro* and *in vivo*, even if some off-target effects still exist, unlike CNO, it does not back converted into clozapine and it is 2,7 times more potent (Thompson et al. 2018). Systemic administration normally responds within 5 to 15 minutes (Rogan und Roth 2011), in our study, DREADD agonist 21 is therefore administered by intraperitoneal injection respectively at the beginning of myocardial ischemic operation and the beginning of reperfusion phase to inhibit lipolysis.

1.3 Crosstalk between heart and adipose tissue after MI

1.3.1 Myocardial infarction

Myocardial infarction, which is due to reduced or stopped blood flow in one or several coronary arteries of the heart leading to insufficient oxygen delivery and thereby tissue death of cardiac muscle, is still nowadays one of the leading causes of death globally, especially in industrial countries. According to the blockage degree of a coronary artery, MI can be subdivided into ST elevation MI, which is characterized by the complete blockage of a coronary artery and non-ST elevation MI, which is characterized by the partial blockage of a coronary artery. Together with unstable angina these entities count as acute coronary syndrome, among which the identification of MI is the occurrence of cell death, which can be estimated by the blood test measurement of troponin (Torres and Moayedi 2007). Blood test of troponin together with infarct sings in electrocardiograms (ECGs) is mainly used for the diagnosis of MI (Varcoe et al. 1975). Atherosclerosis is the leading cause of MI, however, also systemic hypotension after shock and sudden increased oxygen demand after such as fever or hyperthyroidism can also result in myocardial ischemia and subsequent MI (Saleh and Ambrose 2018).

Over the last decades, the mortality rate of acute MI has been significantly reduced, however, the development of heart failure after MI still results in high risks (Lewis et al. 2003). Development of heart failure after MI is closely associated with cardiac remodeling. The progression of heart remodeling can be divided into 3 phases: the inflammatory phase, the reparative and proliferative phase and the maturation phase (Prabhu and Frangogiannis 2016). Leukocyte infiltration resulting from the impairment of vascular endothelial cell integrity due to oxygen deficiency during cardiac ischemia initiates the inflammatory phase (Eltzschig and Eckle 2011). Danger-associated molecular patterns (DAMPs) released by necrotic cells and damaged extracellular matrix activate the innate immune system and induce the expression of proinflammatory cytokines such as IL-1, TNF-α and chemokines as MCP1 and CCL2 by binding to pattern recognition receptors like toll-like receptors (TLRs) (Arslan et al. 2011; Timmers et al. 2012; Haan et al. 2013). These inflammatory molecules promote the adhesion between endothelial cells and leukocytes inducing the infiltration of neutrophils (Yan et al. 2013). The infiltration of neutrophils triggers the transition from inflammatory phase to reparative and proliferative phase. The proteolytic enzymes released by neutrophils help to clear necrotic cells and extracellular matrix debris, furthermore, subsequent apoptosis of neutrophils induces the polarization of macrophages toward an anti-

inflammatory and reparative phenotype (M2), which secretes multiple anti-inflammatory cytokines that suppress tissue inflammation and promote tissue repair (Soehnlein and Lindbom 2010; Boufenzer et al. 2015). Subsequently, the changes of microenvironment induce the trans-differentiation of fibroblasts into myofibroblasts, which develop stress fibers and secrete large amounts of extracellular matrix proteins that maintain the structural integrity of the infarct area and thereby symbolize the proliferative phase (Frangogiannis et al. 2000; Santiago et al. 2010; Turner and Porter 2013). The proliferative phase is finally followed by the maturation phase, which is characterized by de-activation and apoptosis of reparative cells and formation of maturated scar composed of a network of cross-linked collagens (Frangogiannis 2014).

1.3.2 Systemic effects of myocardial infarction

Myocardial infarction has nowadays still a high mortality rate not only because of its own dangers, but also due to its strong systemic implications. MI can impact on the whole body and triggers some responses in other organs such as liver, kidney and adipose tissue (Valori et al. 1967). Many studies reported the correlation between liver enzymes and cardiovascular disease, a recent clinical study demonstrated the association between serum liver transaminases and acute MI (Adibi et al. 2007; Saely et al. 2008; Baars et al. 2016). Elevated serum levels of aspartate transaminases (AST) and alanine transaminases (ALT) which would suggest a NAFLD-type liver injury were determined in patients with acute MI (Baars et al. 2016). Patients with MI have great risks to develop heart failure as a consequence of death of cardiomyocytes and scar formation (Jenča et al. 2021). Cardiac muscle is unable to pump blood well during heart failure, liver, as an organ being largely dependent on blood flow and receiving up to 25 % of cardiac output, often develop manifestations in patients with heart failure (Møller and Bernardi 2013). Reduced arterial perfusion has been suggested as the fundamental mechanisms involved in acute liver damages such as cardiac cirrhosis and congestive hepatopathy (Dunn et al. 1973; Kubo et al. 1987). Besides, MI impacts as well heavily on kidney, and it is still one of the most critical causes of acute kidney injury (Wang et al. 2019). The dropped amount of blood ejected by each contraction during MI leads to the decreased amount of blood that passes through the kidney. Kidney is an organ which can filter waste products from the blood, along with the shortage of blood flow passing through, less waste output is filtered and higher levels of dangerous wastes are getting

accumulated (Goyal et al. 2023). Therefore, MI is not an isolated event only affecting the heart, but it triggers also a number of complications on other organs.

1.3.3 The crosstalk between heart and adipose tissue

During and after MI, several neurohumoral systems are activated as a compensation for the reduced cardiac output, pain and stress due to cardiac injury. Among them, adrenergic stimulation plays a critical role, persistent catecholamine load induces β1 receptors activation in cardiomyocytes and results in increasing cardiac performance and blood pressure (Florea and Cohn 2014). In addition, high level of adrenergic catecholamines in the circulation also activates β3 receptors in peripheral white adipose tissue and is one of the strongest stimuli of lipolysis (Lymperopoulos et al. 2013a). Natriuretic peptides which are elevated during heart dysfunction as well further enhance adipose tissue lipolysis (Sengenès et al. 2000). It has been well known that activated lipolysis in the peripheral white adipose tissue results in high levels of circulating FFAs. Randle cycle describes the competition between glucose oxidation and fatty acids oxidation, namely the fuel selection by tissues (RANDLE et al. 1963). During MI, more acetyl-CoA is yielded from FAO, and glucose oxidation is decreased via inhibition of PDH. FAs oxidation yields acetyl-CoA that becomes a source of lipotoxic intermediates such as ceramides, diglycerides, and reactive oxygen species (ROS), and hence creates lipotoxicity (Perman et al. 2011; D'Souza et al. 2016). Cardio-lipotoxicity relies on the imbalanced uptake and utilization of lipid and results in lipid accumulation in cardiomyocytes (Bertero and Maack 2018). Cardiomyocyte intracellular lipid accumulation is demonstrated to be linked with oxidative stress, which further leads to cardiac apoptosis, necrosis, fibrosis and inflammation (Bertero and Maack 2018). Therefore, cardio-lipotoxicity after MI is one of the leading factors worsening cardiac function and leading to the development of heart failure. In the meanwhile, the repressed glucose oxidation generates lactate and protons, which lead to ionic disturbance and calcium overload in the myocardium and further worsen cardiac function (Tani and Neely 1989). As mentioned in the previous chapter, the binding of catecholamines to $G_{\alpha s}$-coupled receptors on the cell membrane of adipocytes leads to the activation of lipases including ATGL, which is the rate-limiting enzyme that catalyze the initial step of lipid hydrolysis (Young and Zechner 2013). Heart failure as one of the most common complications of MI is the leading cause of eventual death. It has been reported that the activated ATGL due to heart failure contributes to increased production of inflammatory cytokines in adipose tissue, which not

only contributes to the systemic inflammation associated with innate immune cells such as macrophages and worsens cardiac function, but also leads to systemic insulin resistance (Shimizu et al. 2012). Whereas inhibiting ATGL such as by using Atglistatin can improve systolic and diastolic heart function in murine model (Thiele et al. 2022). Previous studies demonstrated that adipocyte specific inhibition of ATGL ameliorated cardiac functional decline and cardiac remodeling by reducing adipose tissue inflammation (Parajuli et al. 2018; Takahara et al. 2021). Furthermore, ATGL deficiency in adipose tissue was identified to prevent left ventricular failure resulted from changes in cardiac lipidome (Salatzki et al. 2018).

1.4 Aims of thesis

Recently, the crosstalk between heart and adipose tissue after MI is more and more under focus. High levels of adrenergic catecholamines during and after MI due to reduced cardiac output, pain and stress, is a driver of lipolysis in the peripheral adipose tissue and results in elevated circulating FFAs levels, which are known to be detrimental to the ischemic myocardium (Essop and Opie 2020). Thereby targeting adipose tissue after MI has been regarded as a promising therapeutic strategy to prevent the worsening of condition (Smeir et al. 2021). However, the adrenergic stimulation of lipolysis is known to be transient, how adipose tissue is getting altered acutely and chronically after MI still remains unclear. Therefore, in this study, first we are eager to find out how MI modulates white adipose tissue during the reperfusion phase and which depot is primarily getting affected.

MI-induced activated lipolysis has been identified as the potential driver of heart failure, which is the leading cause of eventual death in patients with MI. Previous studies reported adipocyte specific inhibition of lipolysis enables to reduce cardiac functional decline and cardiac remodeling (Parajuli et al. 2018; Takahara et al. 2021). Therefore, subsequently, we used an adipocyte-specific inhibitory DREADD system that enables to inhibit lipolysis in a spatio-temporal manner, aiming to investigate the profile of white adipose tissue after blockade of lipolysis, as well as the changes in cardiac function.

2 Materials and methods

2.1 Materials

2.1.1 Chemicals and reagents

Chemicals/Reagents	Supplier
1,4-Dithiothreitol	Carl Roth
4-Hydroxytamoxifen H6278-50 mg	Sigma-Aldrich
2-Mercaptoethanol	Sigmal-Aldrich
Ammonium persulfate	Sigma-Aldrich
Buprenorphinhydrochloride	ESSEX PHARMA
Bovine serum albumin	Sigma-Aldrich
Citrate Buffer pH 6.0 (10x)	ZYTDMED
Chloroform	Carl Roth
Cryocompound	ImmunoLogic
DPBS (1x)	Gibco
DREADD Agonist 21 dihydrochloride SML2392	Sigma-Aldrich
Eosin Y solution 1 % in water	Carl Roth
Glycerin	Carl Roth
Glycin	Carl Roth
Halt™ Protease & Phosphatase Inhibitor Cocktail (100x)	ThermoFischer
10 % Hydrochloric acid	Carl Roth
Hemalum solution acid acc. To Mayer	Carl Roth
Intercept® Blocking Buffer	LI-COR
Isofluran-Piramal	Piramal
Esketamine	Sintetica
N,N,N',N'-Tetramethylethylenediamine	MERCK
Normal goat serum	Cell Signaling
PageRuler™ Prestained Protein Ladder	ThermoFischer

Peanut oil	Sigma-Aldrich
Revert™ 700 Total Protein Stain	LI-COR
Revert™ 700 Wash Solution	LI-COR
ROTICLEAR®	Carl Roth
ROTI® Histofix 4 % Formaldehyd	Carl Roth
Roti®Mount	Carl Roth
ROTI® Mount FluorCare DAPI	Carl Roth
Rotiphorese® Gel 40	Carl Roth
Saccharose	MERCK
Saponin	Sigma-Aldrich
20 % Sodium dodecyl sulfate solution	Sigma-Aldrich
Tween® 20	Carl Roth
TRIS	Carl Roth
TRIzol® Reagent	ThermoFischer
Wheat germ agglutinin, Alexa Fluor™ 488 conjugate	Invitrogen
Xylazinhydrochlorid	Elanco

Table 1: Chemicals and reagents

2.1.2 Buffers

Buffer	Supplier/Composition
Blocking buffer for IHC (cryosections)	10 % (v/v) NGS 0,2 % (w/v) Saponin/PBS
Blocking buffer for IHC (paraffin sections)	10 % (v/v) FCS 1 % (w/v) BSA TBS
Blocking buffer for western blot	50 % (v/v) LI-COR Intercept® Blocking Buffer 50 % (v/v) TBS
4x Laemmli buffer	250 mM Tris (pH=6,8) 8 % (v/v) SDS

	20 % (w/v) Glycerol 0,02 % (v/v) Bromophenol blue 100 mM DTT (freshly added) Millipore water
Lysis buffer for adipose tissue in western blot	20 mM Tris-HCl 1 mM EDTA 255 mM Sucrose Millipore water
PBS	137 mM NaCl 2,7 mM KCl 10 mM Na_2HPO_4 1,8 mM KH_2PO_4 Millipore water
Primary antibody diluting buffer for IHC (cryosections)	2 % (v/v) NGS 0,2 % (w/v) Saponin/PBS
Primary antibody diluting buffer for IHC (paraffin sections)	1 % (w/v) BSA PBS
Primary antibody diluting buffer for western blot	5 % (w/v) BSA TBS-T
RIPA buffer	25 mM Tris 140 mM NaCl 1 mM EDTA 1 % (w/v) Triton X100 0,5 % (w/v) SDS Millipore water
SDS running buffer	25 mM Tris 250 mM Glycine 0,1 % (v/v) SDS Millipore water
Secondary antibody diluting buffer for western blot	50 % (v/v) LI-COR Intercept® Blocking Buffer 50 % (v/v) TBS 0,1 % (v/v) Tween 20

Semi-dry blotting buffer	190 mM Glycine 25 mM Tris 20 % (v/v) Ethanol 0,1 % (v/v) SDS Millipore water
Separating gel (10 %)	10 % (v/v) Acrylamide 250 mM Tris (pH=8,8) 0,1 % SDS 0,2 % (v/v) TEMED 0,025 % (w/v) Ammonium persulfate Millipore water
Stacking gel	5 % (v/v) Acrylamide 125 mM Tris (pH=6,8) 0,1 % (v/v) SDS 0,15 % (v/v) TEMED 0,03 % (w/v) Ammonium persulfate Millipore water
TBS (pH = 7,4)	150 mM NaCl 20 mM Tris Millipore water
TBS-T	0,1 % (v/v) Tween 20 TBS

Table 2: Buffers

2.1.3 Kits

Kit	Supplier
Bio-Plex Pro Mouse Diabetes Adiponectin Assay	BIO-RAD
DAB Substrate Kit	BIOZOL
NEFA-HR Kit	Fujifilm
Pierce™ BCA Protein Assay Kit	ThermoFischer

Platinum® SYBR® Green qPCR SuperMix-UDG	Invitrogen
QuantiTect® Reverse Transcription Kit	Qiagen
RNeasy® Lipid Tissue Mini Kit	Qiagen
RNeasy® Fibrous Tissue Mini Kit	Qiagen
Revert™ 700 Total Protein Stain and Wash Solution Kit	LI-COR
Ultra-Sensitive Mouse Insulin ELISA Kit	Crystal Chem

Table 3: Kits

2.1.4 Primers

Gene	Primer sequence (5' to 3')
Adipoq	fwd: CCA CTT TCT CCT CAT TTC TG rev: CTA GCT CTT CAG TTG TAG TAA C
Cd36	fwd: AGA TGA CGT GGC AAA GAA CAG rev: CCT TGG CTA GAT AAC GAA CTC TG
Cidea	fwd: GTG TTA AGG AAT CTG CTG AG rev: CTA TAA CAG AGA GCA GGG TC
Cox8b	fwd: ATC TCA GCC ATA GTC GTT G rev: CTG CGG AGC TCT TTT TAT AG
Dgat2	fwd: GCG CTA CTT CCG AGA CTA CTT rev: GGG CCT TAT GCC AGG AAA CT
Fasn	fwd: GGA GGT GGT GAT AGC CGG TAT rev: TGG GTA ATC CAT AGA GCC CAG
hM4di	fwd: GAG CCT GGT GAC TGT CGT G rev: AGC TGC CTG TTG ACC TTG AT
Leptin	fwd: GAG ACC CCT GTG TCG GTT C rev: CTG CGT GTG TGA AAT GTC ATT G
Lpl	fwd: GGG AGT TTG GCT CCA GAG TTT rev: TGT GTC TTC AGG GGT CCT TAG

Nudc	fwd: AGA ACT CCA AGC TAT CAG AC rev: CTT CAG GAT TTC CTG TTT CTT C
Plin2	fwd: GAC CTT GTG TCC TCC GCT TAT rev: CAA CCG CAA TTT GTG GCT C
Plin5	fwd: TGT CCA GTG CTT ACA ACT CGG rev: CAG GGC ACA GGT AGT CAC AC
Pln	fwd: AAA GTG CAA TAC CTC ACT CGC rev: GGC ATT TCA ATA GTG GAG GCT C
Pnpla2	fwd: CAA CCT TCG CAA TCT CTA C rev: TTC AGT AGG CCA TTC CTC
Pparg	fwd: AAA GAC AAC GGA CAA ATC AC rev: GGG ATA TTT TTG GCA TAC TCT G
Resistin	fwd: AAG AAC CTT TCA TTT CCC CTC CT rev: GTC CAG CAA TTT AAG CCA ATG TT
Slc2a4	fwd: CAA TGG TTG GGA AGG AAA AG rev: AAT GAG TAT CTC AGG AGG C
Srebp1c	fwd: TGA CCC GGC TAT TCC GTG A rev: CTG GGC TGA GCA ATA CAG TTC
Ucp1	fwd: CTTTTTCAAAGGGTTTGTGG rev: CTTATGTGGTACAATCCACTG

Table 4: Primers

2.1.5 Antibodies

Antibody	Host species	Application	Dilution factor	Primary/ secondary	Supplier
Anti-AKT	Rabbit	Western blot	1:1000	Primary	Cell Signaling
Anti-GFP	Goat	Western blot	1:1000	Primary	Abcam
Anti-GFP	Goat	IHC	1:100	Primary	Abcam
Anti-HA-Tag	Rabbit	IHC	1:800	Primary	Cell Signaling
Anti-Mac2	Rat	IHC	1:150	Primary	CEDARLANE
Anti-p-HSL (s565)	Rabbit	Western blot	1:1000	Primary	Cell Signaling
Anti-PLN	Rabbit	Western blot	1:5000	Primary	Badrilla

Anti-p-PLN (s16)	Rabbit	Western blot	1:5000	Primary	Badrilla
Anti-p-PKA Substrates	Rabbit	Western blot	1:1000	Primary	Cell Signaling
Anti-p-TnI (s23/24)	Rabbit	Western blot	1:5000	Primary	Cell Signaling
Anti-TnI	Rabbit	Western blot	1:5000	Primary	Cell Signaling
Anti-UCP1	Rabbit	IHC	1:500	Primary	Abcam
Anti-UCP1	Rabbit	Western blot	1:1000	Primary	Abcam
Alexa Fluor™ 647 goat anti-rabbit	Goat	IHC	1:200	Secondary	ThermoFischer
Alexa Fluor™ 647 goat anti-rat	Goat	IHC	1:200	Secondary	ThermoFischer
IRDye® 680RD Goat anti-Rabbit	Goat	Western blot	1:10000	Secondary	LI-COR
IRDye® 800CW Goat anti-Mouse	Goat	Western blot	1:10000	Secondary	LI-COR
IRDye® 800CW Goat anti-Rabbit	Goat	Western blot	1:10000	Secondary	LI-COR

Table 5: Antibodies

2.1.6 Technical equipment

Equipment	Supplier
HistoCore MULTICUT	Leica
Keyence microscope BZ X810	Keyence
LEICA CM3050 S	Leica
Mastercycler personal	Eppendorf
NANODROP ONE	ThermoFischer
Semi-Dry Blotter	Peqlab
HEAT SYSTEMS-ULTRASONICS	QSONICA
StepOne Plus Real-Time PCR Detection System	ThermoFischer
SYNERGY microplate reader	SYNERGY

TissueRuptor	Qiagen
TissueRuptor® Disposable Probes	Qiagen
Ultrasound device Vevo 3100	VisualSonics
ZEISS Axio Imager 2	Zeiss

Table 6: Technical equipment

2.2 Methods

2.2.1 Strains

The R26-LSL-Gi-DREADD mice (line 026219) (Zhu et al. 2016a) from The Jackson Laboratory were designed to have the Rosa-CAG-LSL-HA-hM4Di-pta-mCitrine conditional allele (R26-hM4Di/mCitrine). CAG promoter-driven, loxP-flanked STOP cassette and HA-hM4Di-pta-mCitrine coding region were inserted into the ROSA26 locus, HA-hM4Di-pta-mCitrine expression is determined by tissue-specific Cre recombinase expression. C57BI/6J mice (line 005304) (Keane et al. 2011) from Janvier for the Adipoq-CreERT2 BAC transgene were hemizygous and viable and fertile. Tamoxifen induction directed Cre recombinase (Cre/ERT2) to adipose tissue by the promoter/regulatory regions of the mouse adiponectin (Adipoq) locus on the BAC transgene. By crossing these two lines, the expression of hM4Di receptor were able to be generated in an adipose tissue specific and inducible hM4Di expressing mice.

2.2.2 Tamoxifen-treatment

Cre-recombinase mediated removel of the loxP-floxed STOP cassette in DREADD mice was achieved by 5 consecutive days intraperitoneal injection of 4-hydroxytamoxifen (500 µg/mouse) at the age of 10 weeks followed by 2,5 weeks wash-out phase.

2.2.3 Ischemia/Reperfusion operation

12-15 weeks male mice underwent 60 min closed chest ischemia followed by 30 min, 24 h, 7 or 28 d of reperfusion. To induce closed chest ischemia, operation was performed in a two-step procedure. First mice received the ligature, by anesthetizing them with 90 mg/kg BW ketamine/15 mg/kg BW xylazine, intubating and mechanically ventilating them. Then the chest was opened in the 3rd intercostal space, the LAD exposed and the ligature, a 7/0 prolene suture, passed underneath the LAD. To close the ligature at a later time point, a small PE-10 tube was threaded on both ends of the suture, loosely forming a loop around the LAD and the ends of the suture were left in a subcutaneous skin pocket, while ribs and skin were closed. Mice recovered from surgery for 5 - 7 days and then underwent ischemia by anesthetizing them with 2 % isoflurane, opening the skin and exposing the sutures. Ischemia was induced under ECG control by using 5 g weights at each end of the suture. Lipolysis

inhibition was achieved in DREADD-mice by intraperitoneal injection of 3 mg/kg BW DREADD agonist 21 before ischemia and directly at the beginning of reperfusion. Body temperature was maintained at 37.5 °C. Postoperative analgesia was achieved using buprenorphine (0.05 mg/kg BW). To investigate NEFA levels and circulating adipokines, blood was sampled from the tail vein before ischemia and after 30 min of reperfusion.

Operations were performed by Dr. med. Katharina Bottermann and Dominik Semmler.

2.2.4 Echocardiography

Echocardiography was performed using ultrasound device Vevo 3100 (Visual Sonics) and ultrasound probe MX400. Spontaneously breathing animals were anesthetized using 4 % isoflurane in 0,6 mL/min O_2, anesthesia was maintained with 2 % isoflurane. Mice were fixed on a heating table, ECG, temperature and breathing frequency was controlled. Images were taken from parasternal long axis (PSLA) in B-Mode and M-Mode and from parasternal short axis at mid (B-Mode and M-Mode), base and apex (both B-Mode) of the heart. Cardiac volumes (EDV, ESV, SV, CO) and functional parameters (EF, FAC, FS) were calculated using Simpson's protocol (Heinen et al. 2018). Echocardiography was performed by Dr. med. Katharina Bottermann. All experiments were in accordance with the local animal regulations and approved by the local authorities (LANUV NRW, AZ: 81-02.04.2019.A397).

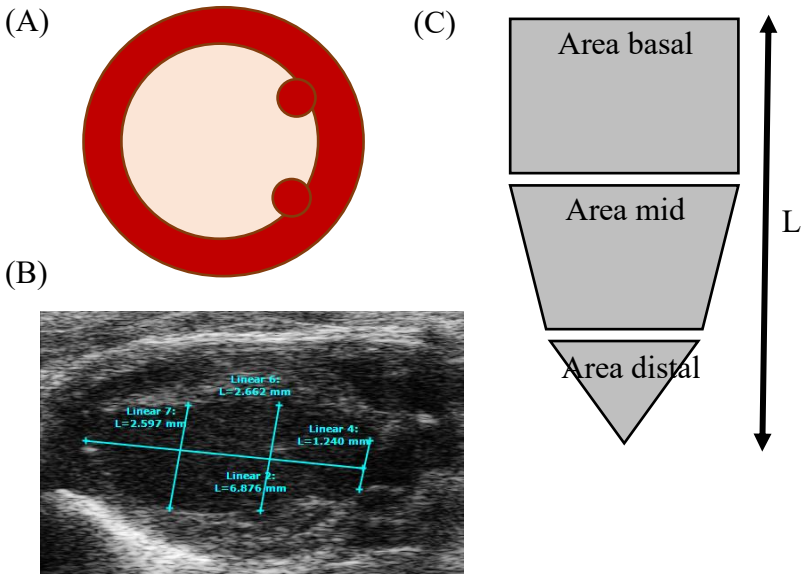

Fig. 6: Illustration of echocardiography. (A) Schematic of a short axis view of the left ventricle. (B) Schematic of the heart how it is seen for calculation of EDV and ESV using Simpson's method. (C) Long axis of a mouse heart with length estimation.

2.2.5 Blood pressure measurement

Blood pressure measurement was performed under anesthesia using isoflurane (2 - 2.5 %) and buprenorphine (0.1 mg/kg, s.c.) was administered for perioperative analgesia. The common carotid artery was exposed through a skin incision (approx. 1.5 cm) on the left ventral side of the neck followed by a ligature and subsequent opening of the vessel. A 1.4 F Millar pressure volume catheter was inserted and the vessel around the catheter closed with a permanent knot. After the stabilization of the blood pressure for 10 min, blood pressure and heart rate were recorded for additional 15 min. After completing the functional measurements, the catheter was removed, and the animals were killed by cervical dislocation.

Blood pressure measurement was performed by PD Dr. Dr. med. André Heinen and Anne Hemmers.

2.2.6 Harvest of gWAT and iWAT

The mice were sacrificed, and the skin opened in the middle of the abdominal cavity, inguinal white adipose tissue could be found underneath the skin (Fig. 7), lymph nodes inside had to be carefully removed. After opening the peritoneum, gonadal white adipose tissue directly connected to the gonads was exposed. The tissue used for gene and protein analysis was first washed in cold 1x PBS and then frozen in liquid nitrogen before storing at -80 °C. The tissue used for histological analysis was washed in cold 1x PBS and then kept in 4 % formalin at 4 °C on a horizontal rotator overnight. On the second day, the tissue was transferred to 1x PBS and kept at 4 °C until paraffin embedding.

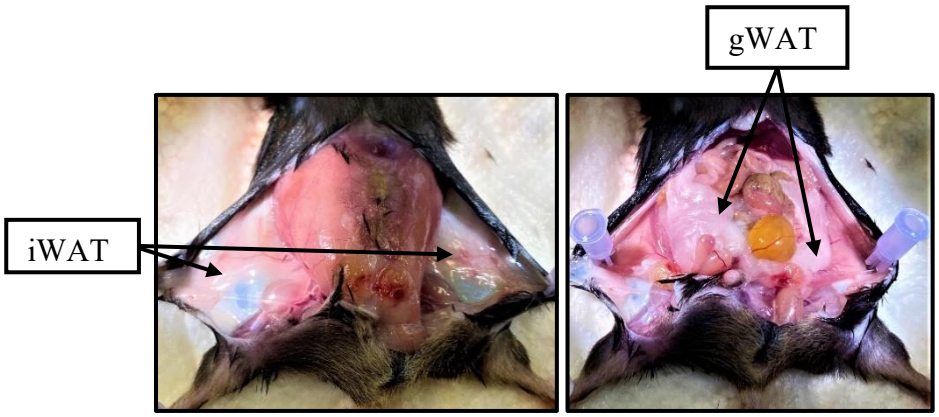

Fig. 7: Anatomical position of gWAT and iWAT. The harvest position of inguinal white adipose tissue and gonadal white adipose tissue. After opening the abdominal cavity, inguinal white adipose tissue was found underneath the skin and after opening the peritoneum, gonadal white adipose tissue was found directly connected to the gonads. gWAT: Gonadal white adipose tissue. iWAT: Inguinal white adipose tissue.

2.2.7 DREADD agonist 21 preparation

10 mg/mL DREADD agonist 21 dihydrochloride stock solution was prepared by dissolving 25 mg DREADD agonist 21 powder in 2,5 mL sterile DPBS. The 2,5 mL stock solution was aliquoted into 100 µL aliquots and kept at -20 °C.

2.2.8 Non-esterified fatty acids (NEFA) measurement

Blood taken from either the tail or the heart was centrifuged twice at 4000 rpm and 4 °C for 5 min, the supernatant namely serum was collected and kept on ice for use. NEFA-HR Assay was used to quantitatively determine the FFAs in serum. It is based on an enzymatic method using 3-methyl-N-ethyl-N-(β -Hydroxyethyl)-aniline (MEHA) as a violet coloring agent. 4 µL standard (0, 0,125, 0,25, 0,5 and 1 mM FUJIFILM NEFA Standard) or sample and 200 µL FUJIFILM NEFA(HR) 1 were pipetted into a Greiner 96 Well Cell Culture F-bottom Plate and incubated at RT on a horizontal rotator for 5 min. After incubation, the plate was measured by SYNERGY microplate reader at a wavelength of 550 nm and the first readouts (A) was obtained. Then 100 µL FUJIFILM NEFA(HR) 2 was added, the plate was incubated at RT on a horizontal rotator for another 5 min and determined again at a wavelength of 550 nm. After having the second readouts (B), B – A was considered to be the measurement value of each standard or sample. An equation was possible to be obtained with the help of the standard series, and the concentration of fatty acids in the sample was able to be obtained.

2.2.9 Microtome cutting

Paraffin-embedded white adipose tissue was sectioned using a microtome at a thickness of 5 µm. To collect large enough sections, the first 500 µm of the section were discarded. Two sections were always collected every 100 µm and 20 sections were collected for each tissue block.

2.2.10 Hematoxylin and eosin staining

Adipocyte size and morphology was analyzed using hematoxylin and eosin staining. 5 µm paraffin sections were deparaffinized 3x 15 min in Roticlear and rehydrated in 100 %, 95 % and 70 % ethanol for each 2 min. The washing steps were started with 1x PBS for 2x 5 min and followed by washing with distilled water for 1 min. The cell nuclei were stained by hematoxylin for 1 min, afterwards the slides were rinsed shortly in tap water and 1 % HCl. Bluing was done by washing slides with running tap water which is mildly alkaline for 10 min. Plasma and extracellular matrix were stained with 1 % eosin for 1 min. Before mounting the sections with Roti®Mount, the slides were dehydrated in 70 %, 95 % and 100 % ethanol for each 2 min and in Roticlear for 5 min.

2.2.11 Immunohistochemistry of adipose tissue paraffin sections

Immunohistochemistry is used to visualize the localization of a specific cell type or protein. Anti-Mac2 antibody was used to analyze macrophage infiltration in white adipose tissue, anti-UCP1 antibody was used to analyze the browning of white adipose tissue. 5 µm paraffin sections were deparaffinized 3x 15 min in Roticlear and rehydrated in 100 %, 95 % and 70 % ethanol for each 2 min. After rehydration, sections were washed in 1x PBS for 2x 5 min. Antigen retrieval, which was used to reduce or eliminate the chemical modifications introduced by formalin and hence gained the detectability of proteins, was performed by boiling slides in citrate buffer at 65 °C for 20 min. Slides were cooled down at RT for at least 10 min before washing 2x 5 min in 1x PBS. Blocking solution, which avoids the unspecific binding of secondary antibody, was prepared by adding 10 % FCS and 1% BSA in TBS. The slices were blocked at RT for 1 h and then incubated with 50-100 µl primary antibody diluted with 1x PBS containing 1 % BSA at 4 °C overnight. On the second day, the slides were washed 3x 5 min in 1x PBS before incubating with secondary antibody, which was diluted with 1x PBS at RT in dark for 1 h. After incubation, slides were washed 3x 5 min in 1x PBS and mounted with ROTI® Mount FluorCare DAPI. The slides were dried in dark at 4 °C overnight before being analyzed with fluorescent microscope.

2.2.12 Cryosectioning

During cryosectioning, the temperature was controlled at -21 °C and the cryo-embedded hearts were sectioned into 5 - 14 µm sections. The first intact section from the apex side that could be selected was marked level 1, 2x 5 µm, 4x 8 µm and 2x 14 µm sections were collected every 500 µm, 10 - 13 levels were collected for each heart.

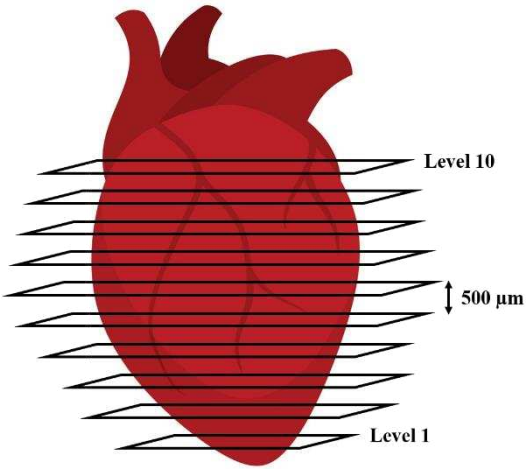

Fig. 8: Cryosectioned levels of one heart. The cryosectioned hearts were cut from the apex side to the basal side, every 500 µm eight 5 – 14 µm sections were collected, 10 – 13 levels were collected for one heart.

2.2.13 Immunohistochemistry of cardiac cryosections

Native hearts were cryo-embedded in cryocompound using -30 to -40 °C cold isopentane. Cryo-embedding allows a better preservation of antigens and therefore better detectability by antibodies. The 8 µm thick cryosections were first fixed with 4 % ice-cold formalin at RT for 10 min. Afterwards, the sections were washed 3x 10 min with PBS. To avoid unspecific binding of secondary antibody, the sections were blocked with 10 % NGS in 0,2 % saponin/PBS at RT for 1 h in a wet chamber. After blocking, the sections were incubated with the primary antibody, which was diluted with 2 % NGS in 0,2 % saponin/PBS overnight at 4 °C in a wet chamber. Before incubating with the secondary antibody, the sections had to be first washed 3x 10 min with 2 % saponin/PBS. The dilution of the secondary antibody was with 2 % NGS in 0,2 % saponin/PBS and the incubation was performed at RT and in dark for 3 h. After incubation, the sections were washed twice with 0,2 % saponin/PBS and once with PBS, each time for 5 min. The slides were mounted with ROTI®Mount FluorCare DAPI and dried in dark at 4 °C overnight before being analyzed with fluorescent microscope.

2.2.14 Quantification of adipocyte size

To determine adipocyte size and morphology, H&E-stained slices of adipose tissue was analyzed using Zeiss Axio Imager 2 microscope and 10x objective. For measurement of adipocyte size, 200 cells per animal were analyzed in ImageJ by drawing manually the outline of each adipocyte (Fig. 9).

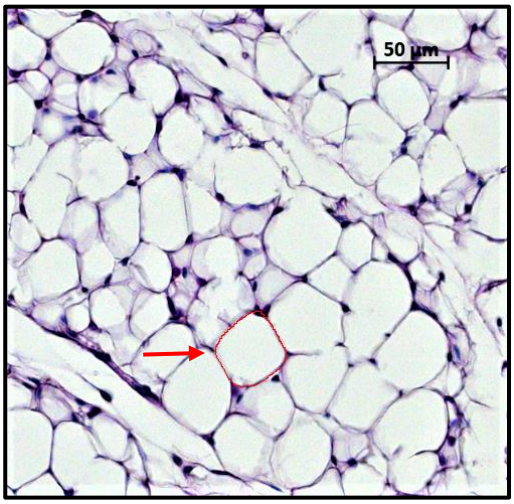

Fig. 9: H&E staining of 5 µm gWAT paraffin section. Red arrow: example of a free hand-drawing adipocyte in ImageJ.

2.2.15 Quantification of macrophage number

For macrophages quantification adipose tissue slices were imaged with Zeiss Axio Imager 2 microscope using a 20x objective after anti-Mac2 fluorescent staining (Fig. 10). The number of all macrophages in the whole section was counted manually using the software ImageJ and normalized to the size of the section. The final macrophage number was noted as the number of macrophages in 1 mm^2 inguinal white adipose tissue.

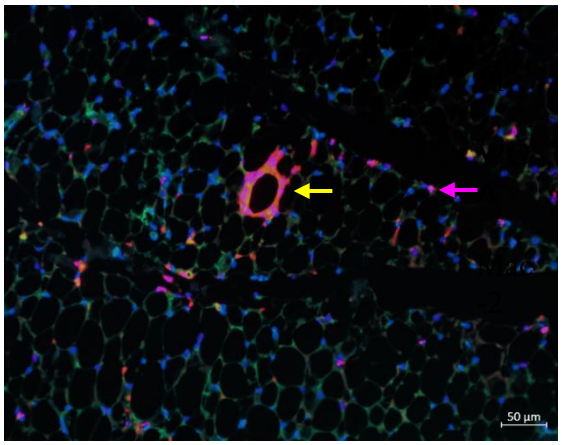

Fig. 10: Anti-Mac2 immunofluorescent staining of inguinal white adipose tissue. Pink arrow: representative anti-Mac2 positive cell; yellow arrow: representative crown-like structure.

2.2.16 Quantification of cardiac scar size

For assessment of scar size all levels (8 µm) of the hearts after 60 min ischemia and 7 d of reperfusion were stained for WGA-Alexa Fluor 488. Whole heart images were taken using fluorescence microscope with the 20x objective. The outline of every scar tissue was drawn by hand in ImageJ. The whole heart section and the left ventricle were also drawn manually. The percent of scar tissue occupying the whole heart section and the left ventricle was calculated respectively.

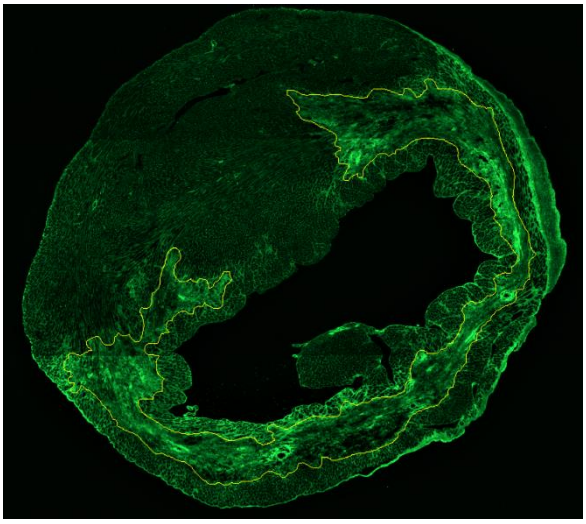

Fig. 11: WGA staining of cryosectioned 8 µm heart section. Yellow line: free hand-drawing of scar tissue in ImageJ. WGA: Wheat germ agglutinin.

2.2.17 Tissue preparation

The protein for western blot analysis was obtained from the lysis of organs or tissues. The lysis buffer for adipose tissue in western blot (Table 2) was used to lyse adipose tissue and RIPA buffer was used to lyse other organs or tissues. Both buffers were supplemented with 1:100 Halt™ Protease & Phosphatase Inhibitor Cocktail (100x), which contains inhibitors against the major classes of proteases and phosphatases and therefore prevents protein degradation during extraction. Each tissue sample was lysed in 500 µL lysis buffer with the help of Qiagen TissueRuptor. After lysis, the homogenate was kept immediately on ice and followed by a centrifugation at full speed and 4 °C for 15 min. After centrifugation, the clear layer containing protein was carefully transferred into a new tube and stored at -80 °C.

2.2.18 Protein concentration determination (BCA)

Protein concentration was determined by Pierce™ BCA Protein Assay Kit. A protein standard series composing of 0, 25, 125, 250, 500, 750, 100, 1500 and 2000 µg/mL albumin and the reagent for protein concentration determination which was prepared by mixing Pierce™ BCA Protein Assay Reagent A with Pierce™ BCA Protein Assay Reagent B at 50:1. The protein from lysis was first diluted 1:5 with lysis buffer, 25 µL albumin standards or diluted protein and 200 µL reagent were pipetted into a Greiner 96 Well Cell Culture F-bottom Plate and incubated at 37 °C for 30 min. The protein concentration was determined by SYNERGY microplate reader at a wavelength of 562 nm.

2.2.19 SDS PAGE

To analyze and quantify relative protein abundance, SDS PAGE followed by western blot analysis was performed. Denatured proteins were separated according to their molecular weights in a 10 % or 15 % self-casted polyacrylamide separating gel. According to protein concentration, the protein sample was diluted with Millipore water and 4x laemmli buffer at a final concentration of 2 µg/µL. Denaturation was done by incubating the samples at 95 °C for 6 min. 50 µg sample was used for analysis. The gel ran in SDS running buffer at a voltage of 100 V for around 15 min and then at 150 V for around 60 min. 5 µL PageRuler™ Prestained Protein Ladder was used as molecular weight reference.

2.2.20 Western blot

Following SDS PAGE, proteins were blotted from the polyacrylamide gel to a nitrocellulose blotting membrane using a Peqlab Semi-Dry Blotter. Before the transfer, gel, membrane and Whatman papers were incubated in blotting buffer (Table 2) for a short while and the western blot "sandwich" (Fig. 12) was prepared. The blotting was run at 105 mA for 60 min at RT. In case two gels were transferred at the same time, the current was doubled to 210 mA.

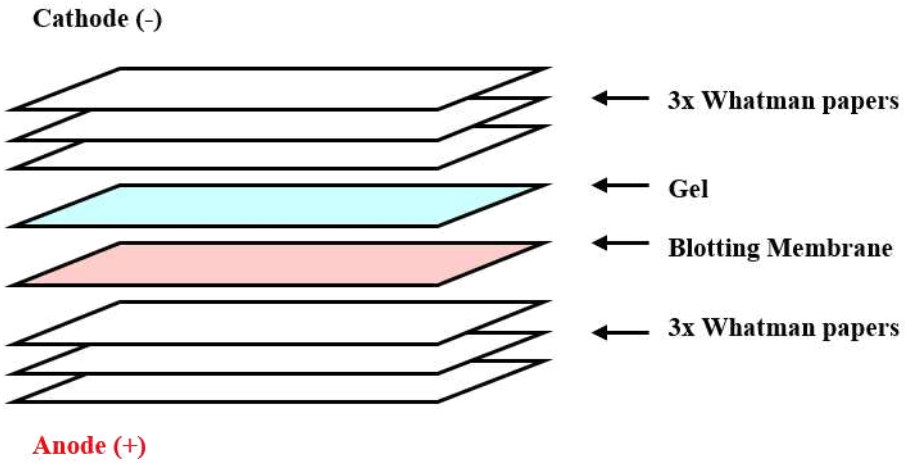

Fig. 12: Western blot "sandwich". Western blot "sandwich" composing of 6 Whatman papers, a polyacrylamide gel and a nitrocellulose blotting membrane. The gel loaded with negatively charged proteins is on the side of cathode, the proteins can be transferred to membrane along with the current.

After blotting, the membrane was stained for total proteins using Revert^{TM} 700 Total Protein Stain protocol, serving as the normalization reference. The membrane was first washed roughly in Millipore water and then incubated in 5 mL Revert^{TM} 700 Total Protein Stain Solution for 5 min in dark at RT while shaking. Afterwards, the dye was washed out twice by 30 s in Revert^{TM} 700 Total Protein Wash Solution and once roughly in Millipore water. After scanning, the membrane was blocked with blocking buffer for Western Blot (Table 2) at RT on horizontal shaker for 1 h and incubated with 5 mL primary antibody solution on a horizontal shaker at 4 °C overnight. Before incubation with 10 mL secondary antibody solution, the membrane was washed 3x 10 min in 10 mL TBS-T at RT on horizontal shaker. The incubation with secondary antibody was at RT on horizontal shaker for 1 h in the dark. Before scanning, the membrane was washed 3x 5 min in 10 mL TBS-T at RT on a horizontal shaker.

2.2.21 ELISA

Ultra-Sensitive Mouse Insulin ELISA Kit which was based on a sandwich enzyme immunoassay was used to check the circulating insulin level. 5 µL standard or serum was diluted with 95 µL diluent from the kit and incubated at 4 °C for 2 h and followed by a careful washing. Afterwards, 100 µL conjugate solution given by the kit was added and the plate was incubated at RT for 30 min followed by a careful washing. 100 µL substrate solution was added then and the plate was incubated again at RT for 40 min. The reaction was stopped by adding 100 µL stop solution. The insulin concentration was measured by SYNERGY microplate reader at a wavelength of 450/630 nm.

2.2.22 Multiplex

Commercially available Bio-Plex Pro Mouse Diabetes Adiponectin Assay and Bio-Plex Pro Mouse Diabetes 8-Plex Assay were used to determine protein levels for leptin, adiponectin, resistin, PAI-1, ghrelin, GIP, GLP-1, glucagon and insulin. Analysis was performed using a Bioplex 200 suspension array system (Biorad, Hercules, CA, USA) according to the manufacturer's instructions. Protein concentrations were calculated from the appropriate optimized standard curves using Bio-Plex Manager software version 6.0 (Biorad, Hercules, CA).

Multiplex analysis was performed by Dr. Stefan Lehr from German Diabetes Center (DDZ).

2.2.23 RNA isolation from peripheral white adipose tissue

RNA of peripheral white adipose tissue was isolated using Qiagen RNeasy® Lipid Tissue Mini Kit. Not more than 100 mg white adipose tissue was homogenized in 1 mL TRIzol with the help of Qiagen TissueRuptor and the homogenate was incubated at RT for 5 min. To separate the homogenate, 200 µL chloroform was added and the sample was shaken vigorously for 15 s followed by centrifugation at full speed and 4 °C for 15 min. The aqueous phase containing RNA was transferred into a new tube and the same amount of 70 % ethanol was added to provide ideal binding conditions allowing the RNA to precipitate among the other components. Up to 700 µL sample including any precipitate that may have formed was transferred to a RNeasy spin column placed in a 2 mL collection tube, RNA was bound to the silica membrane and the column was centrifuged at 8000x g and 4 °C for 30 s. After

centrifugation, the flow-through was discarded and the step was repeated by using the same collection tube if there was any remained sample. 700 µl RW1 buffer, which was used as a stringent washing buffer to remove biomolecules like carbohydrates, proteins and fatty acids bound on the silica membrane, was added and the column was centrifuged at 8000x g and 4 °C for 30 s. After this washing step, the column was washed twice with 500 µL ethanol-containing RPE buffer, which was a mild washing buffer and removed traces of salts. The two washing steps with RPE buffer were followed by centrifugation at 8000x g and 4 °C for respectively 30 s and 2 min. Afterwards, the RNeasy spin column was placed in a new 2 mL collection tube and centrifuged at full speed and 4 °C for 1 min. Finally, RNA was eluted by incubating the RNeasy spin column, placed in a 1.5 mL RNase-free tube, with 30 µL RNase-free water and then centrifuged at 8000x g and 4 °C for 1 min. 1 µL RNA was used for concentration measurement by NANODROP ONE Spectrophotometer. Isolated RNA was stored at -80 °C before use.

2.2.24 RNA isolation from heart tissue

Qiagen RNeasy® Fibrous Tissue Mini Kit was used to isolate RNA from the heart. Not more than 30 mg heart tissue was homogenized in 300 µL RLT buffer by Qiagen TissueRuptor, 590 µL RNase-free water and 10 µL Proteinase K were sequentially added to the homogenate which was afterwards incubated at 55 °C for 10 min and centrifuged at 10000x g for 3 min. The supernatant after centrifugation was transferred into a new tube and the half amount of 100 % ethanol was added. Up to 700 µL sample including any precipitate that may have formed was transferred to a RNeasy spin column placed in a 2 mL collection tube and centrifuged at 8000x g and 4 °C for 30 s. After centrifugation, the flow-through was discarded and the step was repeated by using the same collection tube if there was any remained sample. The membrane was washed twice with 350 µL RWI buffer and each was followed by a centrifugation at 8000x g for 30 s and twice with 500 µL RPE buffer followed by centrifugations at 8000x g respectively for 30 s and 2 min. After washing steps, the RNeasy spin column was placed in a new 2 mL collection tube and centrifuged at full speed and 4 °C for 1 min. Finally, RNA was eluted by incubating the RNeasy spin column placed in a 1.5 mL RNase-free tube with 30 µL RNase-free water and then centrifuged at 8000x g and 4 °C for 1 min. 1 µL RNA was used for concentration measurement by NANODROP ONE Spectrophotometer. Isolated RNA was stored at -80 °C before use.

2.2.25 Reverse transcription

Reverse transcription was performed according to Qiagen QuantiTect® Reverse Transcription Quick-Start Protocol. First, RNA was diluted according to its concentration with right amount of Millipore water reaching a final volume of 12 µL containing 1000 ng RNA. Diluted RNA was mixed with 2 µL 7x gDNA Wipeout Buffer to remove contaminating genomic DNA and incubated in Eppendorf Mastercycler at 42 °C for 2 min. After incubation, 6 µL reverse transcription master mix was prepared for each reaction according to Table 7.

Component	Volume
Quantiscript Reverse Transcriptase	1 µL
Quantiscript RT Buffer, 5x	4 µL
RT Primer Mix	1 µL

Table 7: Components of reverse transcription master mix.

After adding master mix, the sample incubated again in Eppendorf Mastercycler running a program as below (Table 8):

Temperature	Time
42 °C	30 min
95 °C	5 min
4 °C	∞

Table 8: Temperature and time set up of the thermal cycler for reverse transcription.

Before storing the synthesized cDNA at -20 °C, it was first diluted with 100 µL Millipore water reaching a concentration of 1000 ng/120 µL.

2.2.26 Quantitative real time PCR

The amount of an expressed gene can be measured by the number of copies of an RNA transcript (cDNA) of that gene present in a sample. Relative change in gene expression was detected by quantitative real time PCR analysis. qPCR is based on monitoring the amplification of a targeted DNA molecule in real-time. qPCR was performed using Platinum® SYBR® Green qPCR SuperMix-UDG; which contains all components including DNA polymerase, SYBR® Green dye and dNTPs, together with specific primers for the target gene. The detection of PCR product was based on the binding of the fluorescent dye

SYBR Green absorbing light of a certain wavelength into the PCR product. 2,5 µL cDNA with a concentration of 1000 ng/120 µL and 7,5 µL master mix (Table 9), which is composed of 2,5 µL primer pairs and 5 µL SYBR Green was pipetted into a MicroAmp® Fast 96-Well Reaction Plate, which was tightly closed by MicroAmp™ Optical Adhesive Film.

Component	Volume
Forward primer	1,25 µL
Reverse primer	1,25 µL
Platimum® SYBR® Green qPCR SuperMix-UDG	5 µL

Table 9: Components of SYBR Green master mix for Qrt-PCR analysis.

The samples were analyzed by StepOne Plus Real-Time PCR Detection System. The amplification program was set as an initial step at 95 °C for 10 min followed by 40 cycles alternately 95 °C for 15 s and 60 °C for 60 s together. Calculation of relative gene expressions was performed by means of ΔCt method using *Nudc* as reference gene. The calculation of relative gene expressions for each animal is as follows:

$$Value = 2 \text{ ^ } (-\Delta Ct)$$

The mean of all the values from control group was calculated via the calculation above, and this mean value was used as a reference. By dividing each value obtained from the calculation by this mean value, the final values of all the samples were obtained.

2.2.27 Statistical analysis

All the results were reported as mean ± standard error of the mean (SEM). Statistical analysis was performed by GraphPadPrism 9. For comparison of two groups unpaired, two-tailed *t*-test or Mann-Whitney test was used. For comparison of groups with two variables 2-way-ANOVA was used followed by Sidak's multiple comparisons test. Outliers were identified using ROUT test. A *p*-value smaller than 0,05 (*$p < 0,05$) was treated as significant, a *p*-value smaller than 0,01 (**$p < 0,01$) was treated as very significant, a *p*-value smaller than 0,001 (***$p < 0,001$) was treated as highly significant. Trends are shown by *p*-values as numbers as indicated.

3 Results

3.1 Myocardial ischemia worsens cardiac function

To analyze changes in subcutaneous and visceral white adipose tissue after MI, in this study, 3 groups of 12 weeks old C57Bl/6J male mice were subjected to 60 min cardiac ischemia or sham operation and underwent respectively 24 h, 7 d or 28 d of reperfusion. To trace the change of cardiac function during reperfusion, echocardiography was done for 28 d group at baseline, day 7 and day 28 (data acquired by Dr. Katharina Bottermann). At day 7 and day 28, the mice which were subjected to cardiac ischemia operation showed a significantly reduced systolic pump function (Day 7: EF: 37 ± 3.2 %, FAC: 28.9 ± 1.6 %; Day 28: EF: 32.3 ± 3.1 %, FAC: 22.9 ± 4.2 %), and increased end diastolic and systolic volumes (Day 7: EDV: 122.3 ± 6 µl, ESV: 77.5 ± 6.7 µl; Day 28: EDV: 156.2 ± 10 µl, ESV: 106.8 ± 11.1 µl) compared to sham operated mice (Fig. 13A). The ratios of gWAT and iWAT to BW stayed unchanged between sham operated and ischemic operated mice at all the three timepoints (Fig. 13B).

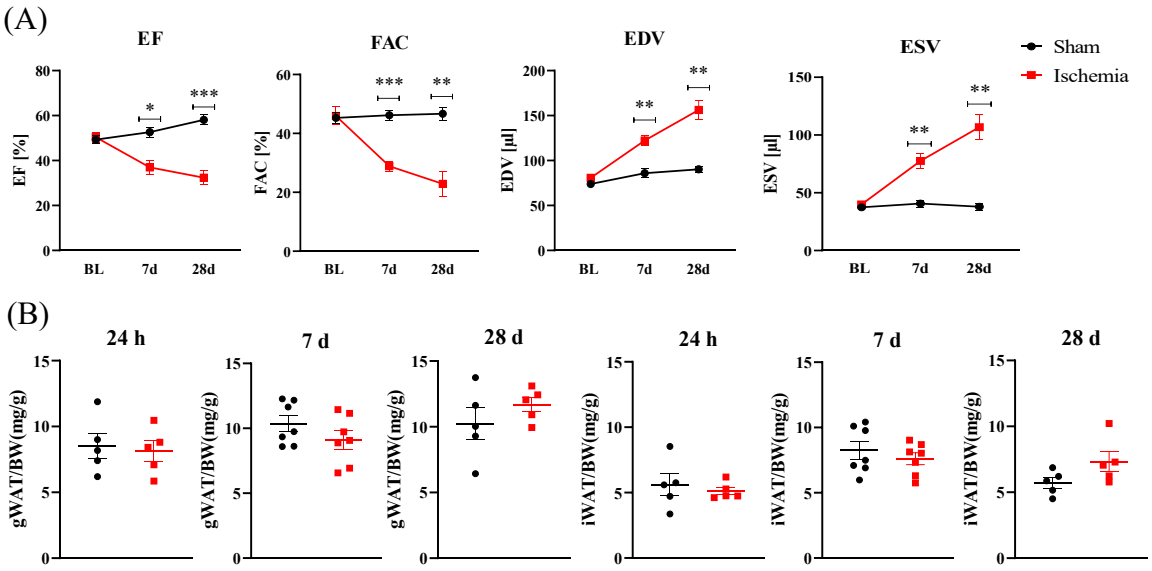

Fig. 13: Echocardiography and ratio of adipose tissue to bodyweight of sham and ischemic operated animals during reperfusion. (A) Ejection fraction, fractional area change, end diastolic volume and end systolic volume at baseline and after 7 d and 28 d of reperfusion (n = 5, data acquired by Dr. Katharina Bottermann). (B) The ratio of gonadal and inguinal white adipose tissue weight to bodyweight (n = 5-7). Mean ± SEM, 2-Way-Anova with Sidak's multiple comparisons test (A) or unpaired , two-tailed t-test (B). (Wang et al. 2022)

3.2 Myocardial ischemia chronically reduced adipocyte size in iWAT

The adipose tissue morphology and adipocyte size were analyzed by H&E staining in 5 μm paraffin sections of gWAT and iWAT. After cardiac ischemia, no major change was found during reperfusion in gWAT, the morphology and adipocyte size were both comparable with sham operated mice. (Fig. 14A,B,C). Elevated NEFA levels after 30 min of reperfusion indicated a stimulation of lipolysis due to cardiac ischemia, therefore, the relative gene expression of the main lipolytic enzyme ATGL (*Pnpla2*) was analyzed, *Pnpla2* expression was revealed to be similar between controls and infarcted mice at all three time points, which was consistent with unchanged adipocyte size during the whole reperfusion phase (Fig. 14D). However, in the subcutaneous depot, namely iWAT, the adipocyte size of infarcted mice after 24 h of reperfusion started to show a significantly increased number of smaller adipocytes (300–350 μm^2) and decreased number of bigger adipocytes over 1500 μm^2. This shift towards smaller adipocyte size was even stronger after 7 d and was the most pronounced after 28 d of reperfusion (Fig. 15A,B). The mean adipocyte size of iWAT was trended to exhibit reduced adipocyte size in infarcted animals after both 24 h and 28 d of reperfusion ($p = 0{,}0744$ and $p = 0{,}0764$) (Fig. 15C). To further investigate the possible underlying reason for decreased adipocyte size in iWAT after cardiac ischemia, gene expression analysis of *Pnpla2* was performed and after 7 d, *Pnpla2* expression started to show a trend in infarcted group towards a higher expression, and *Pnpla2* expression after 28 d of reperfusion was significantly upregulated in iWAT of infarcted animals (Fig. 15D). Taken together, lipolysis is not only induced shortly after cardiac ischemia as seen by increased NEFA levels but also chronically, at least in iWAT, as seen by smaller adipocytes and increased gene expression of ATGL.

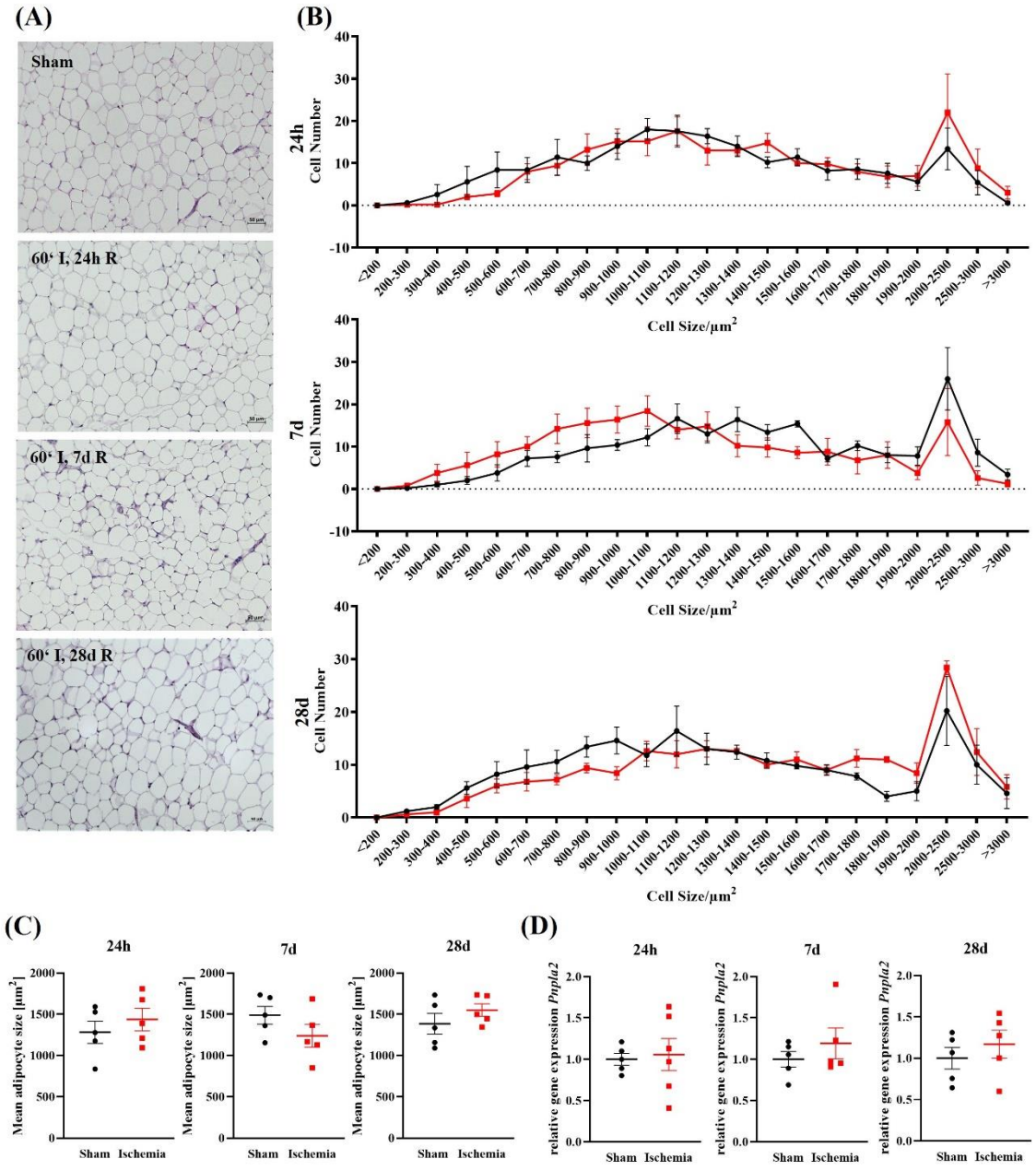

Fig. 14: Cardiac ischemia showed no effect on adipocyte size in gWAT. (A) H&E staining of gWAT in sham and cardiac ischemic operated mice after 24 h, 7 d and 28 d of reperfusion. (B) Adipocyte size distribution in gWAT after 24 h, 7 d and 28 d of reperfusion. (C) Mean adipocyte size of gWAT after 24 h, 7 d and 28 d of reperfusion (D) Relative gene expression of *Pnpla2* in gWAT after 24 h, 7 d and 28 d of reperfusion. n = 5, mean ± SEM, unpaired, two-tailed t-test or Mann-Whitney test. gWAT: Gonadal white adipose tissue. H&E: Hematoxylin and eosin. (Wang et al. 2022)

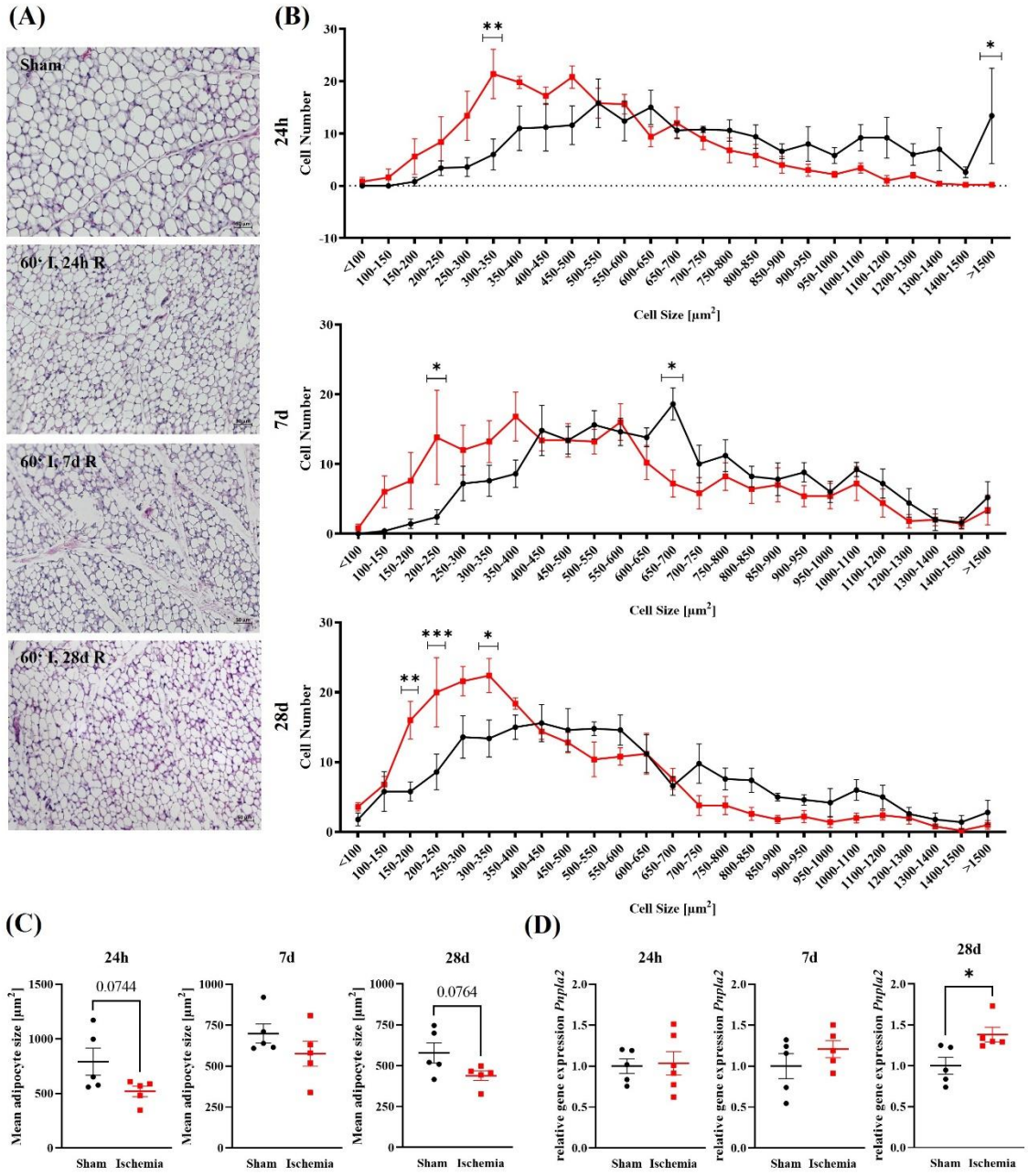

Fig. 15: Cardiac ischemia predominantly reduced adipocyte size in iWAT. (A) H&E staining of iWAT in sham and cardiac ischemic operated mice after 24 h, 7 d and 28 d of reperfusion. (B) Adipocyte size distribution in iWAT after 24 h, 7 d and 28 d of reperfusion. (C) Mean adipocyte size of iWAT after 24 h, 7 d and 28 d of reperfusion (D) Relative gene expression of *Pnpla2* in iWAT after 24 h, 7 d and 28 d of reperfusion. n = 5, mean ± SEM, unpaired, two-tailed t-test or Mann-Whitney test. H&E: Hematoxylin and eosin. iWAT: Inguinal white adipose tissue. (Wang et al. 2022)

3.3 Myocardial ischemia induced browning of iWAT

Smaller adipocyte size has been revealed by H&E staining in the inguinal depot of infarcted animals, moreover, additional morphological changes were revealed by the staining. A large number of adipocytes in iWAT of ischemic operated animals were shown to be multilocular, which is a typical feature of "brown-like" adipocytes (Fig. 16A). To validate the possible browning phenomenon shown by H&E staining, the UCP1-expression which serves mostly as browning marker was analyzed. Since similar number of animals from 24 h, 7 d and 28 d groups showed the browning phenomenon, the 24 h time point group was chosen to analyze the UCP1 expression level. Anti-UCP1 immunofluorescent staining demonstrated the positive UCP1 expression only in iWAT of animals after 1 h ischemia and 24 h of reperfusion (Fig. 16B). To quantitively evaluate UCP1 protein content, the protein levels of UCP1 in sham and ischemic operated mice after 24 h of reperfusion were analyzed by western blot analysis. By using the total protein as reference for analysis, a significantly increased UCP1 protein level was found in infarcted animals (p = 0,0195, Fig. 16C).

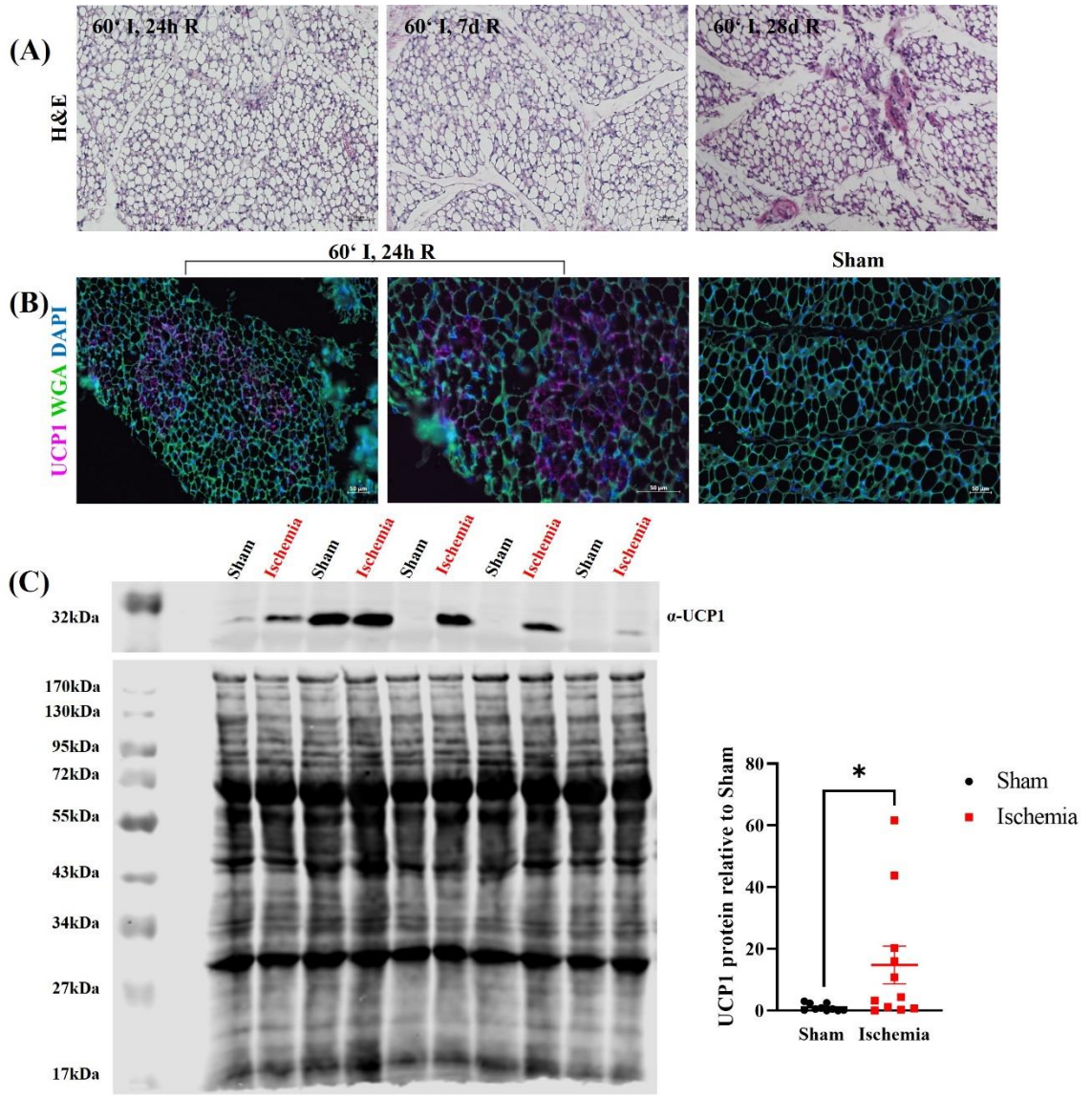

Fig. 16: Cardiac ischemia induced browning in iWAT. (A) H&E staining of iWAT in ischemic operated mice after 24 h, 7 d and 28 d of reperfusion. (B) Anti-UCP1 fluorescence staining of iWAT in sham operated mice and ischemic operated mice after 24 h of reperfusion. (C) Western blot analysis of UCP1 expression in iWAT of sham and ischemic operated mice after 24 h of reperfusion. n = 13, mean ± SEM. ROUT test (Q = 1) identified 3 statistical outliers in the sham group and 2 in the ischemic group which were excluded in western blot analysis and Mann-Whitney test was used for (C). DAPI: 4’,6-diamino-2-phenylindole. H&E: Hematoxylin and eosin. iWAT: Inguinal white adipose tissue. UCP1: Uncoupling protein 1. (Wang et al. 2022)

3.4 Myocardial ischemia reduced lipogenesis in iWAT

Our data show that myocardial ischemia has been suggested to stimulate lipolysis in the peripheral white adipose tissue. Lipolysis and lipogenesis are two important metabolic processes which dynamically maintain the stability of white adipose tissue, therefore, whether and how the lipogenesis was altered due to the increased lipolysis was analyzed in different WAT depots. The relative gene expression of several genes regarding lipogenesis was investigated in controls and infarcted mice, by measuring gene expression, no profound change was found in gWAT, only fatty acid synthase (*Fasn*) after 7 d of reperfusion showed a trend to be upregulated in ischemic animals (Fig. 17). In iWAT however, the lipogenesis seemed to be reduced after cardiac ischemia. Even if the gene expression of the transcription factors PPAR-γ (*Pparγ*) and SREBP-1C (*Srebp1c*) themselves were not affected, the downstream genes involved in lipogenesis were either downregulated or trended to be downregulated. The gene expression of lipoprotein lipase (*Lpl*) was downregulated after 24 h of reperfusion and trended to be downregulated after 7d and 28 d. Fatty acid synthase (*Fasn*) and diacylglycerol acyltransferase 2 (*Dgat2*) both trended to be downregulated only after 24 h of reperfusion in infarcted animals (Fig. 18). This reduced expression of a lipogenic gene signature seemed to be an acute and transient reaction to myocardial ischemia, only *Lpl* trended to be downregulated also at later timepoints, which was in line with persistent smaller adipocyte size in subcutaneous WAT.

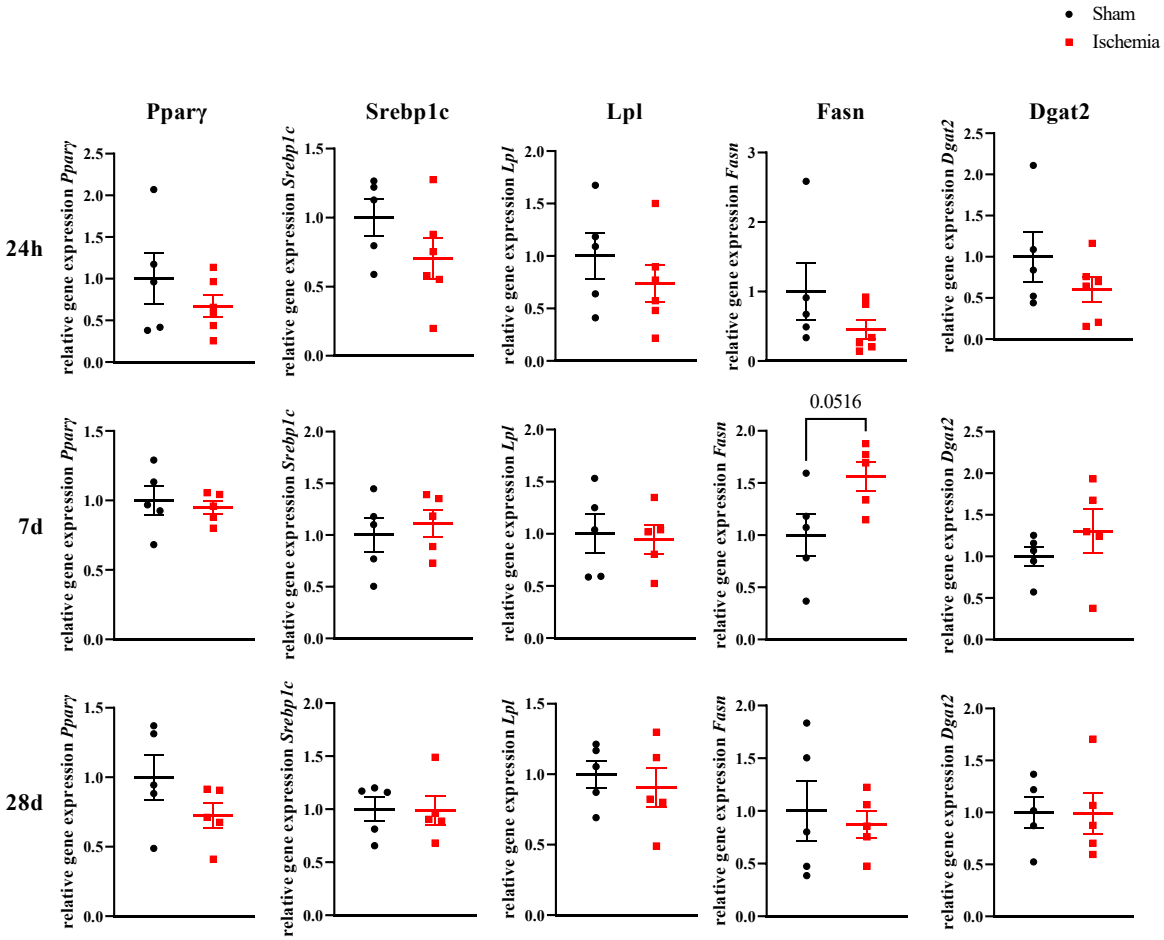

Fig. 17: Cardiac ischemia did not affect lipogenesis in gWAT. Relative gene expression of *Pparγ*, *Lpl*, *Fasn*, *Dgat2* and *Srebp1c* in gWAT after cardiac ischemia and 24 h, 7 d and 28 d of reperfusion. n = 5 - 6, mean ± SEM, unpaired, two-tailed t-test and Mann-Whitney test. Dgat2: Diacylglycerol O-acyltransferase 2. Fasn: Fatty acid synthase. gWAT: Gonadal white adipose tissue. Lpl: Lipoprotein lipase. Pparγ: Peroxisome proliferator-activated receptor gamma. Srebp1c: Sterol regulatory element-binding protein-1c. (Wang et al. 2022)

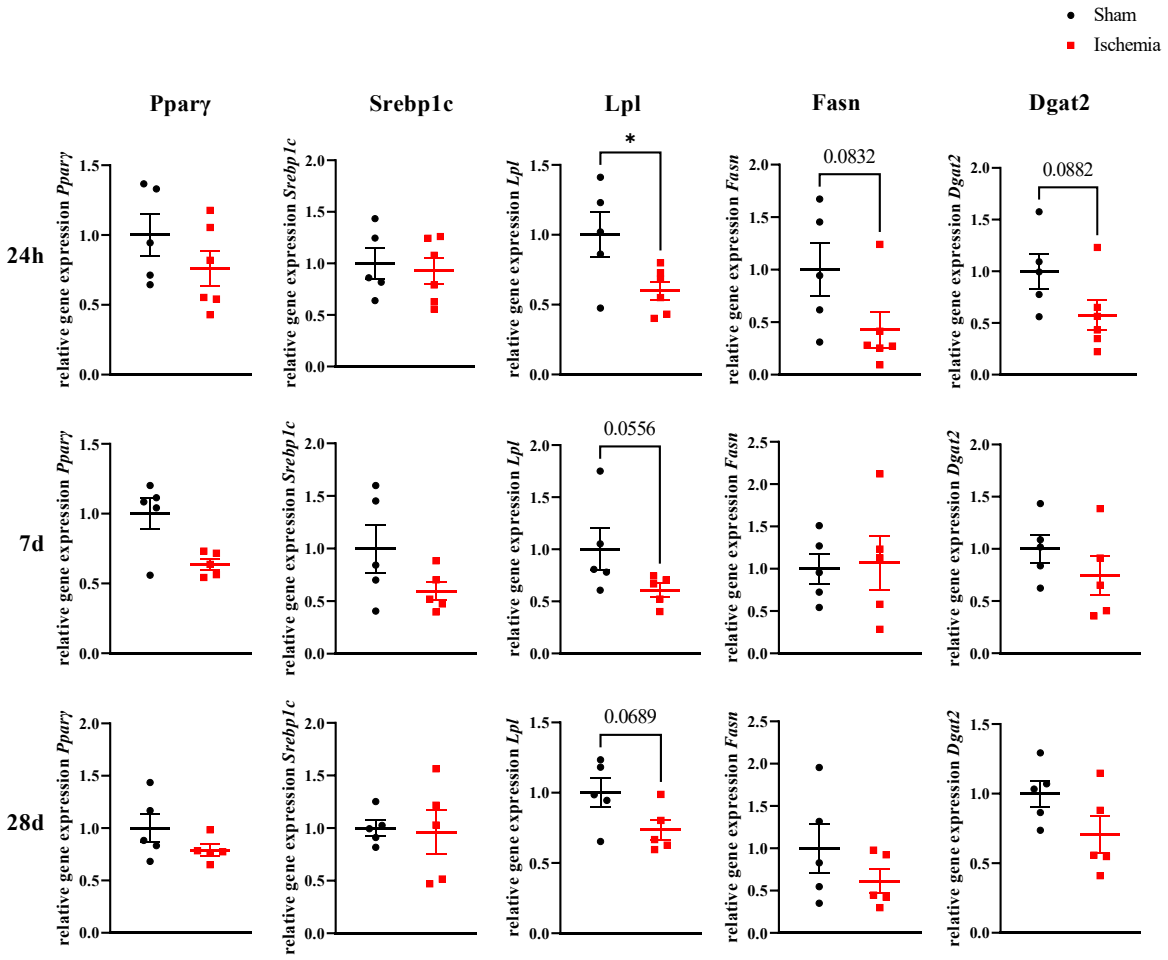

Fig. 18: Cardiac ischemia reduced lipogenesis in iWAT. Relative gene expression of *Pparγ*, *Lpl*, *Fasn*, *Dgat2* and *Srebp1c* in iWAT after cardiac ischemia and 24 h, 7 d and 28 d of reperfusion. n = 5 - 6, mean ± SEM, unpaired, two-tailed t-test and Mann-Whitney test. Dgat2: Diacylglycerol O-acyltransferase 2. Fasn: Fatty acid synthase. iWAT: Inguinal white adipose tissue. Lpl: Lipoprotein lipase. Pparγ: Peroxisome proliferator-activated receptor gamma. Srebp1c: Sterol regulatory element-binding protein-1c. (Wang et al. 2022)

3.5 Myocardial Ischemia increased MAC-2$^+$ macrophage infiltration in iWAT

Besides the browning phenomenon revealed by H&E staining, the staining also showed an increased number of nuclei from non-adipocyte cells after 7 d of reperfusion. Assuming that the tissue was infiltrated with immune cells, anti-Mac2 immunofluorescent staining was performed in both gWAT and iWAT. In line with the assumption, significantly increased number of MAC-2$^+$ macrophages were revealed by the quantification in iWAT of ischemic animals after 7 d of reperfusion. Interestingly, even if the macrophage number stayed unchanged in gWAT, the formation of crown-like structures (CLS), namely the structure composed of macrophages surrounding dead or dying adipocytes, was significantly increased. To analyze if the infiltration lasted longer, gWAT and iWAT of animals after 28 d of reperfusion were also stained by anti-Mac2 and analyzed. The quantification revealed unchanged macrophage number in both depots after 28 d, which means the enhanced macrophage infiltration due to cardiac ischemia is not a long-lasting effect (Fig. 19).

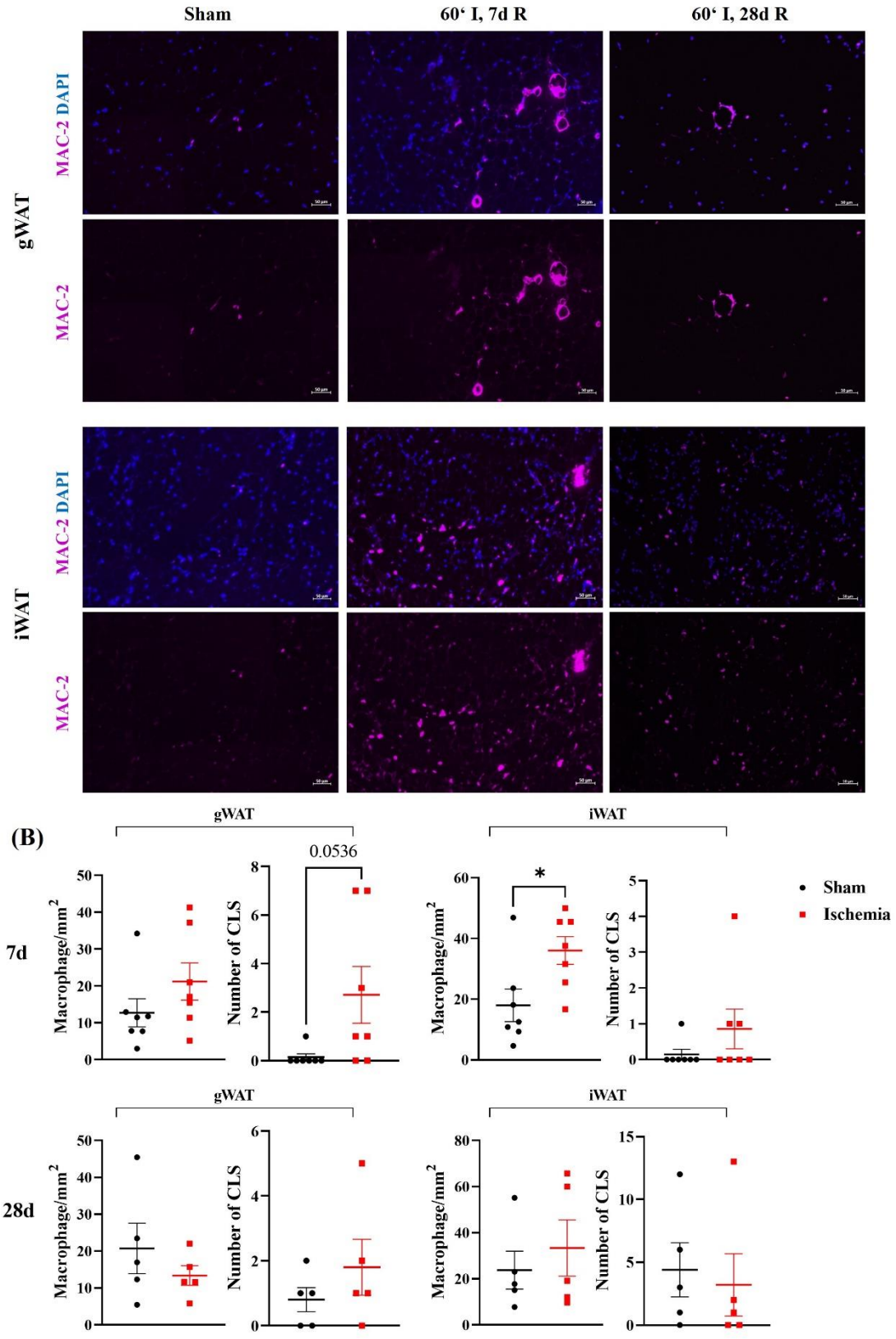

Fig. 19: Macrophage infiltration was increased in iWAT after cardiac ischemia and 7 d of reperfusion. (A) Anti-Mac2 fluorescent staining of gWAT and iWAT after 7 d and 28 d of reperfusion. (B) The number of macrophages and crown-like structures in gWAT and iWAT after 7 d and 28 d of reperfusion. n = 5 - 7, mean ± SEM, unpaired, two-tailed t-test and Mann-Whitney test. DAPI: 4’,6-diamino-2-phenylindole. gWAT: Gonadal white adipose tissue. iWAT: Inguinal white adipose tissue. (Wang et al. 2022)

3.6 Myocardial ischemia reduced adipokine expression in iWAT

Adipose tissue is an important endocrine organ which secretes large number of cytokines and adipokines, some of them are known to be involved in post-infarct remodeling. Therefore, after cardiac ischemia the gene expression of several adipokines was analyzed and the expression pattern of three adipokines which are highly expressed were found to be altered due to myocardial ischemia. Consistent with the changes found after cardiac ischemia in iWAT, the change of adipokine expression was also mainly found in iWAT. gWAT was not much affected by infarction, resistin was the only gene which was downregulated in infarcted animals after 24 h of reperfusion (Fig. 20). However, the gene expression pattern of adipokines was much more affected in iWAT. Adiponectin was downregulated after 24 h of reperfusion and trended to be downregulated after 7 d; leptin was downregulated after 7 d and resistin was downregulated after 24 h. None of the genes was differently expressed after 28 d of reperfusion in both depots, which revealed that the disturbance of adipokine expression due to myocardial ischemia was transient (Fig. 21).

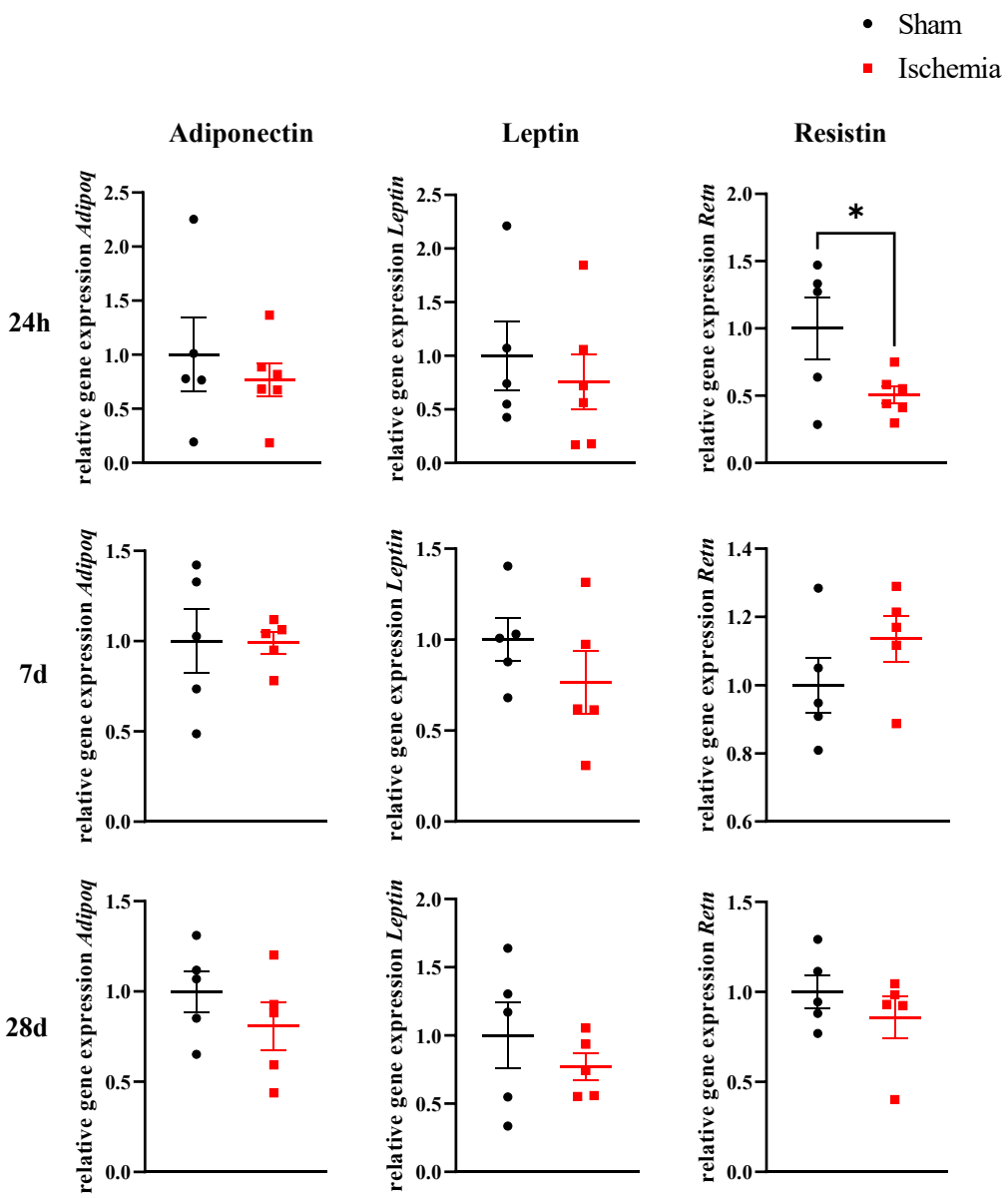

Fig. 20: Cardiac ischemia did not change adipokine gene expression in gWAT. Relative gene expression of *Adipoq*, *Leptin*, and *Retn* in gWAT after cardiac ischemia and 24 h, 7 d and 28 d of reperfusion. n = 5 - 6, mean ± SEM, unpaired, two-tailed t-test and Mann-Whitney test. gWAT: Gonadal white adipose tissue. (Wang et al. 2022)

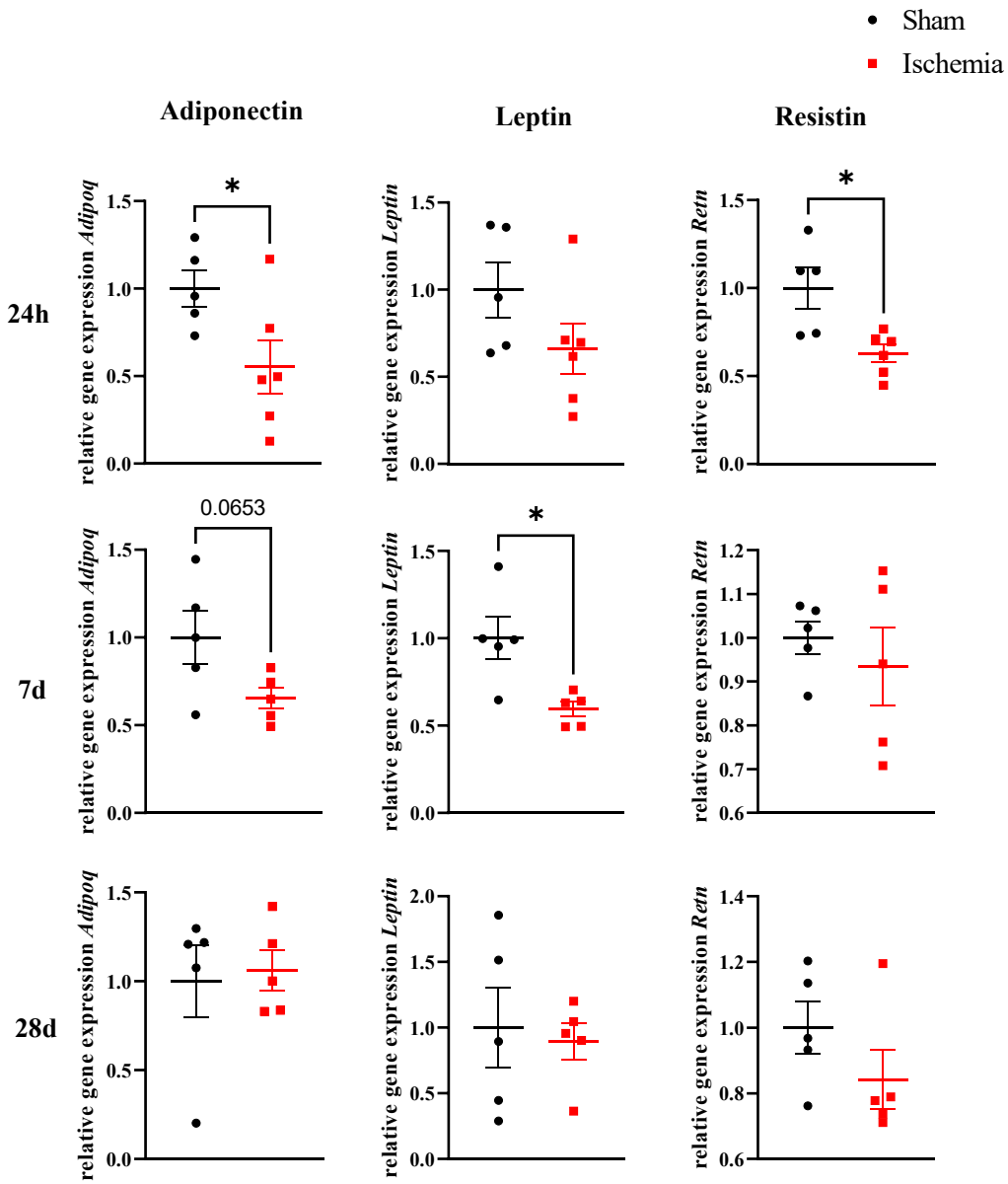

Fig. 21: Cardiac ischemia reduced adipokine gene expression in iWAT. Relative gene expression of *Adipoq*, *Leptin*, and Retn in iWAT after cardiac ischemia and 24 h, 7 d and 28 d of reperfusion. n = 5 - 6, mean ± SEM, unpaired, two-tailed t-test and Mann-Whitney test. iWAT: Inguinal white adipose tissue. (Wang et al. 2022)

3.7 Inducible adipocyte specific inhibitory DREADD enables spatio-temporally specific inhibition of lipolysis

3.7.1 Successful expression of inducible adipocyte specific inhibitory DREADD in white adipose tissue

To inhibit lipolysis of peripheral white adipose tissue in a spatio-temporal specific manner, the mice being able to express adipocyte specific inhibitory DREADD were used for analysis. The intraperitoneal injection of 4-hydroxytamoxifen enables the Cre-Lox recombination and thereby hM4Di expression. To visualize successful receptor expression, the receptors are tagged by hemagglutinin epitope tag (HA), which is followed by a P2A sequence and another mCitrine reporter, which is a yellow-green variant of Citrine YFP. P2A is a self-cleaving peptide which can induce ribosomal skipping during translation of a protein. After translation, the fused protein will be split into 2 parts, mCitrine will enter the cytoplasm, which allows to visualize transcriptional activity and thereby construct expression, whereas HA-fused DREADDs are located on the cell membrane allowing to determine, the detailed spatial localization of receptors in the cell (Fig. 22).

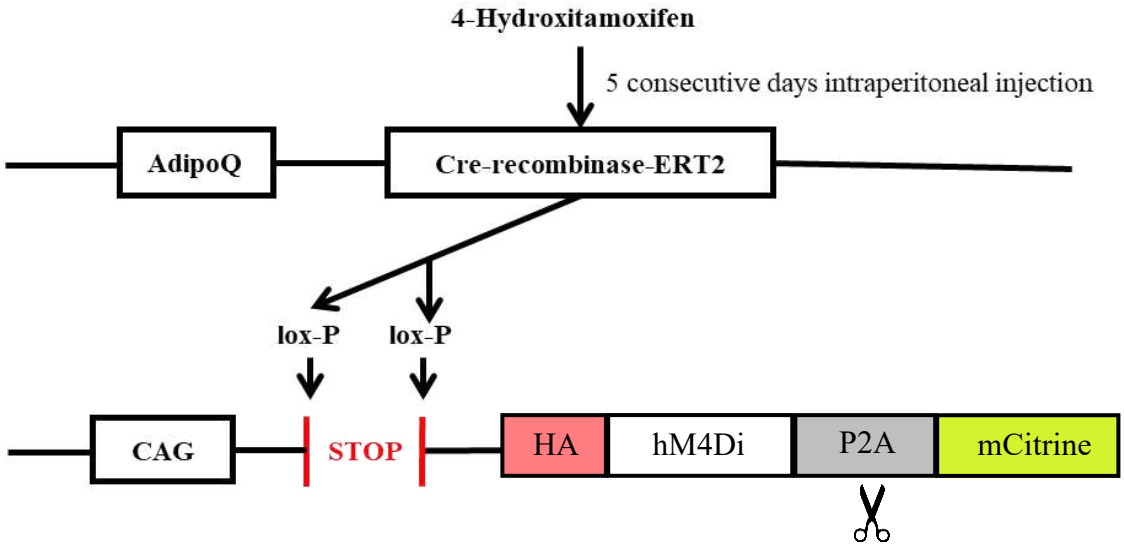

Fig. 22: Inducible adipocyte specific inhibitory DREADD expression system. The hM4Di receptors, which are under control of the strong ubiquitous adipocyte specific promotor CAG, are able to express after intraperitoneal injection of 4-hydroxytamoxifen that enables the Cre-Lox recombination. The receptors are tagged by HA and mCitrine reporters, which allow for detection of expression. P2A is a self-cleaving peptide, after translation, mCitrine enters the cytoplasm, HA-fused receptors are located on the cell membrane. DREADD: Designer receptor exclusively activated by designer drugs. HA: Hemagglutinin epitope. P2A: Self-cleaving peptides.

To analyze if the receptors were successfully expressed in white adipocytes, mCitrine expression was analyzed immunochemically in paraffin sections of gWAT of Cre+/hM4Di- and Cre+/hM4Di+ animals by anti-GFP DAB staining. Different from hM4Di- controls, linking HRP to primary antibody oxidized DAB and formed dark-brown products in the adipocytes of hM4Di+ mice revealing a high expression of mCitrine and thus also hM4Di receptors (Fig. 23A). For a more specific analysis of receptor expression, the relative gene expression of *hM4Di* was investigated in gWAT and iWAT of 4-hydroxytamoxifen induced animals. Another control group, namely Cre-/hM4Di+ group was added into the experiments. As expected, no *hM4Di* gene expression was seen in Cre+/hM4Di- mice, whereas very surprisingly a low expression was found in Cre-/hM4Di+ mice. Comparing to the receptor gene expression in Cre+/hM4Di+ mice, which was highly significant in both gWAT and iWAT, the relative gene expression of *hM4Di* in Cre-/hM4Di+ mice count 1,92 % in gWAT *and 1,53 % in iWAT (Fig. 23B).*

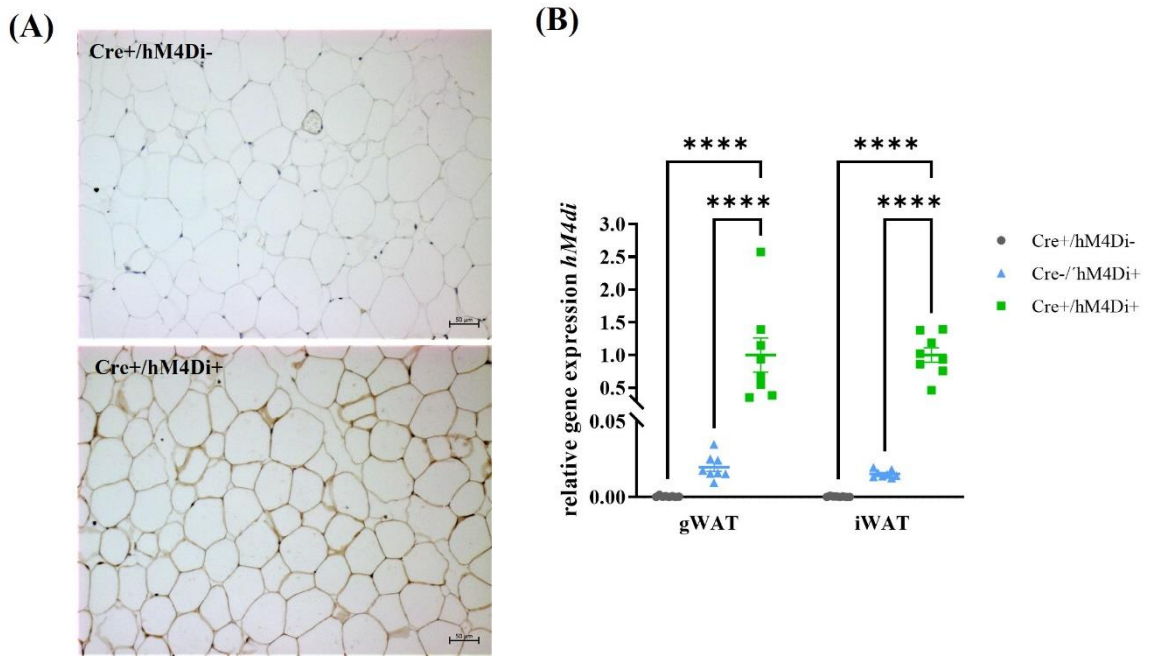

Fig. 23: Successful expression of hM4Di in WAT of induced ischemic mice. (A) Anti-GFP DAB staining of gWAT. (B) Relative gene expression of *hM4di* in gWAT and iWAT. n = 8, mean ± SEM, 2-Way-ANOVA with Sidak's multiple comparisons test. DAB: 3,3'-Diaminobenzidine. GFP: Green fluorescent protein. gWAT: Gonadal white adipose tissue. iWAT: Inguinal white adipose tissue.

3.7.2 Visible expression of inducible adipocyte specific inhibitory DREADD in other organs of non-induced animals

The receptors were designed to be inducible expressed only in an adipocyte specific manner, HA-hM4Di and mCitrine expression should be strictly limited to adipose tissue and the expression should not be detectable prior to induction of Cre-recombinase. To exclude any leakiness of the system, the receptor expression was also investigated in heart, liver and skeletal muscle. Different from this expectation, GFP expression was visible in white and brown adipose tissue prior to Cre-recombinase induction in Cre+/hM4Di+ mice and Cre-/hM4Di+ mice in western blot analysis, with iWAT having the strongest GFP signal. In addition to the expression in adipose tissue, weak but visible GFP signals were able to be seen in the heart, liver and skeletal muscle prior to Cre-recombinase induction in all hM4Di+ mice (Fig. 24). The protein expression of GFP prior to Cre-recombinase induction and in other organs revealed the leakiness of the STOP codon.

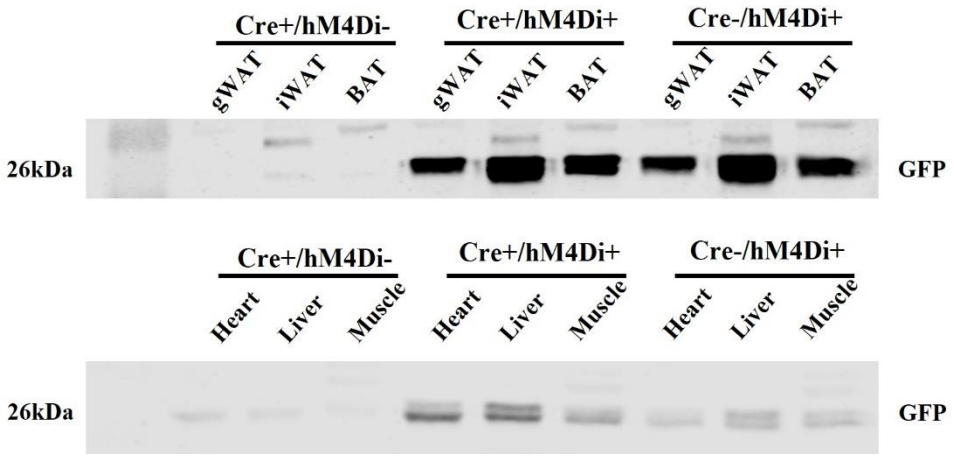

Fig. 24: Visible GFP expression in adipose tissue and other organs prior to Cre-recombinase induction. Western blot analysis of GFP expression in gWAT, iWAT, BAT, heart, liver and skeletal muscle. BAT: Brown adipose tissue. GFP: Green fluorescent protein. gWAT: Gonadal white adipose tissue. iWAT: Inguinal white adipose tissue.

To quantitatively compare the expression level of hM4Di prior to and after the induction of Cre-recombinase, the protein expression level of GFP was analyzed in gWAT and iWAT of induced and non-induced animals. Visible GFP expression was found in all the hM4Di+ animals, however, a much lower GFP expression was revealed in both gWAT and iWAT of non-induced mice. The GFP expression level of non-induced animals showed to be 20 % of induced mice in gWAT, and 26 % of induced mice in iWAT. In non-induced mice, comparing to Cre+/hM4Di+ group, the GFP expression was even lower in Cre-/hM4Di+ mice (Fig. 25).

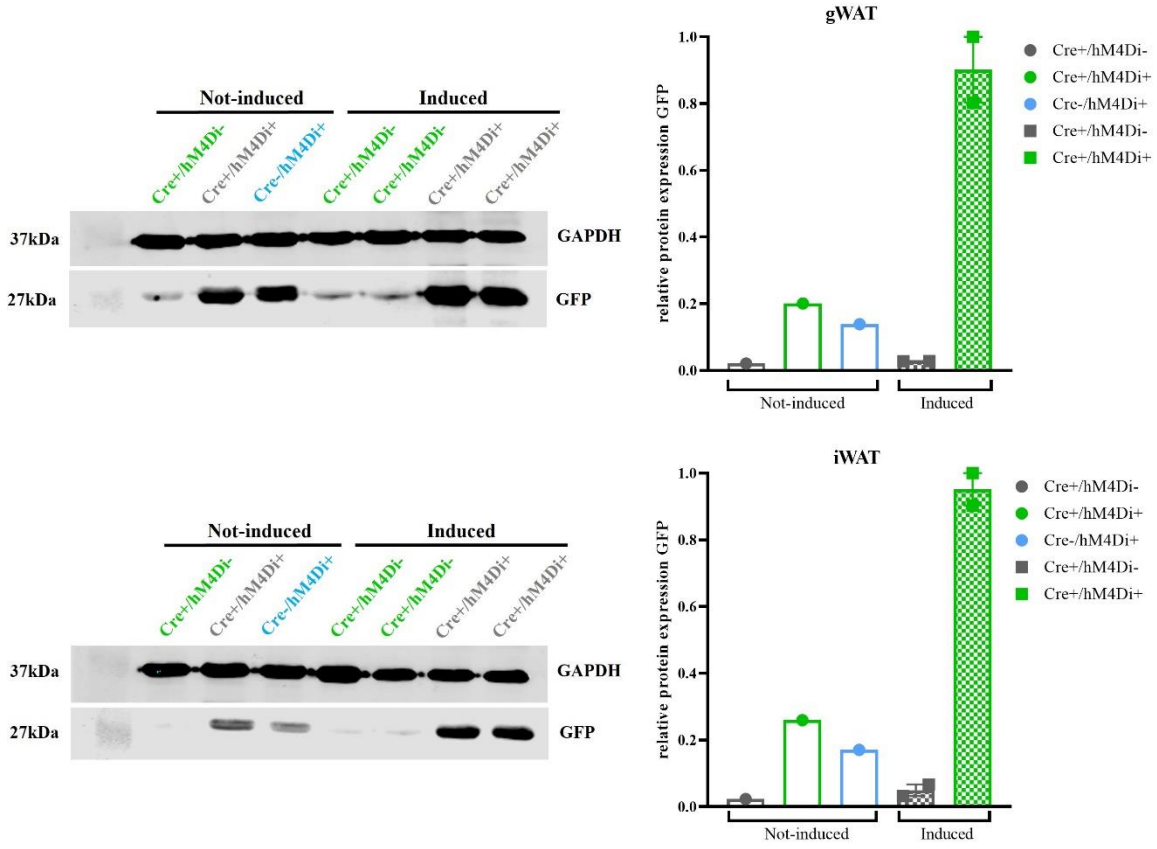

Fig. 25: Weak GFP expression in WAT prior to Cre-recombinase induction. (A) Western blot analysis of GFP in gWAT of animals prior to or after 4-hydroxytamoxifen induction. (B) Western blot analysis of GFP in iWAT of animals prior to or after 4-hydroxytamoxifen induction.

As GFP protein expression had been detected in other organs including the heart, the expression level of hM4Di in the heart was critical to find out. The protein expression level of GFP was first compared between white, brown adipose tissue and heart in western blot analysis. The analysis revealed visible GFP signals only in hM4Di+ mice after Cre-recombinase induction. GFP showed to most highly express in inguinal depot and highly expressed in gonadal depot. Comparing to the expression level of GFP in WAT, visible but much weaker GFP expression was found in BAT and heart, the protein expression level of GFP in the heart was only 18 % of that in iWAT. (Fig. 26A). Besides, the relative gene expression level of *hM4Di* was investigated in iWAT, BAT and heart. In line with western blot analysis, the quantification revealed a much lower receptor gene expression in the heart compared to that in iWAT, the relative gene expression of *hM4Di* in the heart was only 2,5 % of the expression in iWAT (Fig. 26B). Furthermore, echocardiography revealed no difference in ejection fraction, fractional area change, end diastolic volume, end systolic volume and heart rate between baseline and after giving DREADD agonist 21 (CP21) (Fig. 26C), which confirmed the low expression of hM4Di in the heart did not exhibit any functional effect.

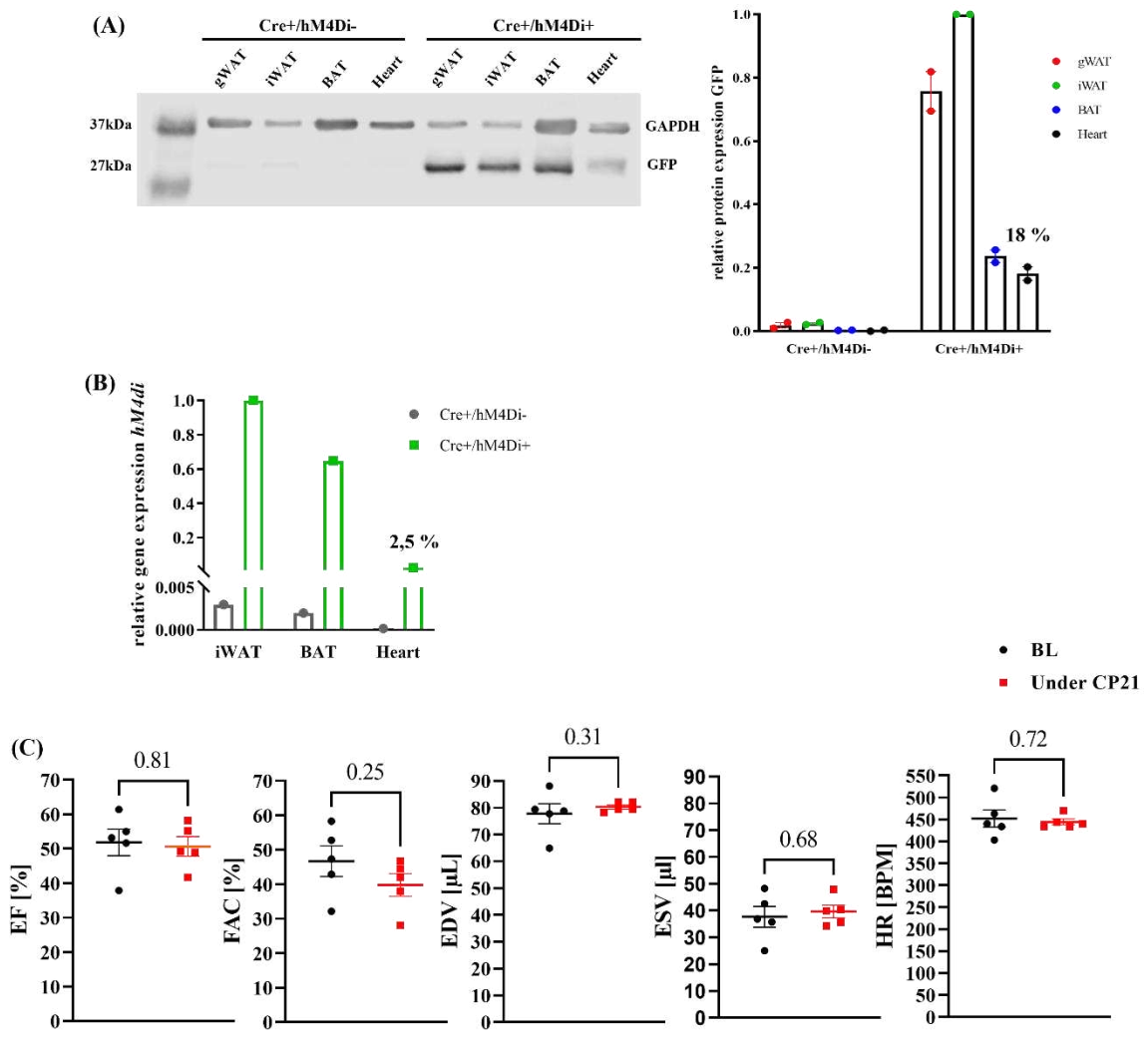

Fig. 26: Very low hM4Di expression in the heart. (A) Western blot analysis of GFP in gWAT, iWAT, BAT and heart. (B) Relative gene expression of *hM4Di* in iWAT, BAT and heart. (C) Comparable cardiac function between baseline and under CP21 in Cre+/hM4Di+ mice revealed by echocardiography analysis. BAT: Brown adipose tissue. BL: Baseline. GAPDH: Glyceraldehyde 3-phosphate dehydrogenase. GFP: Green fluorescent protein. gWAT: Gonadal white adipose tissue. iWAT: Inguinal white adipose tissue.

3.8 Agonist-dependent acute inhibition of lipolysis in DREADD mice after MI

As indicated, the receptors were successfully expressed in gWAT and iWAT, to activate the receptors, DREADD agonist 21 which is an agonist for muscarinic-based DREADDs was given to the animals at the beginning of ischemia and at the beginning of reperfusion. To investigate if lipolysis due to cardiac ischemia could be successfully inhibited, blood was taken from the tail of control mice and hM4Di expressing mice before ischemia (baseline) and after 30 min of reperfusion. The blood after 24 h of reperfusion was taken from the heart during harvest. NEFA assay was used to analyze circulating FAs level and revealed an increase in plasma NEFA levels in Cre+/hM4Di- and Cre-/hM4Di+ control mice after 30 min of reperfusion due to ischemia while this was significantly suppressed in Cre+/hM4Di+ mice. Cre-/hM4Di+ mice showed a slightly lower NEFA level compared to Cre+/hM4Di- mice, however this difference was not significant. The circulating NEFA levels went back to baseline in all the animals after 24 h of reperfusion, which indicated an only transient increase in NEFA after cardiac ischemia (Cre+/hM4Di-: BL: 0,195 ± 0,019 mmol/L, 30' R: 0,589 ± 0,069 mmol/L; Cre-/hM4Di+: BL: 0,161 ± 0,017 mmol/L, 30' R: 0,505 ± 0,058 mmol/L; Cre+/hM4Di+: BL: 0,195 ± 0,021 mmol/L, 30' R: 0,336 ± 0,033 mmol/L). (Fig. 27).

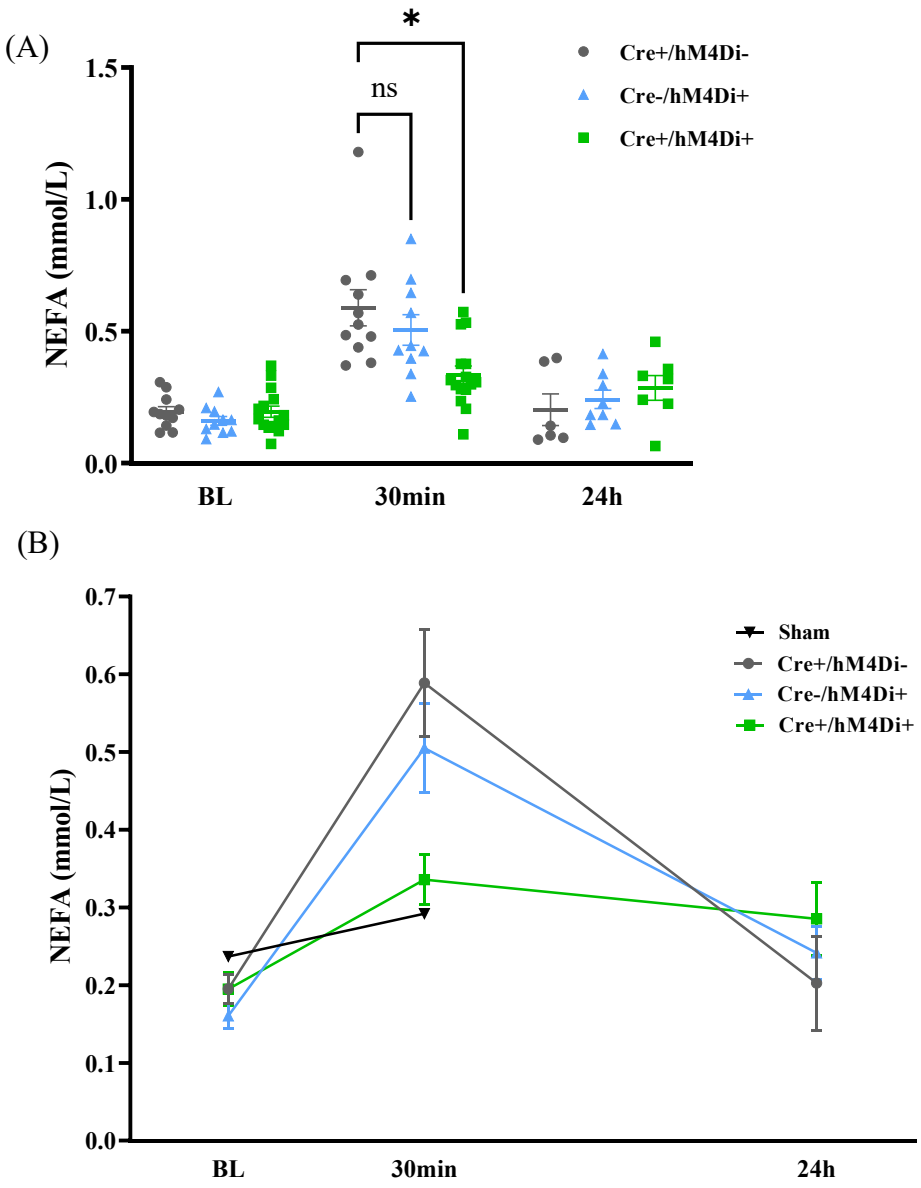

Fig. 27: The serum NEFA level was acutely and significantly decreased after MI in induced Cre+/hM4Di+ mice. (A and B) Tail blood was collected at baseline and after 30 min of reperfusion in Cre+/hM4Di-, Cre-/hM4Di+ and Cre+/hM4Di+ ischemic operated mice. The ischemia led to upregulated serum NEFA levels after 30 min of reperfusion, whereas Cre+/hM4Di+ mice showed significantly downregulated NEFA level compared to Cre+/hM4Di- and Cre-/hM4Di+ mice. Blood from the heart was collected during harvest after 24 h of reperfusion, NEFA levels of all groups went back to baseline. n = 6 - 15, mean ± SEM, 2-Way-ANOVA with Sidak's multiple comparisons test. BL: Baseline. MI: Myocardial infarction. NEFA: Non-esterified fatty acids.

3.9 Improved cardiac systolic function in DREADD mice after MI and 7 d of reperfusion

To investigate if inhibition of lipolysis after MI by activation of the adipocyte specific inhibitory DREADD system could alter cardiac function post-ischemia, echocardiography which is routinely used to monitor cardiac function, was used to analyze the animals at base line and after 7d of reperfusion. The results revealed an improved cardiac systolic function in Cre+/hM4Di+ animals after 1 h ischemia and 7 d of reperfusion, which is depicted by increased ejection fraction (Cre+/hM4Di-: 31,9 ± 6,7 %; Cre-/hM4Di+: 33,7 ± 4,2 %; Cre+/hM4Di+: 40,2 ± 6,7 %), increased fractional area change (Cre+/hM4Di-: 22,7 ± 8,3 %; Cre-/hM4Di+: 26,6 ± 6,8 %, Cre+/hM4Di+: 34,1 ± 9,8 %) and improved stroke volume (Cre+/hM4Di-: 39,2 ± 9,7 µL; Cre-/hM4Di+: 39,3 ± 6,3 %, Cre+/hM4Di+: 47,2 ± 6,7 µL) (Fig. 28A). As hM4Di expression was also detected in the heart, Cre-/hM4Di+ animals were used as a second control group and analyzed as well. Compared to Cre+/hM4Di- animals, they did not show significant difference but showed a significantly reduced cardiac ejection fraction compared to Cre+/hM4Di+ animals (Fig. 28B). Therefore, from this point on Cre+/hM4Di- animals served as the only control group in the following experiments.

Since improved cardiac systolic function might be due to reduced aortic pressure, additional intra-aortic pressure measurements were performed in mice after 7 d of reperfusion. Systolic, diastolic and mean arterial pressure were unchanged between the two groups, indicating that the improved cardiac systolic function was either due to an intrinsic enhanced contractile function or a reduction in scar size (Fig. 28C).

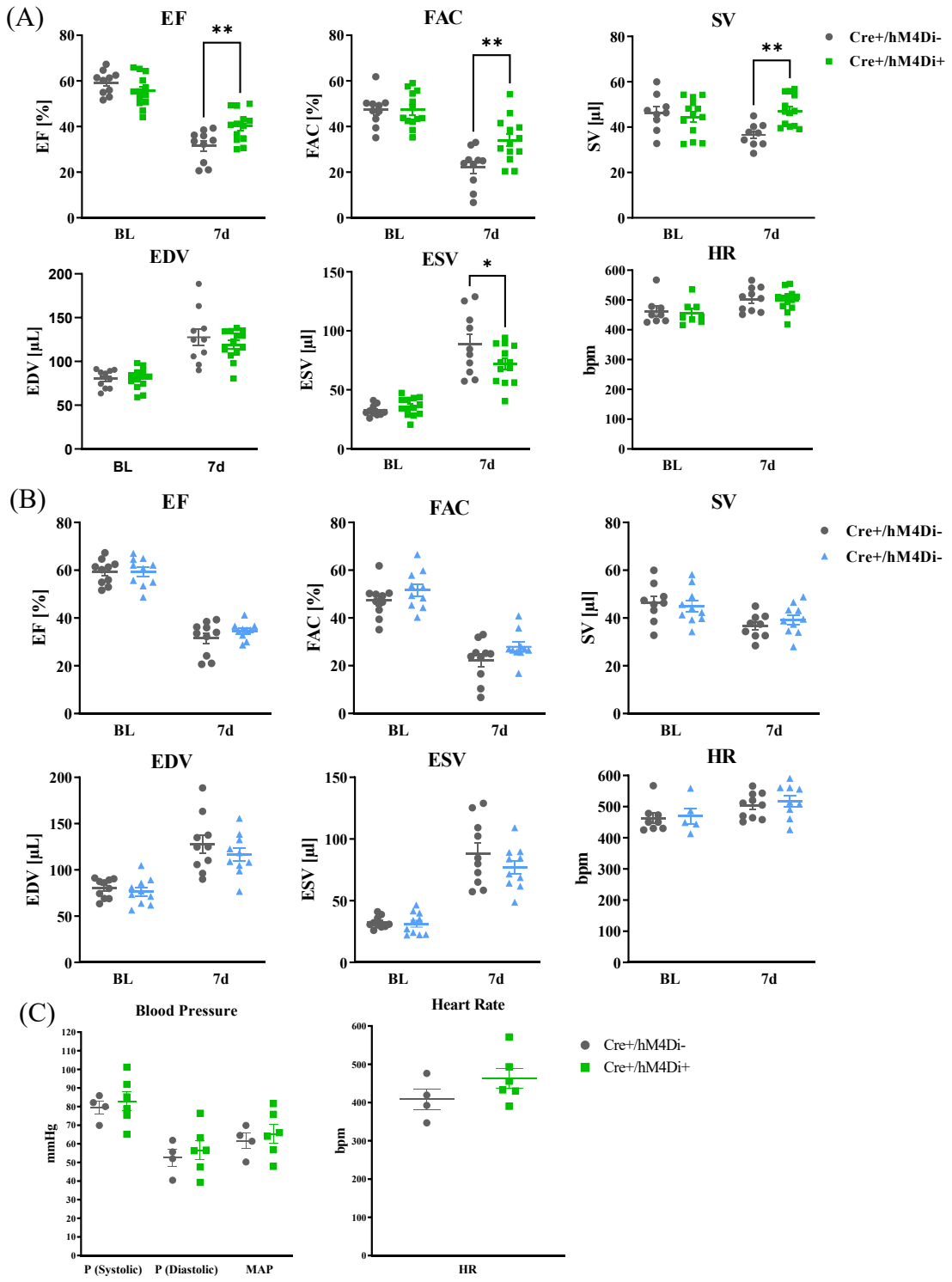

Fig. 28: Improved cardiac systolic function after acute inhibition of lipolysis. (A) Improved cardiac systolic function in hM4Di expressing mice after 1 h ischemia and 7 d of reperfusion, as depicted by increased EF, FAC and SV (B) Comparable cardiac function between two control groups revealed by echocardiography. (C) Unchanged blood pressure and heart rate in hM4Di expressing mice after 7 d of reperfusion. n = 4 – 13, mean ± SEM, 2-Way-ANOVA with Sidak's multiple comparisons test or unpaired, two-tailed *t*-test. EDV: End diastolic volume. EF: Ejection fraction. ESV: End systolic volume. FAC: Fractional area change. HR: Heart rate. SV: Stroke volume.

Accordingly, the scar size was analyzed after 7 d of reperfusion using wheat germ agglutinin (WGA) staining, which is often used for labeling cell membranes and fibrotic scar tissue (Emde et al. 2014). Snap frozen heart tissue was cryosectioned and the first 10 sections (level 1 to level 10) from the apex side were used for the quantification. WGA staining was evaluated under fluorescent microscope, the scar tissue could be clearly seen in green color (Fig. 29A). 14,06 ± 4,90 % of the whole heart and 17,37 ± 5,97 % of left ventricle was shown to be fibrotic scar tissue in Cre+/hM4Di- mice and 12,96 ± 5,89 % of the whole heart and 15,93 ± 7,31 % of left ventricle was shown to be fibrotic scar tissue in Cre+/hM4Di+ mice (Fig. 29B), a difference which was not statistically significant.

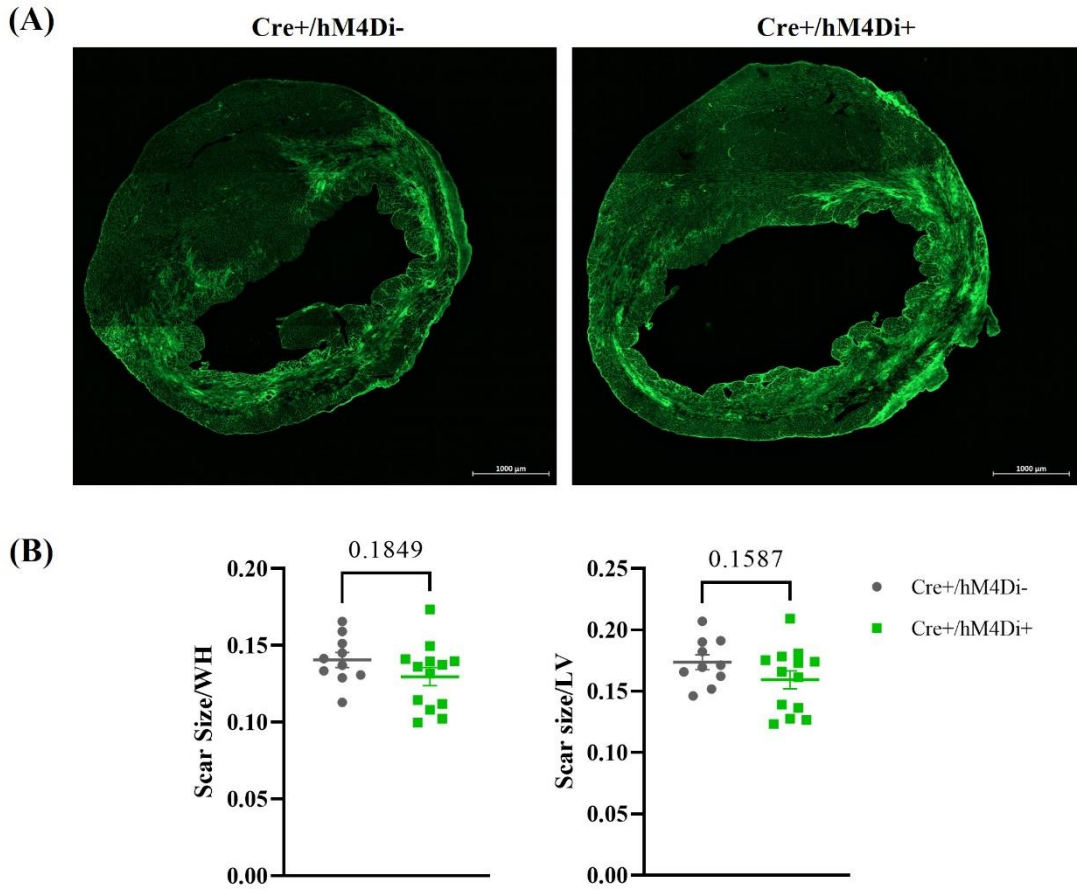

Fig. 29: Comparable scar size between Cre+/hM4Di- and Cre+/hM4Di+ mice after 7 d of reperfusion. (A) WGA fluorescence staining of cryosectioned heart tissue of Cre+/hM4Di- and Cre+/hM4Di+ ischemic mice after 7 d of reperfusion. (B) Analysis of scar size to the whole heart area and left ventricular area. n = 10 – 13, mean ± SEM, unpaired, two-tailed *t*-test. WGA: Wheat germ agglutinin.

3.10 Changes in white adipose tissue due to acute inhibition of lipolysis after MI

3.10.1 Acute inhibition of lipolysis during and after MI did not change morphology of white adipose tissue

A series of morphological changes of iWAT have been revealed in C57BL/6J mice after myocardial ischemia: 1) smaller adipocyte size in iWAT; 2) browning of iWAT and the appearance of crown-like structures in gWAT; 3) increased infiltration of MAC-2+ macrophages in iWAT. To investigate if the acute inhibition of lipolysis using the inducible adipocyte specific inhibitory DREADD system could reverse or change the effects caused by cardiac ischemia, cell size, browning and macrophage infiltration were analyzed.

H&E staining revealed unchanged adipocyte size after 1 h ischemia and 24 h of reperfusion in gWAT and iWAT between hM4Di expressing mice and control mice (Fig. 30). The cell morphology of gWAT was shown to be typical white adipocytes, and similar to what has been found in iWAT after MI, the adipocytes of inguinal depot after ischemia and 24 h of reperfusion all turned to be smaller and some of them showed to be multilocular, which is the typical morphology of brown adipocytes. The increased number of nuclei could also be found in iWAT of control mice and hM4Di expressing mice. However, H&E staining did not show if there was any difference in browning and macrophage infiltration between the two groups, therefore, further browning analysis and macrophage infiltration analysis were performed. The protein expression level of UCP1 and the relative gene expression of several browning markers were investigated to analyze the browning effect. Even if a significantly reduced UCP1 protein level could not be found by western blot analysis in hM4Di expressing mice after 24 h of reperfusion, the browning level trended to be decreased after acute inhibition of lipolysis (p-value = 0,1754, Fig. 31A). In line with UCP1 protein expression level, the relative gene expression of browning markers also showed slightly reduced expression levels in hM4Di expressing mice (Fig. 31B). The results revealed that acute inhibition of lipolysis using DREADD system was able to partly reverse the browning effect in iWAT after MI.

Due to the enhanced macrophage infiltration in iWAT of C57BI/6J mice after cardiac ischemia and 7 d of reperfusion and the findings of increased number of nuclei in H&E staining after 7 d of reperfusion, iWAT of control and hM4Di expressing mice was stained by anti-Mac2 immunofluorescence staining after MI and 7 d of reperfusion. Increased

number of macrophages, comparable to the numbers seen before in sham vs. ischemia, was found in iWAT after 1 h ischemia and 7 d of reperfusion with or without acute inhibition of lipolysis, however, no difference was overt between the two groups (Average macrophage number: sham operated: 17,98 ± 5,35 pro mm^2; ischemic operated: 36,04 ± 4,57 pro mm^2; Cre+/hM4Di-: 26,61 ± 4,58 pro mm^2; Cre+/hM4Di+: 27,19 ± 5,07 pro mm^2, Fig. 32). This finding indicates that the enhanced macrophage infiltration in iWAT after MI is not due to the acute lipolytic activation.

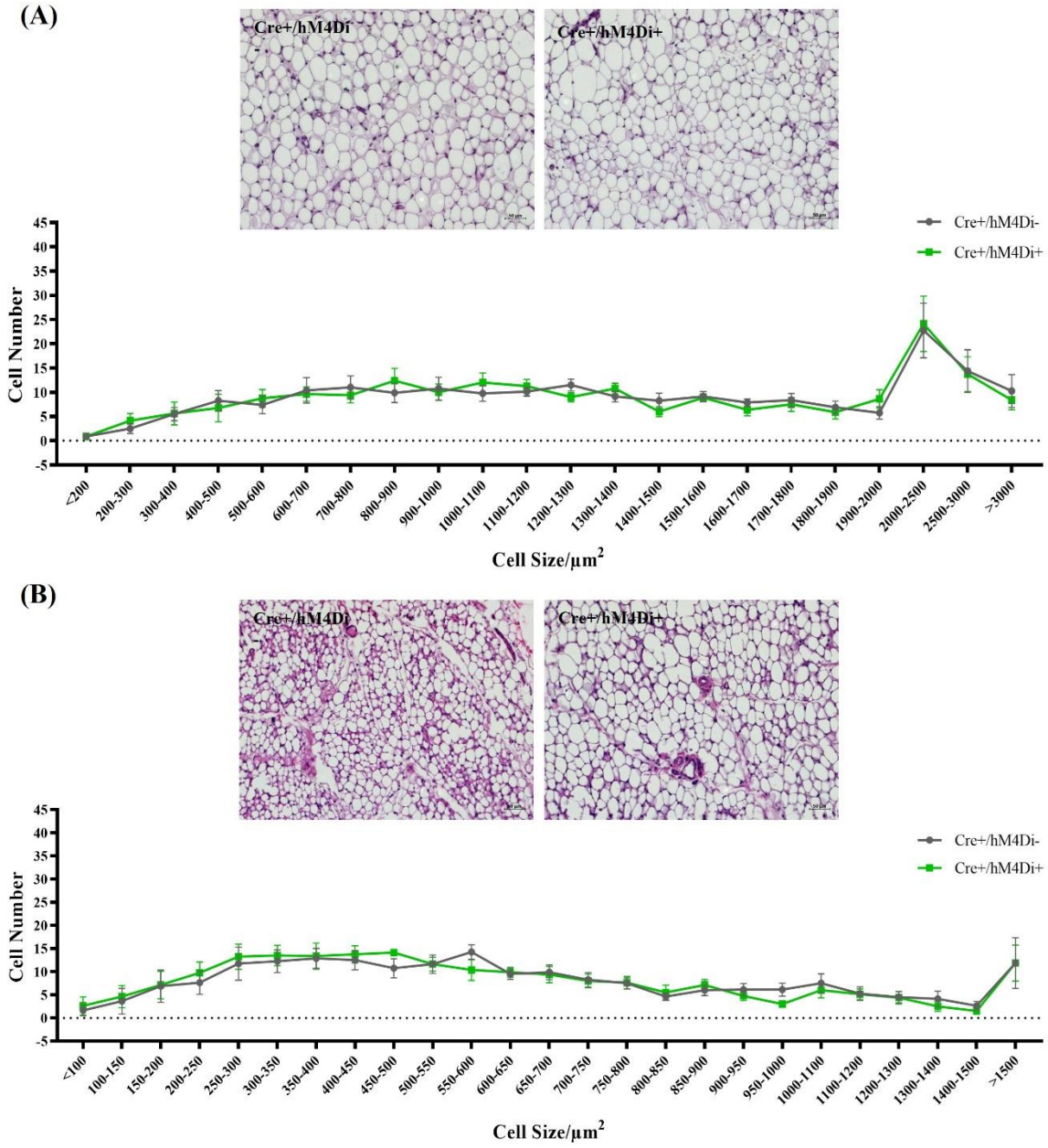

Fig. 30 : Acute inhibition of lipolysis after cardiac ischemia did not affect adipocyte size in gWAT and iWAT. (A) H&E staining of gWAT and adipocyte size distribution curve after 24 h of reperfusion. (B) H&E staining of iWAT and adipocyte size distribution curve after 24 h of reperfusion. gWAT: Gonadal white adipose tissue. H&E: Hematoxylin and eosin. iWAT: Inguinal white adipose tissue.

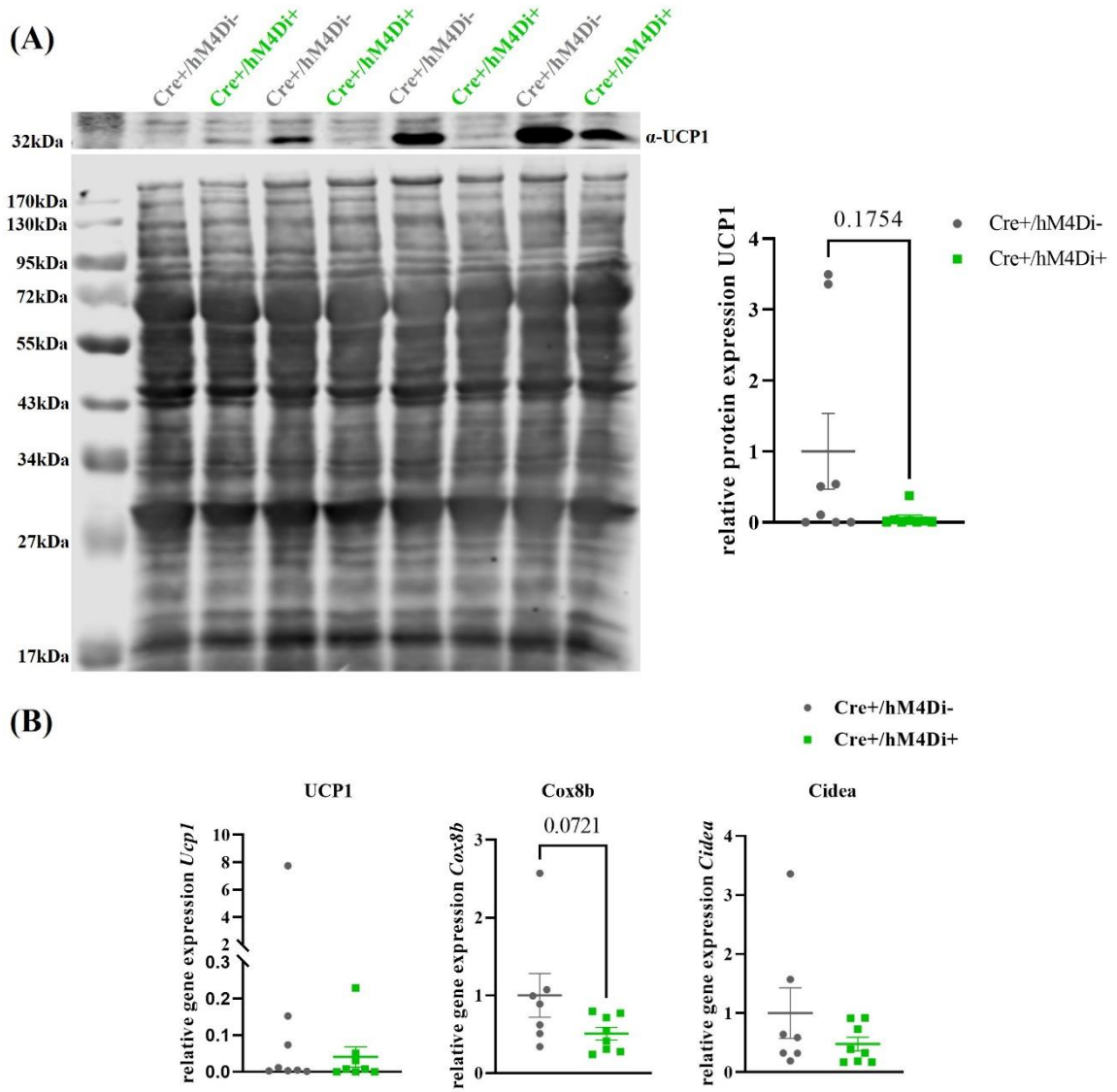

Fig. 31 : The browning of iWAT induced by cardiac ischemia was partly reduced by acute inhibition of lipolysis. (A) Western blot analysis of UCP1 expression in iWAT of hM4Di- and hM4Di+ mice after 24 h of reperfusion. (B) Relative gene expression of Ucp1, Cox8b and Cidea in iWAT after 24 h of reperfusion. n = 7 - 8, mean ± SEM, Mann-Whitney test. Cidea: Cell death activator. Cox8b: Cytochrome c oxidase subunit 8B. iWAT: Inguinal white adipose tissue. Ucp1: Uncoupling protein 1.

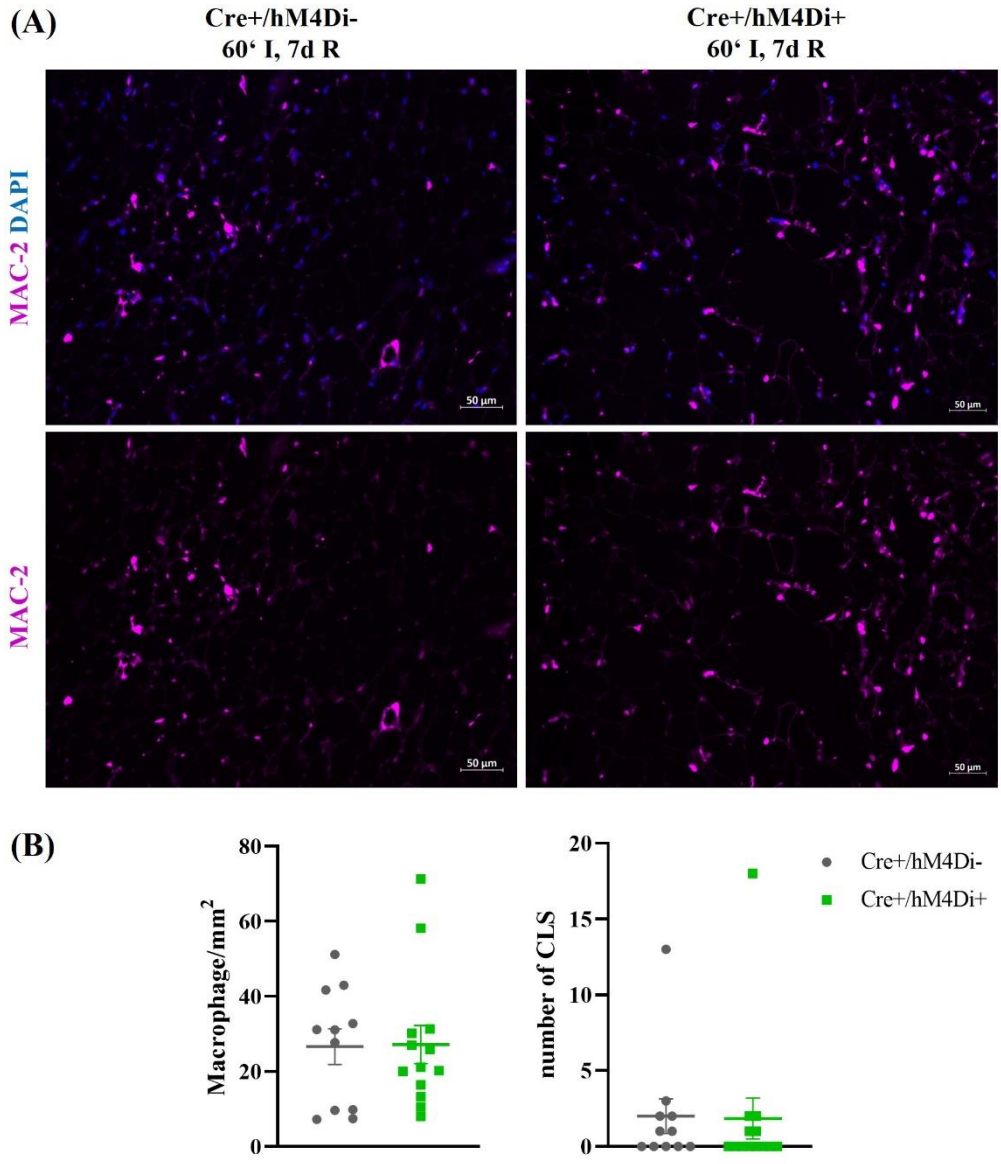

Fig. 32 : Acute inhibition of lipolysis did not alter MAC-2+ macrophage infiltration in iWAT induced by cardiac ischemia. (A) Anti-Mac2 immunofluorescent staining of iWAT after 7 d of reperfusion. (B) Quantification of number of macrophages and CLSs in iWAT after 7 d of reperfusion. n = 11 - 13, mean ± SEM, Mann-Whitney test. CLS: Crown-like structure. DAPI: 4’,6-diamino-2-phenylindole. iWAT: Inguinal white adipose tissue.

3.10.2 Acute inhibition of lipolysis did not affect lipogenesis after MI and 24 h of reperfusion

Cardiac ischemia was associated with reduced lipogenesis in iWAT as downstream targets of the transcription factors PPAR-γ (*Pparγ*) and SREBP-1C (*Srebp1c*) like *Lpl*, *Fasn* and *Dgat2* were downregulated. To investigate if acute inhibition of lipolysis after MI using DREADD system could reverse or alter the gene expression profile regarding lipogenesis, the relative gene expression of transcription factors *Pparγ*, *Srebp1c* and their downstream genes *Lpl*, *Fasn* and *Dgat2* was analyzed in gWAT and iWAT of mice which express or do not express hM4Di after MI and 24 h of reperfusion. The analysis showed an unchanged gene expression profile regarding lipogenesis in both gWAT and iWAT (Fig. 33), indicating that also these alterations in the gene expression profile could not be reversed by acute inhibition of lipolysis.

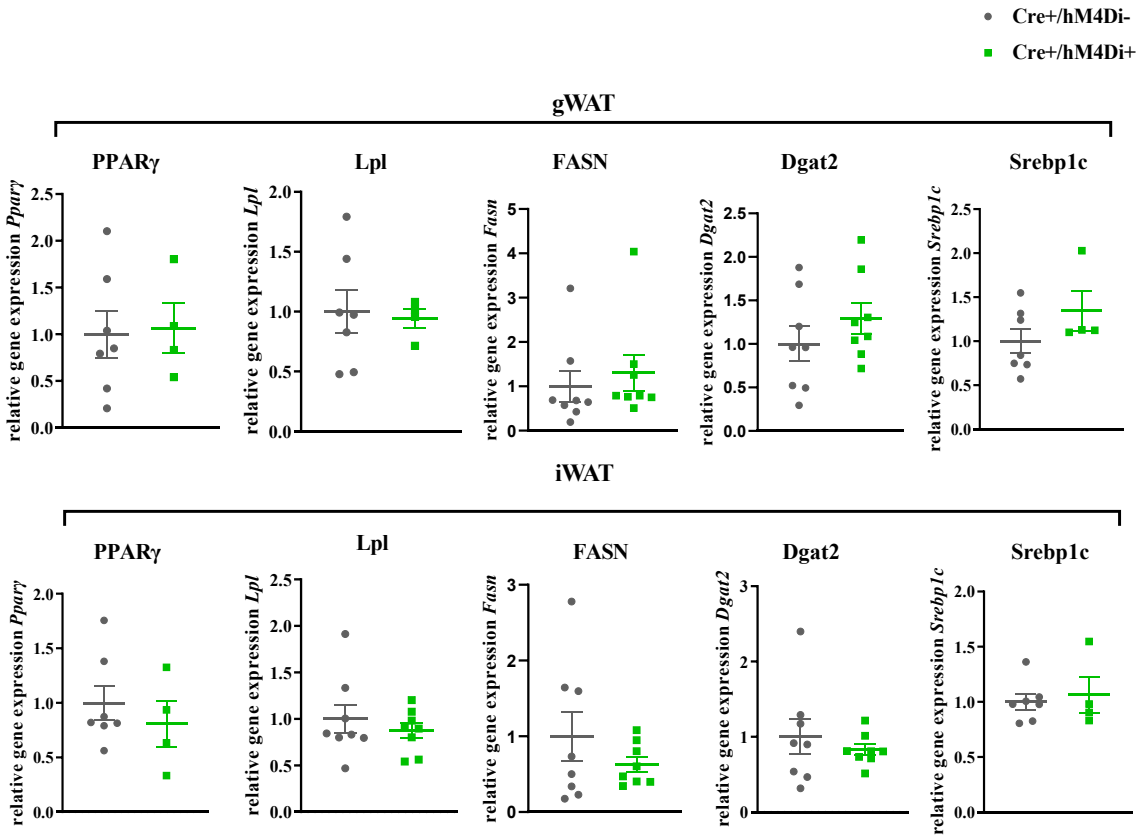

Fig. 33 : Acute inhibition of lipolysis did not affect lipogenesis after 24 h of reperfusion. Relative gene expression of *Pparγ*, *Lpl*, *Fasn*, *Dgat2* and *Srebp1c* in hM4Di- and hM4Di+ ischemic mice after 24 h of reperfusion. n = 5 - 6, mean ± SEM, unpaired, two-tailed t-test and Mann-Whitney test. Dgat2: Diacylglycerol O-acyltransferase 2. Fasn: Fatty acid synthase. gWAT: Gonadal white adipose tissue. iWAT: Inguinal white adipose tissue. Lpl: Lipoprotein lipase. Pparγ: Peroxisome proliferator-activated receptor gamma. Srebp1c: Sterol regulatory element-binding protein-1c.

Acute inhibition of lipolysis did not change adipokine gene expression profile after MI and 24 h of reperfusion

Next to the lipogenic gene expression profile also adipokines like adiponectin, leptin and resistin were shown to be reduced in iWAT after cardiac ischemia. To investigate if acute inhibition of lipolysis using the DREADD system might impact adipokine expression, *Adipoq*, *Leptin* and *Resistin* expression was analyzed in gWAT and iWAT after MI and 24 h of reperfusion in mice with or without hM4Di expression. Comparing to control mice, the adipokine gene expression profile was not altered in both depots, indicating that adipokine expression is not coupled to acute lipolytic activation (Fig. 34).

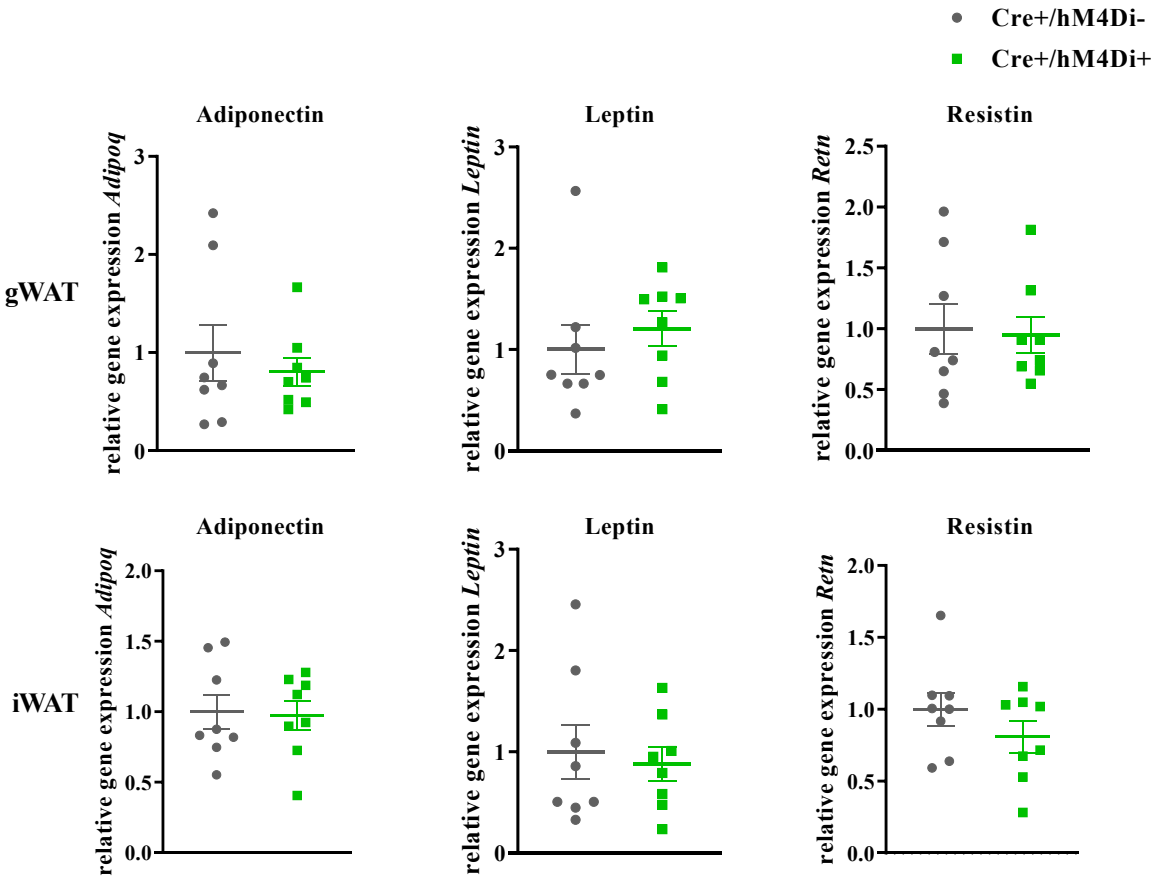

Fig. 34 : Acute inhibition of lipolysis did not affect adipokine gene expression after 24 h of reperfusion. Relative gene expression of *Adipoq*, *Leptin* and *Retn* in hM4Di- and hM4Di+ ischemic mice after 24 h of reperfusion. n = 8, mean ± SEM, unpaired, two-tailed t-test and Mann-Whitney test. gWAT: Gonadal white adipose tissue. iWAT: Inguinal white adipose tissue.

3.10.3 Acute inhibition of lipolysis reduced resistin gene expression after MI and 30 min of reperfusion

The main adipocyte-related alterations in DREADD-expressing mice compared to control mice occurred after 30 min of reperfusion, in terms of decreased circulating NEFA levels in hM4Di expressing mice. To investigate a direct relationship between NEFA level and the gene expression of adipokines, the relative gene expression of adiponectin, leptin and resistin was analyzed in gWAT and iWAT. The analysis revealed none of the adipokines showed any change in gene expression pattern in gWAT. However, in iWAT, gene expression of resistin was reduced (*p*-value = 0,01) in hM4Di expressing mice (Fig. 35).

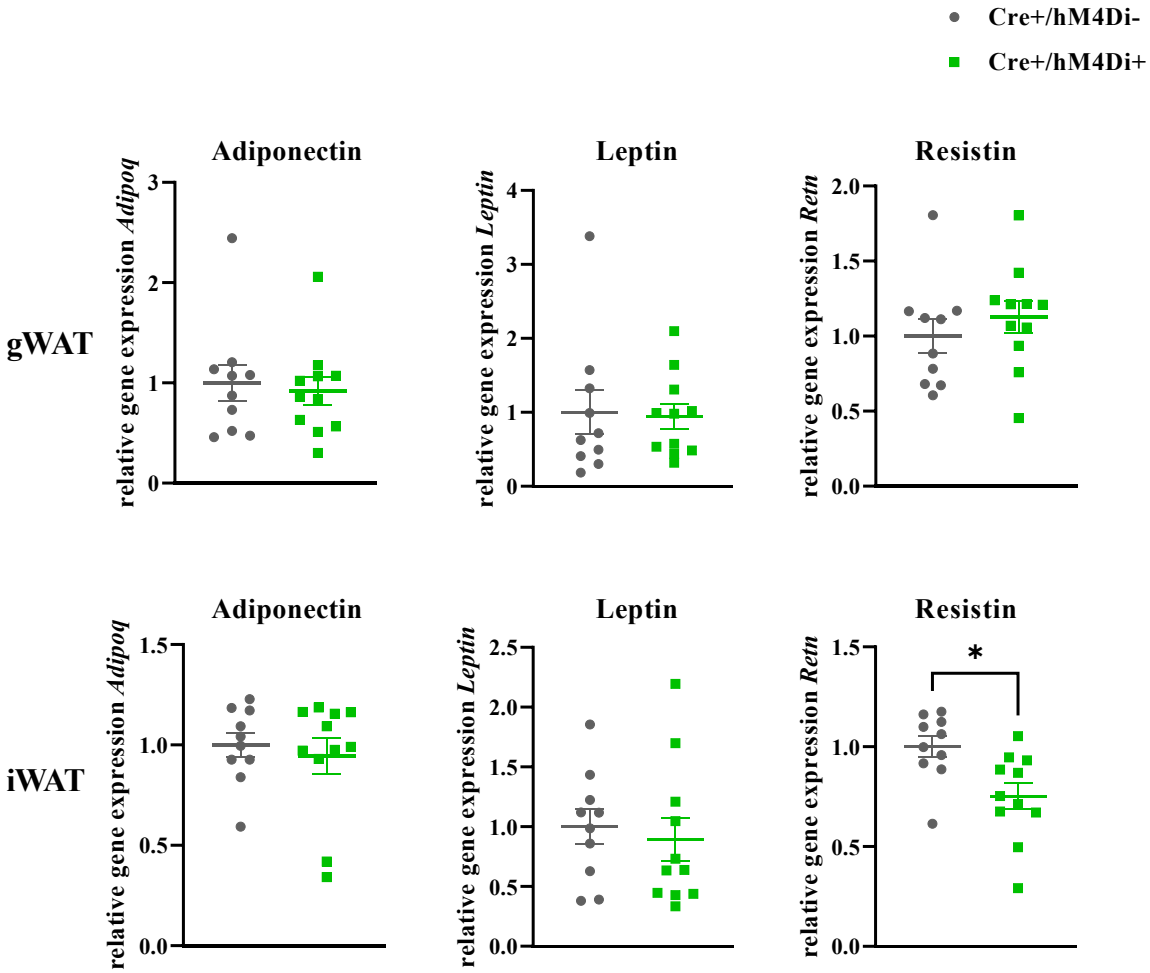

Fig. 35 : Acute inhibition of lipolysis reduced resistin gene expression in iWAT after 30 min of reperfusion. Relative gene expression of *Adipoq*, *Leptin* and *Retn* in hM4Di- and hM4Di+ ischemic mice after 30 min of reperfusion. n = 10 - 11, mean ± SEM, unpaired, two-tailed t-test and Mann-Whitney test. gWAT: Gonadal white adipose tissue. iWAT: Inguinal white adipose tissue.

3.11 Acute inhibition of lipolysis reduced circulating insulin level after MI and 30 min of reperfusion

Based on the finding that reduced NEFA level correlated with reduced resistin gene expression in iWAT of hM4Di expressing mice, the circulating levels of adipokines and hormones related to diabetes were analyzed by multiplex analysis. Despite the alteration found on gene expression level, this was not able to also reduce circulating resistin level in hM4Di+ mice. Other circulating adipokines as leptin, adiponectin and PAI-1 also showed no difference between the two groups, which was in line with the gene expression pattern in white adipose tissue. Interestingly, among the hormones related to diabetes, the circulating insulin level was significantly decreased ($p < 0{,}001$) in hM4Di expressing mice after 30 min of reperfusion while other hormones as ghrelin, GIP and GLP-1 were unchanged (Fig. 36).

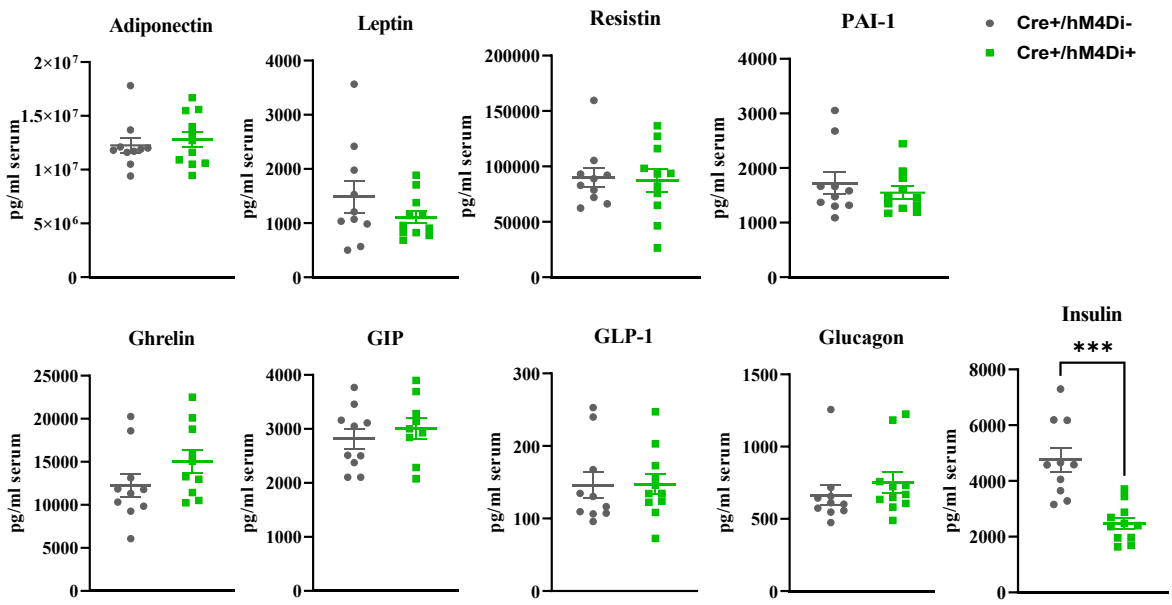

Fig. 36 : Decreased insulin level in circulation after acute inhibition of lipolysis in hM4Di+ mice after 30 min of reperfusion. The circulating level of leptin, adiponectin, resistin, ghrelin, GIP, GLP-1, PAI-1, glucagon and insulin in hM4Di- and hM4Di+ ischemic mice after 30 min of reperfusion. n = 10 - 11, mean ± SEM, unpaired, two-tailed t-test and Mann-Whitney test. GIP: Gastric inhibitory peptide. GLP-1: Glucagon-like peptide 1. PAI-1: Plasminogen activator inhibitor-1.

As the $G_{\alpha i}$ hM4Di receptor was found to be also expressed in other organs like heart, liver and skeletal muscle, we wanted to rule out that reduced circulating insulin level was due to $G_{\alpha i}$-signaling in pancreas. Therefore, hM4Di expression in the pancreas was investigated.

Anti-HA immunofluorescence staining was performed in gWAT and pancreas of hM4Di- and hM4Di+ mice. Positive signals of anti-HA were easily found in gWAT of hM4Di+ mice revealing a high expression of the receptors hM4Di. However, comparing to hM4Di- mice and technical negative control, the pancreas, especially the islets, did not show any positive red fluorescent signals (Fig. 37A). According to the staining, no relevant expression of hM4Di was found in pancreas. Additionally, the protein expression of GFP was analyzed by western blot analysis. Similar to heart, liver and skeletal muscle, pancreas showed as well positive anti-GFP signals in every hM4Di+ mice (Fig. 37B). Even if the protein expression of anti-GFP was seen in hM4Di expressing mice, the qPCR analysis validated the results shown by immunohistochemistry. The relative gene expression of *hM4Di* revealed that the receptors were not expressed in relevant amounts since the Ct values were either above 33,65 or could not be detected at all (Fig. 37C).

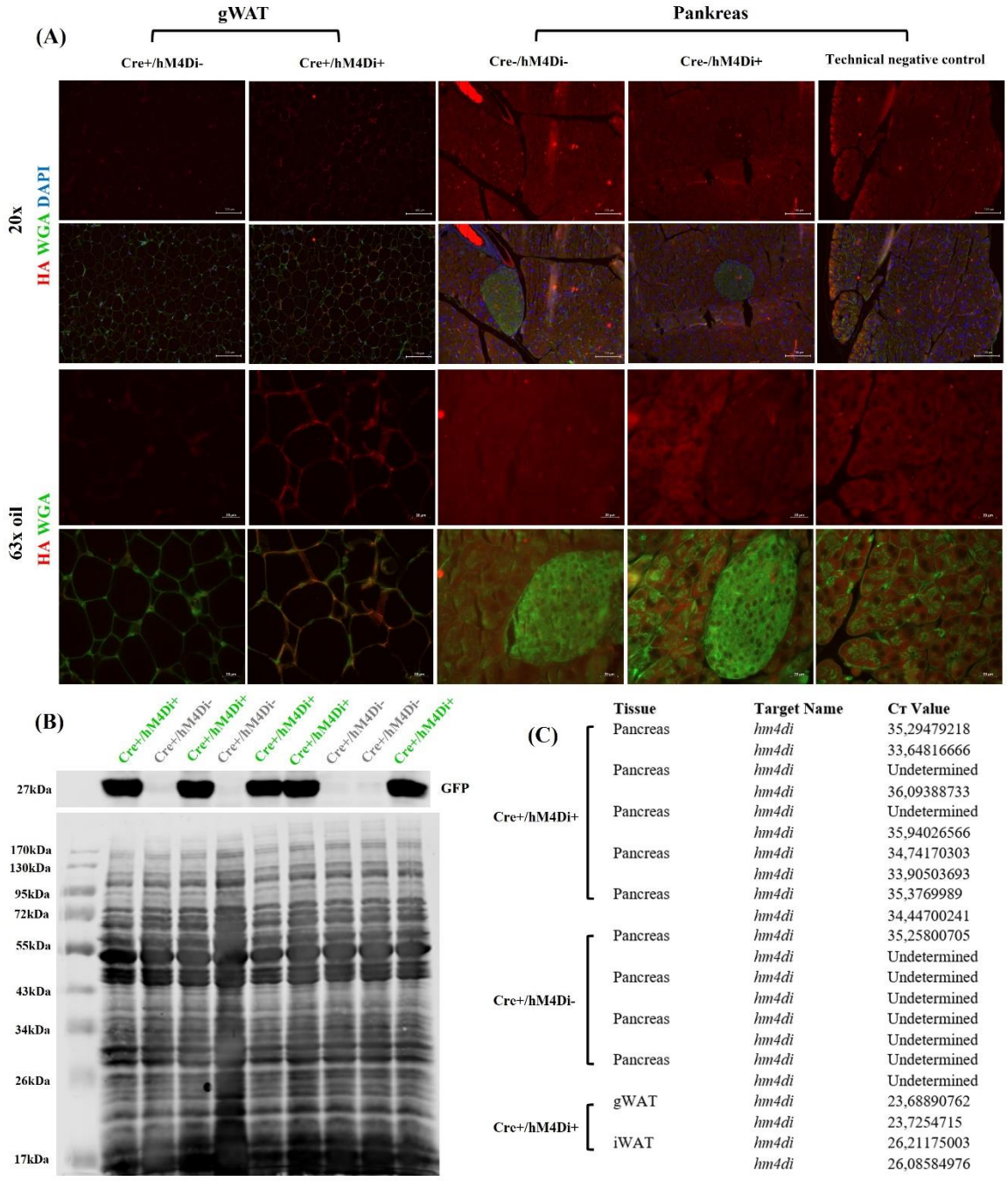

Fig. 37: Expression of hM4Di receptors in white adipose tissue and pancreas. (A) Anti-HA immunofluorescence staining of gWAT and pancreas. (B) Western blot analysis of anti-GFP in the pancreas of hM4Di- and hM4Di+ mice. (C) qPCR analysis of *hM4Di* expression in the pancreas of hM4Di- and hM4Di+ mice. DAPI: 4',6-diamino-2-phenylindole. GFP: Green fluorescent protein. gWAT: Gonadal white adipose tissue. HA: Hemagglutinin epitope. WGA: Wheat germ agglutinin.

To figure out why anti-GFP signals were always able to be detected in the western blot, whereas only little hM4Di gene expression could be detected at mRNA level, the relative gene expression of hM4Di and mCitrine was analyzed respectively in gWAT of Cre-/hM4Di+ and Cre+/hM4Di+ mice after Cre-recombinase introduction. The relative gene expression of hM4Di and mCitrine could both be seen at a low level in Cre-/hM4Di+ mice, however, mCitrine exhibited a higher expression compared to hM4Di. 4,88 % of hM4Di and 9,21 % of mCitrine was expressed in Cre-/hM4Di+ mice compared to the expression in Cre+/hM4Di+ mice (Fig. 38A).

For a functional read out, the circulating insulin level was validated by ELISA. When comparing Cre+/hM4Di+ to Cre+/hM4Di- animals, the insulin level of these mice still trended to be reduced with a *p*-value of 0,1271, supporting the results from the multiplex analysis. More important, no difference could be seen between the two control groups, indicating that indeed the reduction in circulating insulin level was due to the acute inhibition of lipolysis, but not the leakiness of the receptor (Fig. 38B).

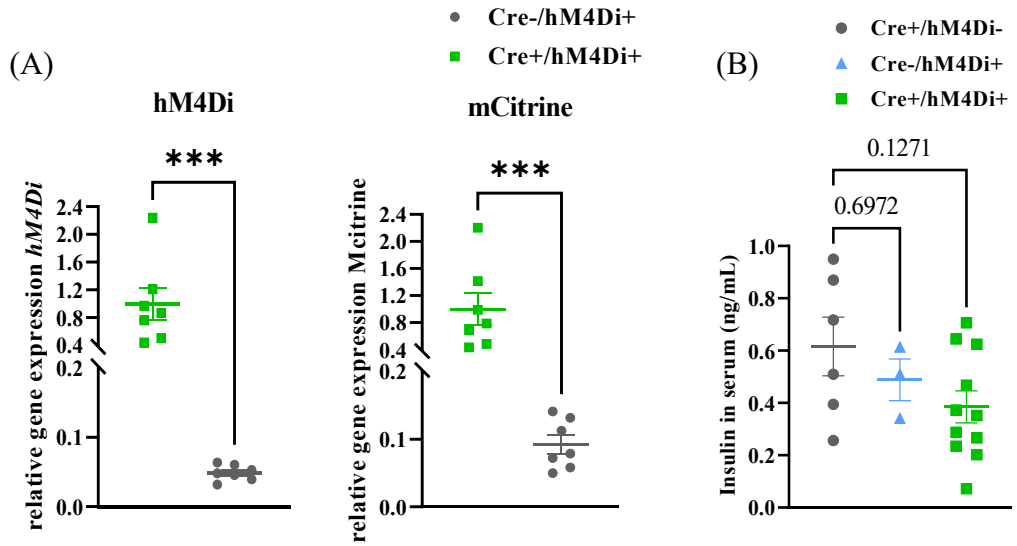

Fig. 38: (A) qPCR analysis of hM4Di and mCitrine in gWAT of hM4Di- and hM4Di+ mice. (B) Analysis of circulating insulin level by ELISA. n = 7 - 11, mean ± SEM, unpaired, Mann-Whitney test (A) or One-Way Annova with Tukey's multiple comparisons test (B). ELISA: Enzyme-linked immunosorbent assay. gWAT. Gonadal white adipose tissue.

To further identify the effects of reduced insulin signaling in the heart after acute inhibition of peripheral lipolysis, the relative expression of several genes which are known to respond to insulin signaling such as the transcription factor *Srebp1c* and its downstream genes *Lpl* and *Fasn*, CD36 (*Cd36*) that imports fatty acids into cardiomyocytes and GLUT4 (*Slc2a4*) that translocates onto the cell membrane after insulin binding and transports glucose into cardiomyocytes, were investigated. Reduced gene expression of GLUT4 was found in remote area (Fig. 39A), however the reduction could not be found in ischemic area (Fig. 39B).

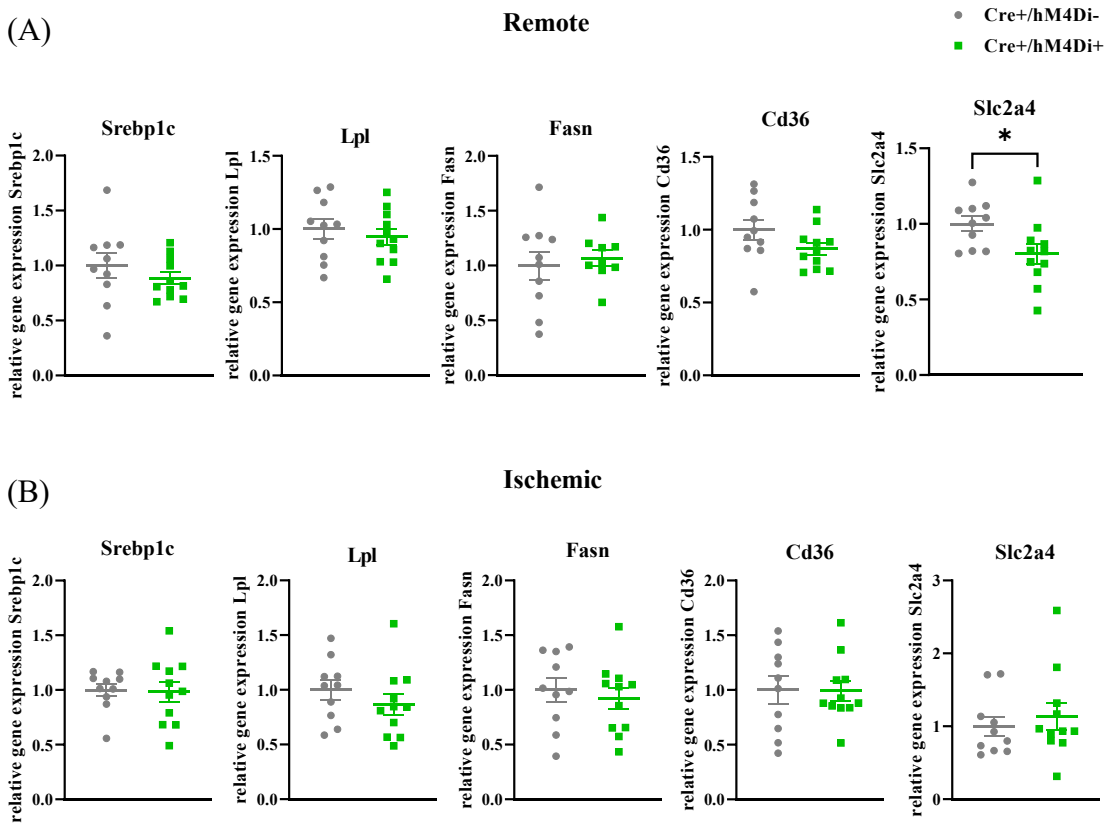

Fig. 39: Acute inhibition of lipolysis reduced GLUT4 gene expression in remote zone after 30 min of reperfusion. The relative gene expression of *Srebp1c*, *Lpl*, *Fasn*, *Cd36* and *Slc2a4* in remote (A) and ischemic (B) zone after MI and 30 min of reperfusion. n = 10-11, mean ± SEM, unpaired, two-tailed t-test. Cd36: Cluster of differentiation 36. Fasn: Fatty acid synthase. Lpl: Lipoprotein lipase. Slc2a4: Glucose transporter type 4. Srebp1c: Sterol regulatory element-binding protein-1c.

3.12 Acute inhibition of lipolysis elevated phosphorylation of PKA substrates in the heart after MI and 30 min of reperfusion

Next to insulin, protein kinase A (PKA) is also known to inhibit the expression and translocation of GLUT4 (Mangmool et al. 2016b). Furthermore, PKA also plays a major role in regulating cardiac contractile function by phosphorylating several targets important for contractility and relaxation of cardiomyocytes (Hanson et al. 2010). PKA-activity was investigated using a broad anti-p-PKA substrates antibody, which indicates changes in phosphorylation of PKA downstream targets. Phosphorylation signals could be clearly detected and hearts of hM4Di expressing mice after 60 min ischemia and 30 min of reperfusion showed a significantly higher phosphorylation of PKA substrates in both remote and ischemic zone (Fig. 40 and Fig. 41). This finding indicates a higher activity of cardiac PKA after inhibition of lipolysis and reduction of circulating NEFA and insulin level.

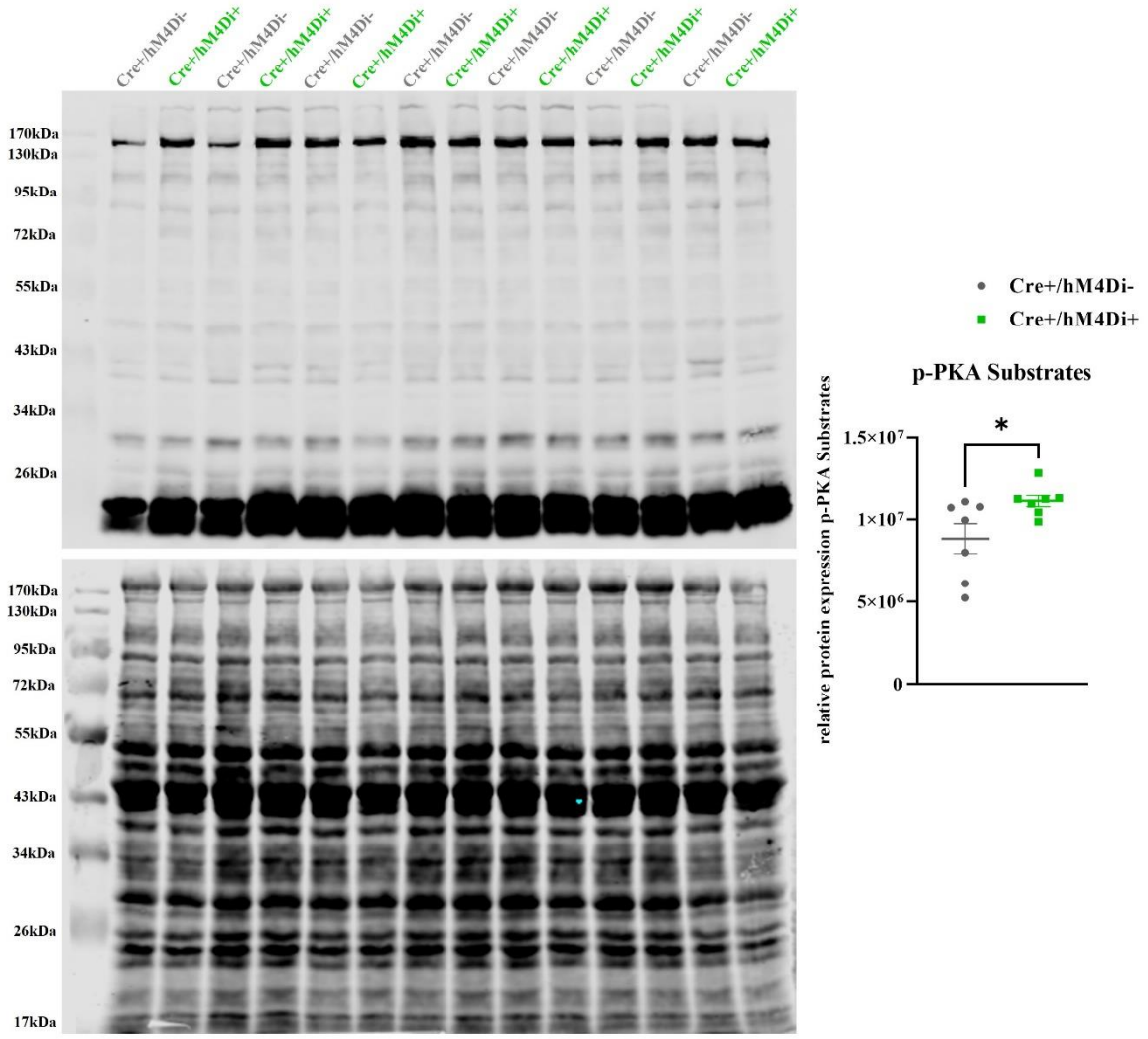

Fig. 40: Acute inhibition of lipolysis increased phosphorylation of PKA substrates in remote zone after 30 min of reperfusion. Western blot analysis of p-PKA substrates and total protein in remote zone of hM4Di- and hM4Di+ mice (p-value = 0,0336). n = 7, mean ± SEM, unpaired, two-tailed t-test. PKA: Protein kinase A.

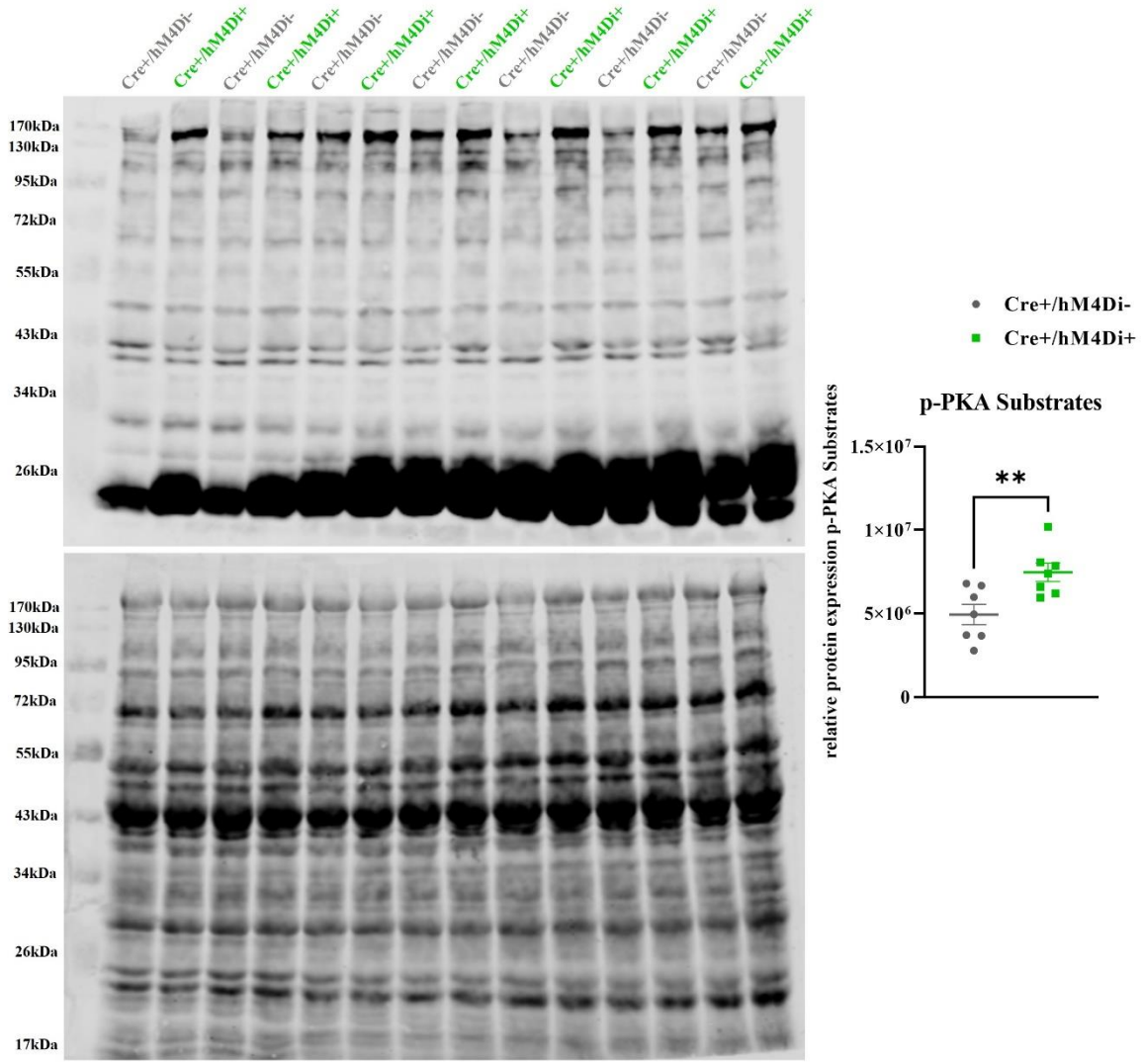

Fig. 41: Acute inhibition of lipolysis increased phosphorylation level of PKA substrates in ischemic zone after 30 min of reperfusion. Western blot analysis of p-PKA substrates and total protein in ischemic zone of hM4Di- and hM4Di+ mice (*p*-value = 0,0091). n = 7, mean ± SEM, unpaired, two-tailed t-test. PKA: Protein kinase A.

Excessive exogenous fatty acids inhibit PKA activity by suppressing accumulation of cAMP in adipose tissue (Mottillo und Granneman 2011b). To investigate if the acutely reduced circulating NEFA levels play a major role in increasing PKA activity in cardiomyocytes, we also analyzed PKA activity in white adipose tissue, and our data were in line with the previous studies. Acute inhibition of lipolysis in DREADD system led to reduced circulating NEFA levels after 30 min of reperfusion (Fig. 27). At this time point, PKA activity was increased in iWAT as revealed by enhanced phosphorylation of PKA substrates (Fig. 42 and Fig. 43). PKA plays an important role in regulating adipocyte lipolysis, activated hM4Di starts Gi signaling pathway and suppresses PKA activity and phosphorylation of its downstream targets like HSL. To show that increased PKA activity due to reduced circulating NEFA levels did not interfere with inhibited lipolysis, we analyzed as well the phosphorylation of HSL (s565). Even though increased PKA activity was detected in iWAT, increased p-HSL (s565) was not found (Figure 44).

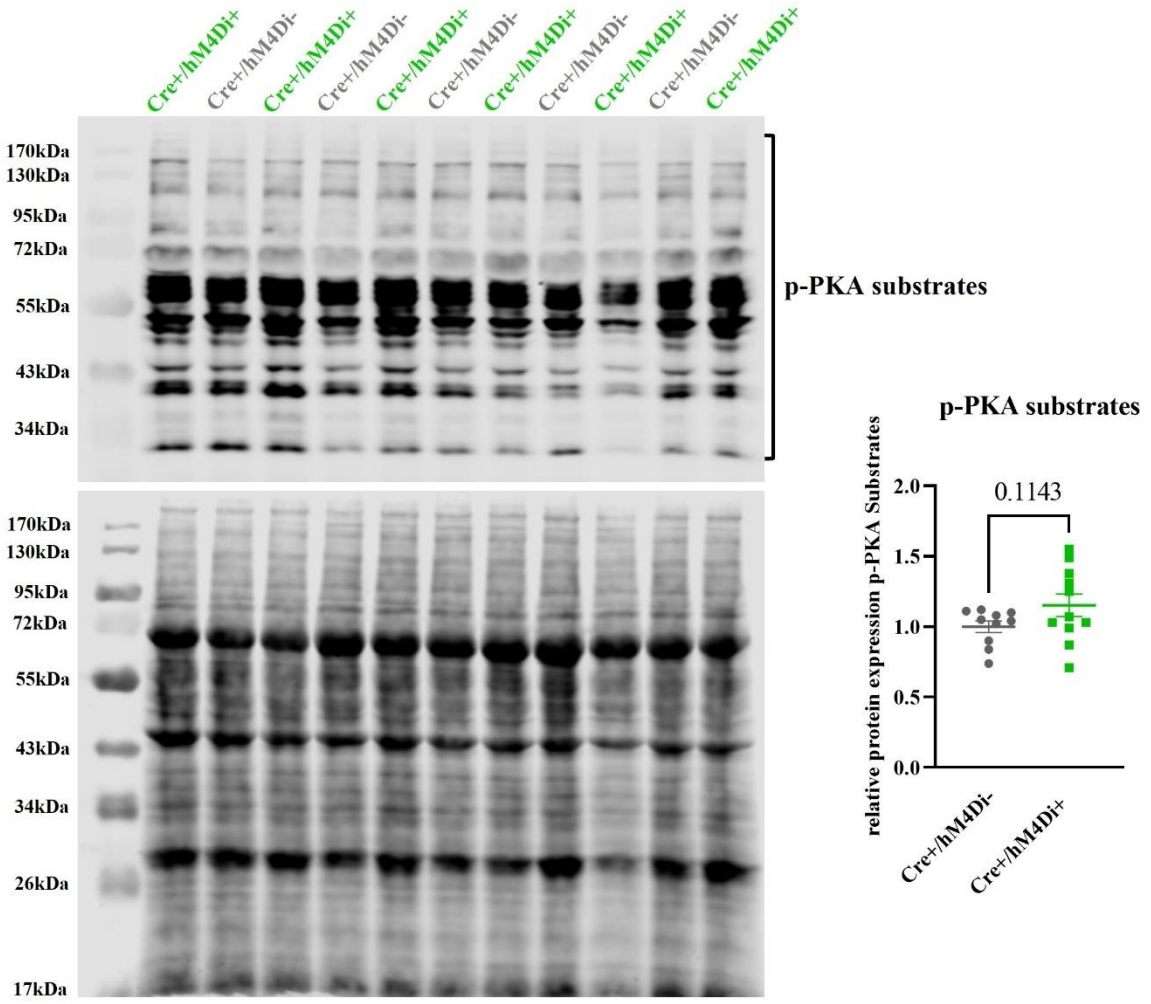

Fig. 42: Phosphorylation of PKA substrates in gWAT after 30 min of reperfusion. Western blot analysis of p-PKA substrates and total protein in gWAT of hM4Di- and hM4Di+ mice. n = 10-11, mean ± SEM, unpaired, two-tailed t-test. gWAT: Gonadal white adipose tissue. PKA: Protein kinase A.

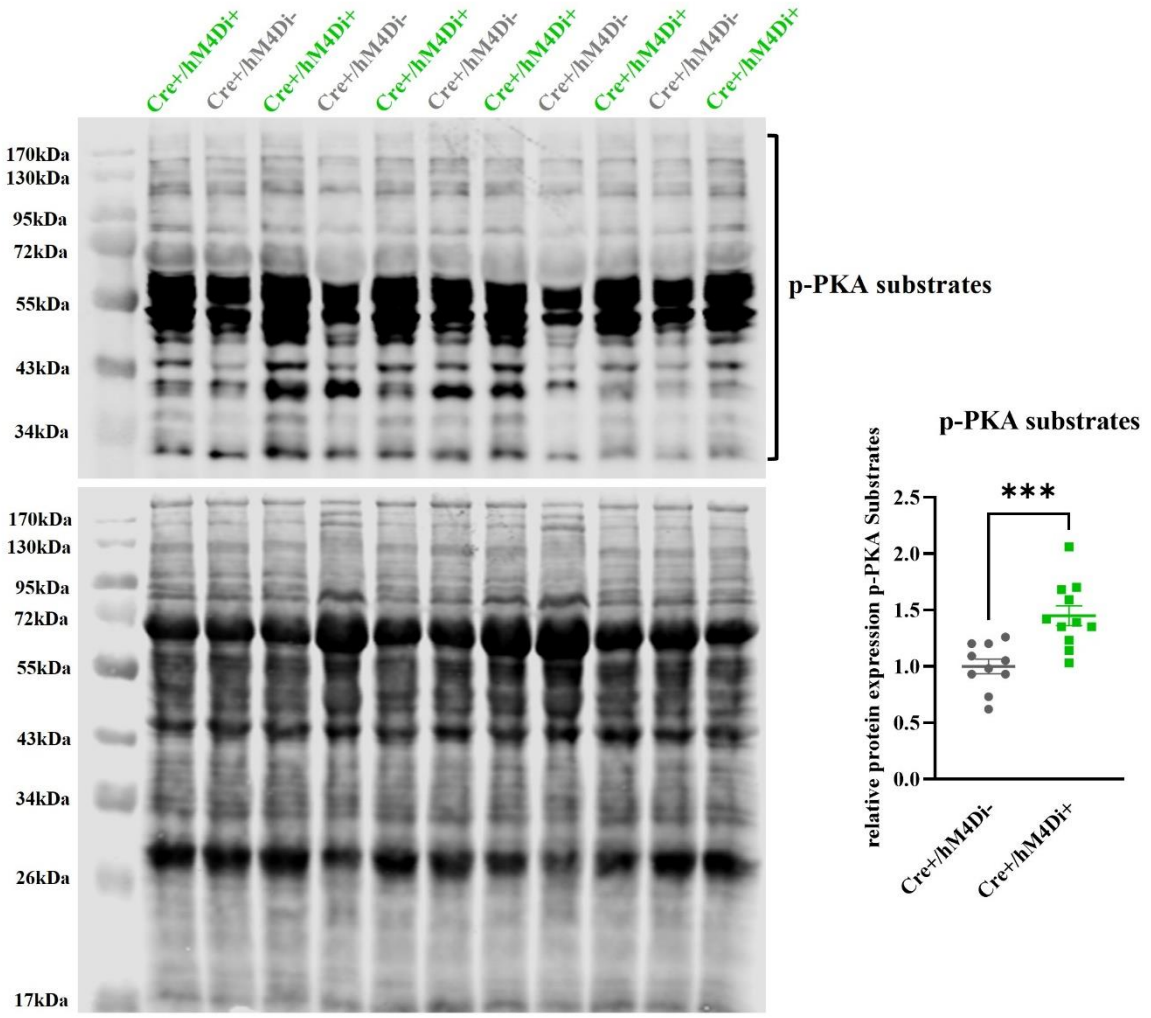

Fig. 43: Reduced circulating NEFA levels increased phosphorylation of PKA substrates in iWAT after 30 min of reperfusion. Western blot analysis of p-PKA substrates and total protein in iWAT of hM4Di- and hM4Di+ mice (p<0,001). n = 10-11, mean ± SEM, unpaired, two-tailed t-test. iWAT: Inguinal white adipose tissue. PKA: Protein kinase A.

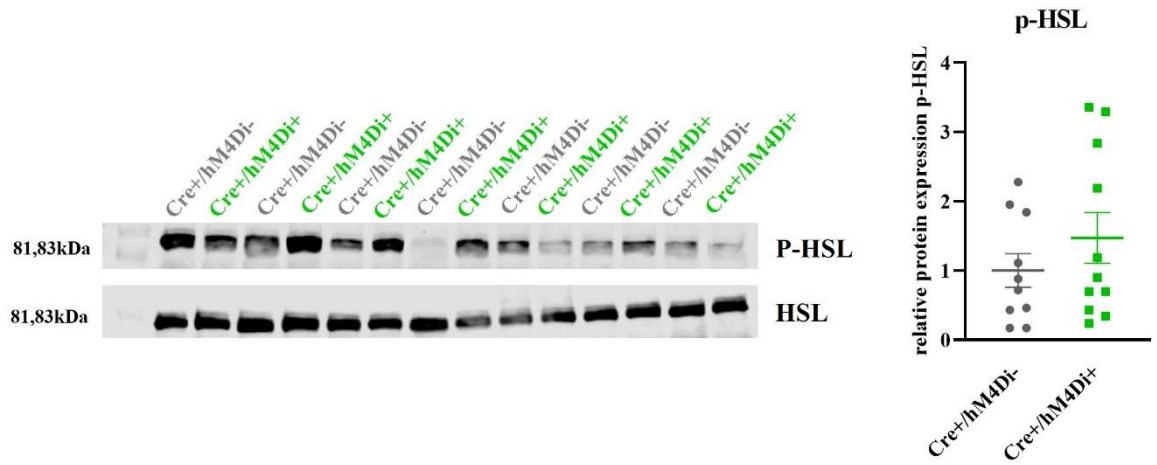

Fig. 44: Increased phosphorylation of PKA substrates did not affect phosphorylation of HSL in iWAT after 30 min of reperfusion. Western blot analysis of HSL and p-HSL (s565) in iWAT of hM4Di- and hM4Di+ mice. n = 10-11, mean ± SEM, unpaired, Mann-Whitney test. iWAT: Inguinal white adipose tissue. HSL: Hormone-sensitive lipase.

Phospholamban (PLN) is an important downstream target of PKA and it inhibits the cardiac muscle sarcoplasmic reticulum Ca^{2+}-ATPase SERCA. Once PLN is phosphorylated by PKA, the inhibition is relieved and SERCA shifts Ca^{2+} from the cytosol into the sarcoplasmic reticulum, being thereby an important regulator of the Ca^{2+} transient in cardiomyocytes (Hagemann and Xiao 2002). A reduced PLN at gene expression level was shown in remote zone of hM4Di+ mice after 30 min of reperfusion (Fig. 45A). To validate this finding, the protein expression level of PLN was analyzed by western blot analysis. Since phosphorylation of PKA downstream targets was found to be upregulated in hM4Di+ mice, also phosphorylation of PLN (s16) was analyzed. The phosphorylation of PLN (s16) and the total protein expression of PLN were investigated by using GAPDH as reference. The alteration of *Pln* gene expression, was not reflected on protein expression level in remote zone of hM4Di+ mice (Fig. 45B). However, in line with increased p-PKA substrate phosphorylation also the phosphorylation of PLN (s16) was upregulated in remote zone and trended to be upregulated in ischemic zone of hM4Di+ mice after 30 min reperfusion (Fig. 45B).

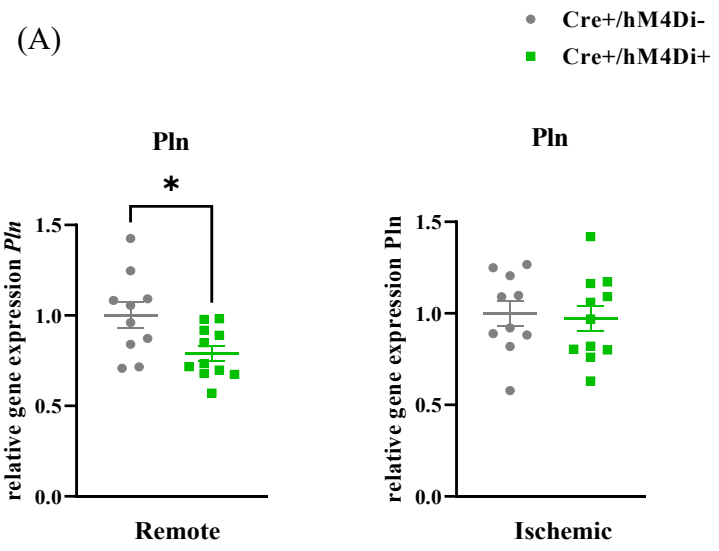

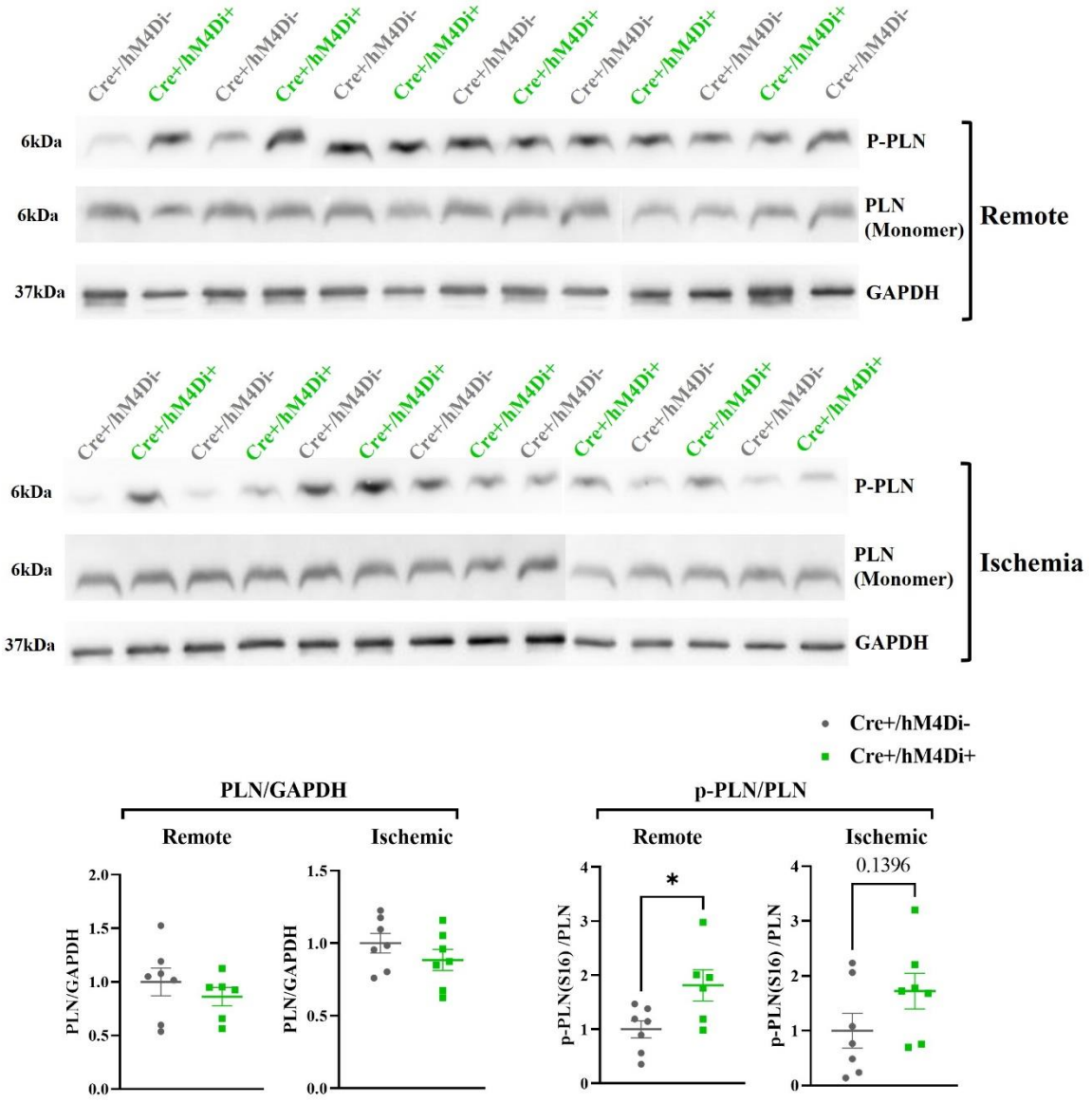

Fig. 45: Acute inhibition of lipolysis reduced *Pln* at gene expression level and increased phosphorylation of PLN (s16) at protein level in remote zone after 30 min of reperfusion. (A) Gene expression analysis of *Pln* in remote and ischemic zones after 30 min of reperfusion. (B) Western blot analysis of PLN and p-PLN (s16) in remote and ischemic zones after 30 min reperfusion. n = 6 - 11, mean ± SEM, unpaired, two-tailed t-test. GAPDH: Glyceraldehyde 3-phosphate dehydrogenase. PLN: Phospholamban.

Ca^{2+} serves as the main second messenger for cardiomyocyte contraction by binding to troponin causing its conformational change and exposing binding sites for myosin, which binds to actin forming crossbridge and allowing the contraction (Betts et al. 2013). Troponin I is also a known target of PKA, phosphorylation enables faster relaxation of cardiomyocytes (Betts et al. 2013). The phosphorylating level of troponin I at serine 23 and 24 was investigated, and though it did not reach statistical significance, also the phosphorylation of troponin I (s23/24) showed a strong trend towards an increase with a *p*-value of 0,0786 in remote zone of hM4Di+ mice (Fig. 46), further confirming an elevated PKA-activation in remote zone of hearts after acute inhibition of lipolysis.

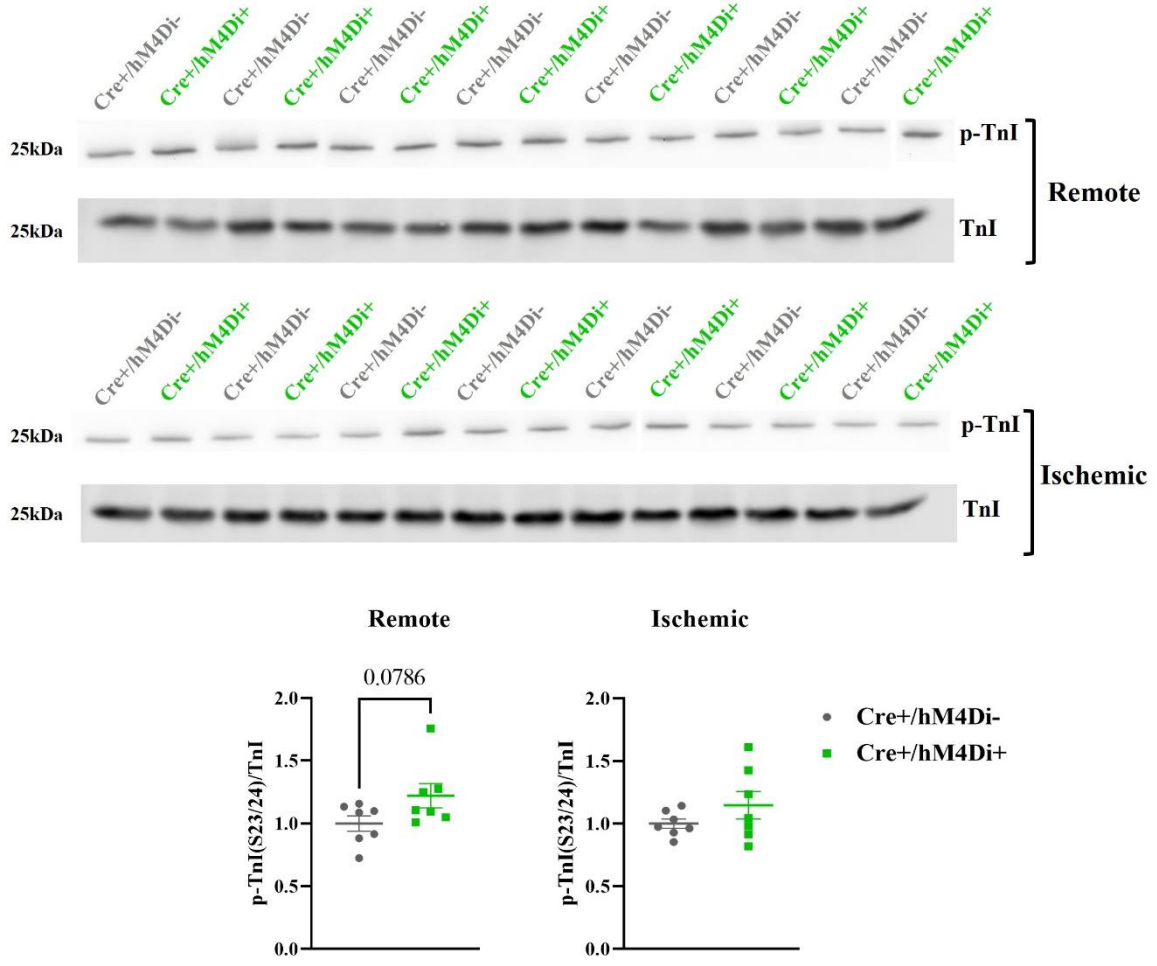

Fig. 46: Acute inhibition of lipolysis trended to reduce phosphorylation of TnI (s23/24) in remote zone after 30 min of reperfusion. Western blot analysis of TnI and p-TnI (s23/24) in remote and ischemic zones after 30 min reperfusion. n = 7, mean ± SEM, unpaired, two-tailed t-test. TnI: Troponin I.

4 Discussion

4.1 Cardiac ischemia induces changes in subcutaneous white adipose tissue

Myocardial infarction (MI), which is due to reduced blood flow in a coronary artery of the heart and leads to damage of myocardium has strong systemic implications. Several factors such as decreased cardiac output, pain, distress and death of cardiomyocytes result in the elevation of circulating catecholamine levels (Valori et al. 1967). The elevated catecholamine levels impact on different organs including adipose tissue and result there in increased lipolysis (Schreiber et al. 2019). Due to the close crosstalk between the heart and adipose tissue, adipose tissue and lipolysis has been suggested as therapeutic target in cardiac pathologies (Smeir et al. 2021). While several studies investigated lipolysis in the context of pressure overload induced heart failure, little is known about the impact of MI in adipose tissue beyond the acute stimulation. In this study, C57Bl/6J male mice went through sham or cardiac ischemic closed-chest operation, and increased lipolysis could be proven by upregulated NEFA levels after 30 min of reperfusion by Heba Zabri, which is in line with the published data (Yue et al. 2003; Oliver 2014). The weight of white adipose tissue was analyzed during the reperfusion phase for up to 28 d of reperfusion, however cardiac ischemia did not induce any weight change in visceral or subcutaneous depots (Fig. 13B). As well known, white adipose tissue is subdivided into subcutaneous and visceral depots. Visceral adiposity has been demonstrated to be an important trigger in activating several pathways of metabolic syndromes (Matsuzawa et al. 2011; Pekgor et al. 2019). However, according to our findings, MI in a lean mouse model mainly induces alterations in the subcutaneous white adipose tissue. The alterations include:

1) Morphological changes in subcutaneous white adipose tissue as small adipocyte size, browning and increased MAC-2^+ macrophage infiltration. More formation of crown-like structures can be found in visceral white adipose tissue.
2) Reduced lipogenesis in subcutaneous white adipose tissue as shown by reduced lipogenesis-relevant gene expression.
3) Reduction in adipokine gene expression mainly in the subcutaneous depot.

4.1.1 Cardiac ischemia induces morphological changes in subcutaneous white adipose tissue

The morphological analysis of white adipose tissue first revealed a sustained reduction of adipocyte size in subcutaneous depot (Fig. 15A). The adipocyte size distribution showed the trend towards smaller adipocytes was getting stronger during the reperfusion phase, animals at day 28 had the maximal number of small adipocytes and the minimal number of large adipocytes (Fig. 15B). This finding was associated with an upregulated ATGL gene expression, which started to show a trend of increase after 7 d and was significantly increased after 28 d (Fig. 15D). The reduction of adipocyte size and upregulation of ATGL gene expression are in line with the previous knowledge that cardiac ischemia induced adrenergic stimulation, which stimulates lipolysis and thereby results in smaller lipid droplets and smaller adipocyte size due to lipid cleavage (Schreiber et al. 2019). However, according to my data cardiac ischemia induces lipolysis not only acutely but also has chronical effects.

Next to size reduction a large number of subcutaneous adipocytes were shown to be multilocular, which is the typical feature of brown adipocytes. These beige or brite (brown-in white) adipocytes are located in white adipose tissue but share the same phenotype as brown adipocytes, which have a high number of mitochondria and can be detected by high expression of UCP1 (Bargut et al. 2017). Recent studies indicate that the browning process starts in response to certain stimuli such as exercise and cold exposure, which activate directly the SNS to release catecholamines that stimulate β_3-adrenergic receptors (Scheel et al. 2022). The browning process is more prone to start in subcutaneous depots since the adipocytes there are predominantly smaller and are much easier to get differentiated (Gustafson and Smith 2015). In this study, the browning in subcutaneous depot was confirmed by upregulated UCP1 expression at protein level (Fig. 16). The most likely explanation for browning of subcutaneous white adipose tissue in this study is the acute β_3-adrenergic stimulation due to cardiac ischemia since control mice underwent anesthesia and sham operation in the same manner as cardiac ischemic operated mice, which revealed that the browning was not due to other experimental procedures like surgical trauma (Longchamp et al. 2016). In addition, previous studies demonstrated that natriuretic peptides, which are secreted from cardiomyocytes and highly released after acute MI, promote browning in the same manner as adrenaline by activating mTORC1 (Liu et al. 2018; Durak-Nalbantić et al. 2012).

Histological analysis also revealed in this study an increased infiltration of MAC-2^+ macrophages in subcutaneous depot and formation of crown-like structures in visceral depot after 7 d of reperfusion (Fig. 19). It has long been known that obesity of adipose tissue is often associated with the appearance of inflammation as M1-like macrophages which are the main driver of inflammation infiltrate adipose tissue. A previous study has demonstrated that macrophage infiltration was found in leptin-deficient and leptin receptor-deficient induced obese mice (Xu et al. 2003). In our mouse model, both in subcutaneous and visceral depot during the reperfusion phase for up to after 28 d (Fig. 13B), leptin gene expression was significantly downregulated after 7 d of reperfusion in subcutaneous depot, which was in line with the observation of increased macrophage number. Moreover, to investigate if the adipose tissue inflammation after MI was a persistent effect, the number of macrophages after 28 d of reperfusion was analyzed as well. In 28 d mice, no difference in inflammation was revealed in subcutaneous depot between cardiac ischemic and sham operated mice, which was also in line with the unchanged leptin gene expression after 28 d of reperfusion (Fig. 21). Our study confirmed again a correlation between macrophage infiltration and reduced leptin secretion.

FFAs are important extracellular and intracellular molecules and are thought to be important for remodeling of adipose tissue, stimulated lipolysis leads to increased amount of FFAs, previous studies showed that acutely stimulated lipolysis induced by β-adrenergic stimulation is closely linked with accumulation of adipose tissue macrophages (Mottillo et al. 2007; Morris et al. 2011). Cardiac ischemia leads to increased β-adrenergic stimulation, which is one of the strongest stimuli for lipolysis in white adipose tissue, in our ischemic mice model, more macrophages were found after cardiac ischemia and 7 d of reperfusion, this finding was in line with the published data from previous studies. Furthermore, another study from 2010 revealed that after stimulation of lipolysis, the inflammatory profile of white adipose tissue was reduced again after 3 weeks in mice, in which the lipolysis was induced by caloric restriction (Li et al. 2010). Even if in this mice model, the lipolysis was induced by caloric restriction, this published data was in line with our finding that the macrophage number was significantly increased after 7 d of reperfusion but showed no difference again after 28 d (Fig. 19). So, our data validated again the relationship between lipolysis and the accumulation of macrophages: cardiac ischemia stimulates lipolysis and thereby induces the accumulation of macrophages, however, this immune response changes dynamically during the reperfusion phase. Lipolysis induced accumulation of macrophages

was more profound in subcutaneous depot, a slight increased number of macrophages in visceral depot was mainly due to the formation of crown-like structures, which are formed by dead or dying adipocytes surrounded by macrophages and serve as a histological marker of local inflammation. The previous study indicated that crown-like structures are prevalent in visceral depot compare with subcutaneous depot, which was also in line with our finding (Murano et al. 2008).

4.1.2 Cardiac ischemia reduces lipogenesis in subcutaneous white adipose tissue

As the balance between lipolysis and lipogenesis is an important determinant for fat build-up and lipolysis was proven to be upregulated due to cardiac ischemia, the investigation of lipogenesis in the different depots was of interest. Lipogenesis encompassing fatty acid synthesis and subsequent triglyceride synthesis takes place in liver and adipose tissue. In adipose tissue the expression of lipogenic genes is mostly mediated by the transcription factors SREBP-1 and PPAR-γ (Kersten 2001). In our study, the gene expression of these two transcription factors was unchanged (Fig. 17 and 18), which is in line with a previous study where transgenic mice with overexpression of SREBP-1c only markedly elevated cholesterol metabolism, and genes regarding lipogenesis stayed unchanged in white adipose tissue (Shimomura et al. 1998). Despite unchanged gene expression of transcription factors, the reduced expression of downstream genes of SREBP-1 and PPAR-γ still indicated a reduced lipogenesis after MI in subcutaneous depot (Fig. 18). The gene expression of fatty acid synthase (FASN) and diacylglycerol O-acyltransferase 2 (DGAT2), which catalyze fatty acid synthesis both trended to be downregulated after cardiac ischemia and 24 h of reperfusion in subcutaneous depot. This change in gene expression pattern revealed that the lipogenic reaction to cardiac ischemia was fast and transient, since the gene expression went back to baseline after 7 d and 28 d of reperfusion (Fig. 18).

In addition to the synthesis of fatty acids from non-lipid precursor, namely a process called *de novo* lipogenesis, lipoprotein lipase, which is partly secreted from adipocytes and is an enzyme responsible for the degradation of triglyceride-rich lipoproteins in the intraluminal space of capillaries, also mediates fatty acids uptake and is transcriptional regulated by PPAR-γ (Bartelt et al. 2013; Wang and Eckel 2009). In our study, the gene expression of

LPL was reduced after 24 h of reperfusion and still trended to be reduced after 7 d and 28 d, this was in line with persistent smaller adipocytes in subcutaneous depot (Fig. 18).

Interestingly, reduced lipogenesis together with increased lipolysis and increased browning are hallmarks of adipose tissue found in cancer patients (Weber et al. 2022). This might indicate that cardiac ischemia re-modulates white adipose tissue in an unfavorable manner.

4.1.3 Cardiac ischemia reduces adipokine expression in subcutaneous white adipose tissue

Adipose tissue is not only an organ storing fat and supplying energy, but is also regarded as an important endocrine organ which secretes a large number of cytokines and adipokines. To investigate whether and how cardiac ischemia modulates adipokine expression pattern will help to better understand the metabolic status of the body after cardiac ischemia. Our study revealed a reduction of adipokine expression after cardiac ischemia especially in the subcutaneous depot.

Adiponectin is an adipokine primarily produced in adipose tissue which regulates lipid metabolism and has anti-inflammatory effects (Nguyen 2020). Previous studies indicated that adiponectin promoted triglyceride accumulation and suppressed lipolysis in adipocytes (Fu et al. 2005; Wedellová et al. 2011). In my thesis, an increased lipolysis and decreased lipogenesis were already revealed in subcutaneous depot of cardiac ischemic operated mice, which matches to the reduced adipokine expression after 24 h of reperfusion and still trended to be downregulated after 7 d (Fig. 21). In addition, adiponectin was reported to be cardioprotective and directly related to myocardial infarction. High plasma adiponectin levels are revealed to be associated with a lower risk of MI (Pischon et al. 2004), and adiponectin levels were found to rapidly decrease after acute MI during the first 72 hours and nearly normalize again after 7 days in humans (Kojima et al. 2003). Our study not only validated this finding, but also suggested that the reduction of adiponectin secretion was mainly from the subcutaneous depot. Moreover, the protective effect of adiponectin on the heart is also reflected in reducing infarct size and inhibiting apoptosis (Shibata et al. 2005). In addition, the nuclear receptor PPAR-γ was indicated as a key transcriptional factor that controlled adipokine gene expression including adiponectin (Guo et al. 2017; Iwaki et al. 2003). LPL, which is the downstream target of PPAR-γ showed a reduction in gene expression in subcutaneous depot of cardiac ischemic operated mice after 24 h of reperfusion

and trended to be downregulated after 7 d (Fig. 18). The gene expression data of adiponectin and LPL fit to each other spatially and temporally in my thesis.

Next to adiponectin, leptin, which regulates long-term energy balance was also shown to be cardioprotective. Leptin resistance promotes impaired cardiac metabolism, increases fibrosis, vascular dysfunction and enhances inflammation (Poetsch et al. 2020).Circulating leptin levels were found to be elevated in humans at day 2 to day 3 after MI (Fujimaki et al. 2001; Khafaji et al. 2012). In our mice model, leptin was reduced in the subcutaneous depot at transcriptional level and it seemed that the reduction neither react to cardiac ischemia rapidly nor very chronically, since the reduced leptin expression was only found after 7 d of reperfusion (Fig. 21). In addition, the lack of leptin was demonstrated to closely link with macrophage infiltration in adipose tissue. Therefore, the reduced gene expression data of leptin after 7 d of reperfusion in subcutaneous depot of cardiac ischemic mice fit to the result of macrophage accumulation after 7 d.

Resistin, which is involved in glucose metabolism and insulin signaling was found to have inflammatory profile leading to an increased expression of several other pro-inflammatory cytokines (Milan et al. 2002; Silswal et al. 2005; Gualillo et al. 2007). Resistin was also suggested to show direct association with cardiovascular disease. Several human studies suggested that resistin plays an important role in the pathogenesis and progression of atherosclerosis (Codoñer-Franch and Alonso-Iglesias 2015), clinical studies also demonstrated the positive correlation between high circulating resistin levels and hypertension in humans (Badoer et al. 2015) and high plasma resistin levels were suggested to have an increased risk of myocardial infarction (Weikert et al. 2008). However, the role of resistin after MI is still unclear, as previous studies revealed that plasma levels of resistin were either increased or unchanged in humans (Gruzdeva et al. 2014; Korah et al. 2011). Our study surprisingly revealed a transient reduced resistin expression in both visceral and subcutaneous depot after cardiac ischemia. PRDM16, which is very selectively expressed in brown adipose tissue and therefore serves as a marker of browning, represses white adipose tissue specific genes including resistin through the direct interaction with C-terminal binding proteins (Seale et al. 2007; Kajimura et al. 2008). The browning found in subcutaneous depot after myocardial ischemia and 24 h of reperfusion could help to explain the reduction of resistin seen at the same time point. Myocardial ischemia seemed not to modulate visceral white adipose tissue that much, the formation of crown-like structures which are dead or dying adipocytes surrounded by macrophages was the only change revealed by our study.

So far, no study has revealed any direct association between the formation of CLSs and resistin levels, however, resistin was known to be exclusively secreted by adipocytes in rodents (Rajala et al. 2002). In our mice, more CLSs were seen in the visceral depot after cardiac ischemia and 24 h of reperfusion. CLSs are dead or dying adipocytes surrounded by macrophages, increased CLS number suggests increased number of dead or dying adipocytes. This indicates that less adipocytes can secrete resistin and might help to explain the reduced resistin expression.

4.2 Successful expression of hM4Di in white adipose tissue and its leaky expression

In our study, DREADD expression was induced by using Cre-loxP technique. The adipocyte specific promotor of adiponectin (AdipoQ) was used to drive expression of CreERT2-recombinase, tamoxifen-activated Cre-recombinase could then excise the loxP-flanked STOP codon between CAG-promotor and DREADD construct. Therefore, the hM4Di-receptor and the reporter should only be expressed after Cre-recombinase induction and in an adipocyte specific manner. However, during the analysis of DREADD construct expression, the reporter mCitrine was not only found to be expressed in adipose tissue, but also in other tissues such as heart, liver and skeletal muscle already prior to Cre-recombinase induction (Fig. 24). The Cre-independent expression revealed a leakiness of the STOP codon similar to several previous studies which demonstrated as well the low-level or leaky expression of recombinant proteins in the absence of activated Cre-recombinase (Fischer et al. 2019; Kallunki et al. 2019; Lavin et al. 2020). To further characterize the leaky expression, hM4Di expression level was compared prior to and after Cre-recombinase induction and a much lower mCitrine expression counting around 20 % of that after Cre-recombinase induction was revealed both in gWAT and iWAT in the absence of Cre activity (Fig. 25). One of the big advantages of DREADD system is its two-way selectivity of receptor-agonist pair, even if hM4Di express independent from Cre activity, without applying DREADD agonist 21, the $G_{\alpha i}$ signaling pathway will not be activated and inhibition of lipolysis will not be started. Therefore, without application of the DREADD agonist, the low-level expression of hM4Di in the absence of Cre activity can nearly be ignored.

As a main goal of the thesis was to investigate the implantation of lipolysis on cardiac function after MI, the leaky expression of hM4Di in the heart is of course also of great

concern. G protein-coupled receptors are reported to play key roles in regulating cardiac function. Muscarinic receptors, which are an important family of GPCRs, are present in the heart. Among the five subtypes of muscarinic receptors, M2 and M4 are coupled to Gi and lead to reduced PKA activity, reduced L-type Ca^{2+} channel current in the heart, they suppress as well the hyperpolarization-activated cyclic nucleotide-gated 4 channel (HCN4) and in turn reduce the pacemaker current (Grogan et al. 2023). M2 is demonstrated as the predominant subtype in the human heart and to be essential for stress response in the murine heart, M4 can only be detected at mRNA level but not at protein level in the human heart and the presence of M4 at a functional level in rodents is still unclear (Saternos et al. 2018; Wang et al. 2001; Tomankova et al. 2015). The reporter protein mCitrine was used to measure DREADD-construct expression in adipose tissue after induction of Cre-recombinase and revealed to be the highest in iWAT, high in gWAT, low in BAT and the lowest in the heart. The receptor hM4Di expression in the heart only counts 18 % of that in iWAT at protein level and 2,5 % at mRNA level (Fig. 26A,B). Furthermore, echocardiography analysis showed EF, FAC, EDV, ESV and heart rate were all not altered after receiving DREADD 21 agonist, which revealed the low expression level of $G_{\alpha i}$ protein-coupled receptors in the heart did not have any functional effect (Fig. 26C).

Multiplex analysis revealed that transient inhibition of lipolysis led to significantly reduced circulating insulin levels after MI and 30 minutes of reperfusion (Fig. 36). Insulin is known to be secreted from pancreatic islets and secretion is tightly controlled by GPCRs (Thor 2022). To validate the reduced circulating insulin levels were not due to the leaky expression of hM4Di in the pancreas, hM4Di expression was investigated in the pancreas. Similar to the visible GFP signals seen in other organs, positive GFP signals could also be detected in the pancreas of Cre+/hM4Di+ mice prior to Cre-recombinase induction by western blot analysis (Fig. 37). However, both immunofluorescence staining of anti-HA and qPCR analysis of *hM4Di* revealed negative receptor expression. Wondering if the leakiness mainly led to mCitrine expression, qPCR analysis of hM4Di and mCitrine was performed in Cre-/hM4Di+ and Cre+/hM4Di+ mice after Cre-recombinase introduction. The analysis revealed that the leaky expression of both hM4Di and mCitrine existed, however the leakiness led to 1,9 times higher mCitrine expression than hM4Di. A recent study from Osanai in 2022 demonstrated that the transgene on 3'- site of a P2A sequence is more likely to have Cre-independent expression, which is due to the 5'- site transgene promoter like activity (Osanai et al. 2022). Since the expression of multiple transgenes under control of a single promoter

is often desired, they also suggested that the solution to a large extent reduce the leaky expression was by inclusion of an additional lox-STOP-lox cassette between 3'- site transgene and P2A sequence (Osanai et al. 2022). To investigate if the leakiness might lead to functional difference, an additional control group Cre-/hM4Di+ was included in some experiments. The circulating levels of fatty acids measured by NEFA assay showed a reduction in Cre+/hM4Di+ mice after MI and 30 minutes of reperfusion compared to both control groups, which suggested that the leakiness did not affect the inhibition of lipolysis after MI in white adipose tissue (Fig. 27). Furthermore, the measurement of circulating insulin levels using ELISA revealed no difference between Cre+/hM4Di- and Cre-/hM4Di+ control groups while insulin in circulation still trended to be reduced in Cre+/hM4Di+ mice after MI and 30 minutes of reperfusion, as also observed in multiplex analysis, which suggested again that the leakiness did not functionally disturb insulin secretion (Fig. 38).

4.3 The effect of transient inhibition of lipolysis using DREADD system after MI on white adipose tissue

Myocardial ischemia has been proved to modulate white adipose tissue in a depot-specific manner. To investigate, if acute inhibition of lipolysis after MI by using DREADD system induces any changes in white adipose tissue, key findings from the sham vs. ischemia study were also investigated in DREADD animals. Cardiac ischemia reduces adipocyte size in subcutaneous depot due to increased lipolysis during and after MI. The cell size distribution in gWAT and iWAT is comparable with that of ischemic C57BI/6J mice, whereas no difference was revealed between hM4Di+ mice and control mice (Fig. 30). This indicates that acute inhibition of lipolysis was not able to reverse the effect in iWAT caused by myocardial ischemia. Furthermore, the cell morphology was also similar to that of ischemic C57BI/6J mice. The adipocytes in gWAT showed typical white adipocyte morphology, some of the adipocytes from inguinal depot showed multilocular phenotype which is the typical character of browning due to cardiac ischemia induced increased β-adrenergic stimulation (Wang et al. 2022). Acute inhibition of lipolysis partly reduced browning levels revealed by western blot analysis of anti-UCP1 (p-value = 0,1754) and validated by qPCR analysis of one of the browning markers *Cox8b* (p-value = 0,0721) (Fig. 31). The relationship between lipolysis and browning is still unclear, however, some studies demonstrated that the appearance of browning goes often along with an increased lipolysis. A previous study

mentioned that burn injury induced browning of white adipose tissue as well as increased lipolysis (Abdullahi et al. 2019). Another recent study reported that an activation of dopamine receptor D1, which is also a catecholamine receptor, increased cAMP accumulation, the activity of PKA, the phosphorylation of HSL and the expression levels of ATGL, which all in turn induced an increased lipolysis and browning (Yu et al. 2022). Furthermore, a reduced browning level was found in adipose tissue-specific ATGL knockout murine model from a previous study (Kaur et al. 2021). From this, it is reasonable to suspect that the increased lipolysis during and after MI also partly results in the browning of white adipose tissue, and an inhibition of lipolysis after MI is able to reduce the browning levels.

Another morphological change induced by cardiac ischemia is the increased infiltration of MAC-2^+ macrophages in subcutaneous depot after MI and 7 days of reperfusion. To investigate if acute lipolysis is responsible for inflammation, the same experiment was performed in DREADD mice after MI and 7 days of reperfusion. Both hM4Di+ mice and control mice showed more MAC-2^+ macrophages, which were comparable with the number of ischemic C57BI/6J mice, but no difference was detected between these two groups (Fig.32). This suggests that the acute inhibition of lipolysis was not able to reverse the effect caused by cardiac ischemia. Similar to the findings regarding macrophage infiltration, acute inhibition of lipolysis also did not affect lipogenesis after MI and 24 hours of reperfusion, which reduced in subcutaneous depot due to cardiac ischemia (Fig. 33).

The expression profile of several adipokines were reduced after myocardial ischemia in iWAT, to investigate if acute inhibition of lipolysis could reverse or further alter the adipokine expression, the adipokines were investigated at gene expression level. No difference was revealed between hM4Di positive mice and control group after MI and 24 hours of reperfusion (Fig. 34). In view of reduced NEFA levels in hM4Di positive mice after 30 minutes of reperfusion I wondered if adipokine gene expression could be directly affected by NEFA levels. Indeed, the proinflammatory adipokine resistin was found to be less expressed in iWAT, however, this reduction did not lead to reduced circulating levels. (Fig. 35 and 36). A previous study demonstrated that resistin induced lipolysis in mice *in vivo*, in cultured mouse adipose tissue explants as well as in cultured human subcutaneous adipocytes (Ort et al. 2005). In our hM4Di positive mice, lipolysis was inhibited after 30 minutes of reperfusion, thus a reduced resistin mRNA expression level in adipose tissue could be expected. Furthermore, previous studies also showed that the circulating resistin

levels were in many cases differently altered from the mRNA expression level of resistin in adipose tissue (Rajala et al. 2004; Barnes und Miner 2009).

4.4 Acute inhibition of lipolysis using DREADD system after MI improves cardiac systolic function

Myocardial infarction is a disease with systemic implications that can impact on many organs including adipose tissue (Valori et al. 1967). The increased β-adrenergic stimulation due to reduced cardiac output is one of the strongest stimuli of the peripheral lipolysis (Lymperopoulos et al. 2013b). Thereby, adipose tissue has been discussed as a promising therapeutic target to improve cardiac function after MI. In our study, we used an inducible adipocyte specific inhibitory DREADD model to spatio-temporally inhibit lipolysis after MI. Echocardiographic analysis revealed an improved cardiac function after 7 d of reperfusion, which was depicted by increased EF, FAC and SV (Fig. 28). We could exclude that the improved cardiac systolic function was due to a reduction in aortic pressure or scar size, we suspected it was because of an intrinsic enhanced contractile function (Fig. 28 and 29), hence we suspected a better contractile function of the remote myocardium in these animals. In terms of circulating NEFA levels, the most profound adipocyte-related effect was found after 30 min of reperfusion (Fig. 27) and multiplex analysis revealed a significantly reduced circulating insulin level at this time point in hM4Di expressing mice (Fig. 36). As well known, the heart is the unique organ that continuously pumps without any fatigue and a large amount of ATP needs to be generated to fuel the contractile apparatus and ionic pumps (Abel 2021). Therefore, myocardial metabolism is highly dependent on substrate availability, and changes in circulating insulin can deeply influence the cardiac metabolism by influencing the substrate uptake by cardiomyocytes (Abel 2021).

In the heart, insulin signaling is transduced to downstream pathways via PI3K and AKT. The binding of insulin to insulin receptors (IRs) or insulin-like growth factor 1 receptors (IGF1Rs) phosphorylates insulin receptor substrates 1/2 (IRS1/2) and then activates PI3K, which phosphorylates AKT. A higher AKT activity promotes the translocation of GLUT4 and CD36, which respectively conduct the glucose and fatty acid uptake (Abel 2004, 2021), AKT also directly and indirectly regulates several other downstream molecules such as FoxO1, GSK3, TSC1/2 and mTORC1 and thereby modulates many cellular processes (Skurk et al. 2005; Abel 2021). To investigate insulin signaling in the heart, the mRNA levels

of transcription factor SREBP-1C (*Srebp-1c*), which is known to be indirectly regulated by AKT through mTORC1, and its downstream genes LPL (*Lpl*) and FASN (*Fasn*) were analyzed, however the transcriptional level was unchanged (Fig. 39). Furthermore, gene expression analysis revealed an unaltered mRNA level of fatty acid transporter CD36 but a reduced mRNA level of glucose transporter GLUT4 in remote area of the heart (Fig. 39). Activated insulin signaling is known to promote the translocation of GLUT4 from intracellular compartment to the plasma membrane (Abel 2004), nevertheless, it is still unclear if insulin signaling can impact on the expression level of GLUT4. Protein kinase A (PKA), a central regulator of cardiac performance, was demonstrated to inhibit insulin-induced GLUT4 expression and translocation by regulating GSK2 activity (Mangmool et al. 2016a).

Western blot analysis of phosphorylation of PKA downstream targets revealed upregulated PKA-activity in both ischemic and remote zones of hM4Di expressing mice (Fig. 40 and 41). In both skeletal muscle and adipocytes, insulin is known to decrease cAMP-dependent activity by activating PDE3B (Brink et al. 1998; Yang and Yang 2016). The circulating insulin level was significantly reduced in hM4Di expressing mice after 30 min of reperfusion. In addition, also NEFA were suggested to suppress PKA activity in previous studies. Even though PKA is well known to promote lipolysis in adipocytes by directly activate HSL and indirectly activate ATGL, excessive exogenous fatty acids can suppress PKA activity by suppressing adenylyl cyclase (AC) activity and cAMP production (Mottillo und Granneman 2011a). Interestingly, I could also show an increased PKA-activity in iWAT (Fig. 43), which is in line with reduced NEFA level and its suppressive effect on PKA activity. Since PKA plays an important role in modulating cardiac contractile function, we speculated that the increased PKA activity is the underlying cause for improved cardiac function by inhibition of lipolysis.

Phospholamban (PLN) is a downstream target of PKA, which is highly involved in regulating cardiac contractile function. (Takahashi et al. 2006). SERCA is an ATPase that pumps Ca^{2+} from the cytosol to the sarcoplasmic reticulum, PLN suppresses SERCA activity under basal state. Once it gets phosphorylated by PKA at serine 16, the inhibition of SERCA activity is relieved and sarcoplasmic reticulum Ca^{2+} load is increased called positive lusitropic effect (Takahashi et al. 2006; Masterson et al. 2011). The increased SERCA activity enables to pump Ca^{2+} from intracellular compartment into sarcoplasmic reticulum and Ca^{2+} is again released into intracellular compartment via ryanodine receptor during the

next contraction cycle. Increased cytosolic Ca^{2+} concentration promotes the myocardial contractility called positive inotropic effect. Defective Ca^{2+} uptake by SERCA and release by ryanodine receptor are both demonstrated as a hallmark of heart failure (Hasenfuss et al. 1994; Wehrens et al. 2003). Gene expression analysis of PLN (*Pln*) showed a reduction in *Pln* gene expression in remote zone of heart of hM4Di expressing mice after 30 min of reperfusion, however, this reduction was not seen at protein expression level (Fig. 45). In line with increased PKA activity, the phosphorylation of PLN was increased in remote zone (Fig. 45), which confirmed the view that enhanced PKA activity found in hearts of hM4Di expressing mice was associated directly with a better relaxation and indirectly with an improved contractility.

PKA phosphorylates another downstream target troponin I at serine 23 and 24, which prevents the binding of actin to myosin during cardiac muscle relaxation. The phosphorylation of troponin by PKA causes its conformational change, which alters the myofilament response to Ca^{2+}. Ca^{2+}- binding enables the formation of crossbridge by actin and myosin and allows the contraction (Betts et al. 2013). In our study, even though a statistical difference was not detectable, the phosphorylation of troponin I trended to be upregulated in remote zone of heart of hM4Di expressing mice (Fig. 46). This validated again the increased phosphorylation of PKA and suggested an improved contractile function due to direct positive lusitropic effect and indirect positive inotropic effect.

4.5 Conclusion

MI-induced peripheral lipolysis modulates white adipose tissue in a depot-specific manner, as the subcutaneous depot gets more affected than the visceral depot. The changes of subcutaneous white adipose tissue include: The adipocytes size of subcutaneous depot decreases during the reperfusion phase suggesting an increased lipolysis after MI. The effect is detected as early as 24 h of reperfusion, stronger after 7 d and most pronounced after 28 d. This goes along with browning of white adipocytes. Increased MAC-2+ macrophage infiltration after 7 d of reperfusion was also observed in the subcutaneous depot. Reduced lipogenic gene expression profile as well as reduced adipokine gene expression were shown in subcutaneous depot too. Taken together, the alterations found after MI in the subcutaneous depot reveal that lipolysis after MI is not only stimulated acutely but also chronically and further impacts adipose tissue in terms of inflammation and endocrine function.

The acute inhibition of lipolysis using inducible adipocyte specific inhibitory DREADD system was able to partly reverse the browning effect after MI in subcutaneous depot, but could not reverse or change the other effects seen in white adipose tissue. The inhibitory DREADDs, which should be adipocyte-specific and inducible expressed, express at a low level prior to 4-hydrotamoxifen induction and in other organs due to a leakiness of the stop codon. Nevertheless, the leakiness did not show any major functional effect in heart, adipose tissue or pancreas. The inhibitory DREADD system enables an acute suppression of lipolysis and thus an acutely reduced circulating NEFA level, which goes along with a reduced circulating insulin level. The following mechanism is speculated: Reduced circulating NEFA and insulin level promote the accumulation of cAMP in cardiomyocytes and thereby increase PKA activity. Increased PKA activity suppresses the gene expression of glucose transporter GLUT4, and promotes the phosphorylation of PLN. Increased PLN phosphorylation enhances SERCA activity and stimulates the calcium flux between sarcoplasmic reticulum and the cytoplasm, the increased calcium flux in cardiomyocytes indirectly improves contractile function (Fig. 48).

The improved systolic function after 7 d of reperfusion is neither due to reduced aortic pressure nor reduced fibrotic scar tissue. Despite the lipolysis in adipose tissue is only acutely inhibited, the acute inhibition is enough to increase PKA activity and the phosphorylation of its downstream targets like PLN after 30 min of reperfusion. Increased PLN phosphorylation suggests an enhanced contractile function of cardiomyocytes, and this

enhanced contractile function is suggested to be the main reason for improved cardiac systolic function at later reperfusion phase.

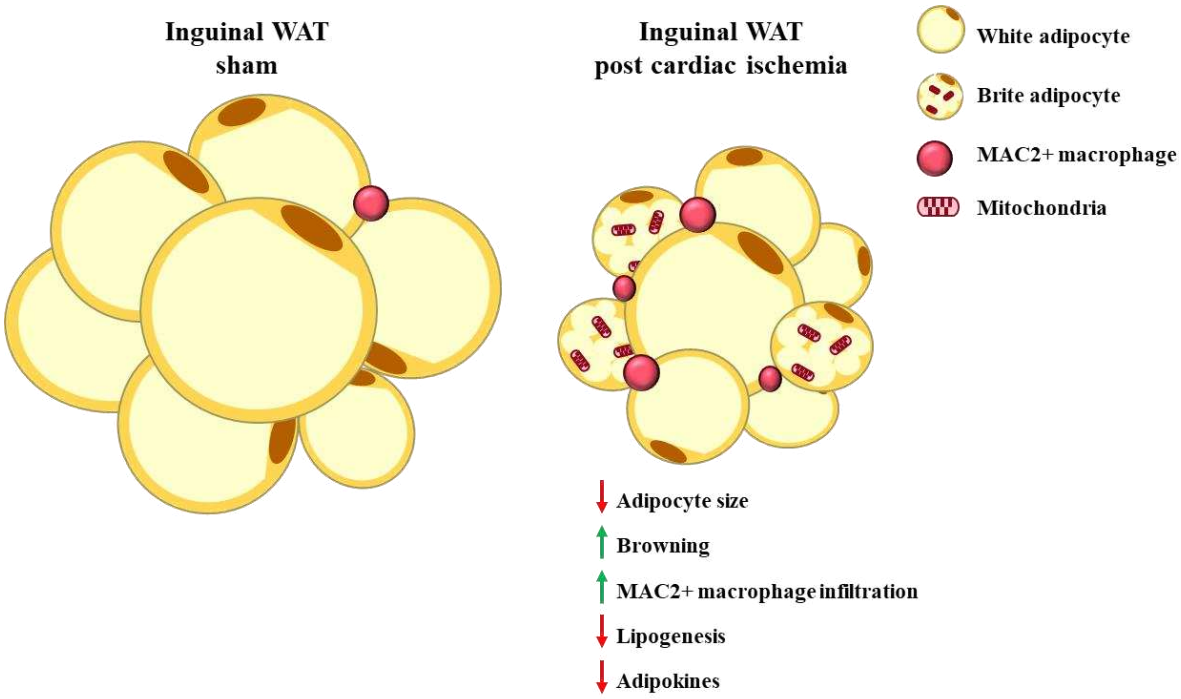

Fig. 47: Cardiac ischemia modulates predominantly subcutaneous white adipose tissue. Cardiac ischemia induces a series of morphological changes in subcutaneous depot (inguinal WAT) including: smaller adipocyte size, browning of white adipocyte and infiltration of MAC2+ macrophages. Lipogenesis and adipokines are reduced by cardiac ischemia at a gene expression level. Brite: Brown-in-white. WAT: white adipose tissue.

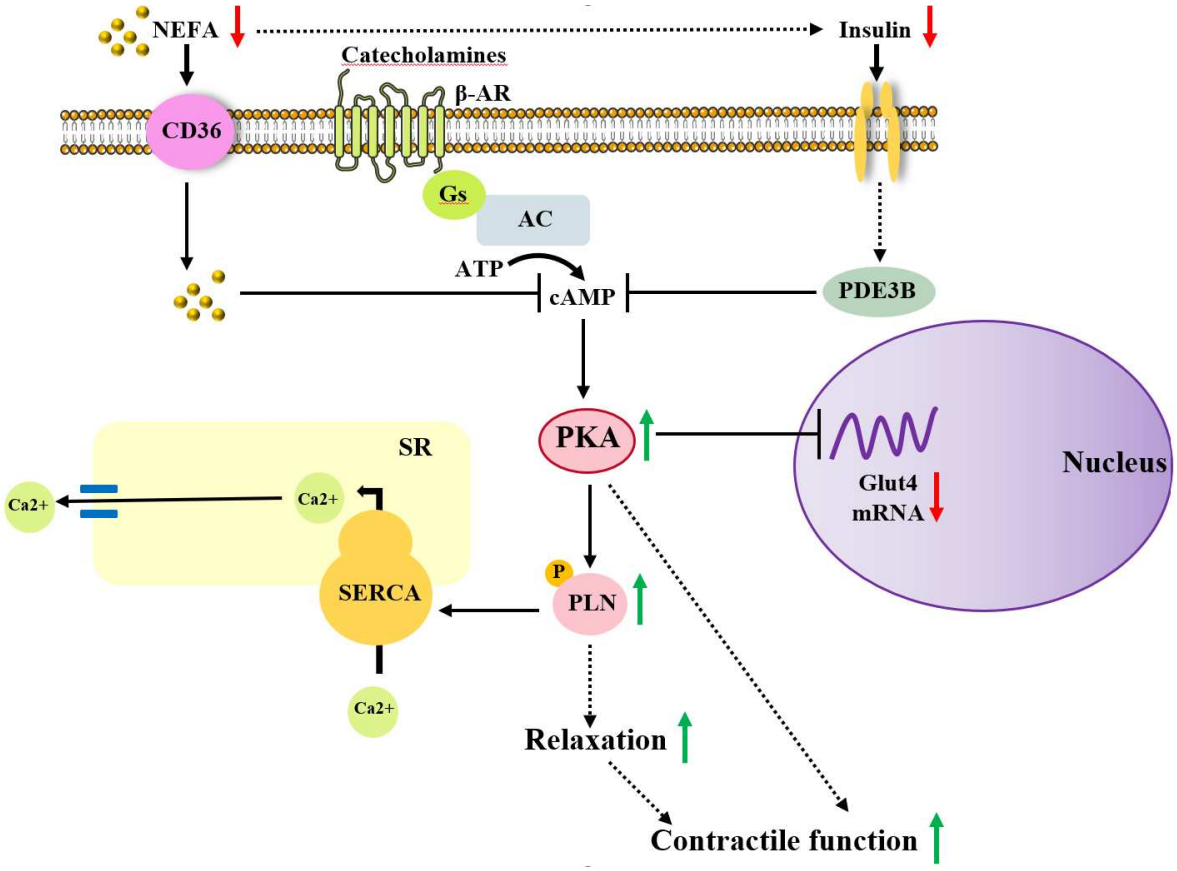

Fig. 48: Acute inhibition of lipolysis after MI improves cardiac systolic function. Acute inhibition of lipolysis using inducible adipocyte specific inhibitory DREADD system acutely reduced circulating NEFA levels and insulin levels, which increase PKA activity by promoting cAMP accumulation. Enhanced PKA activity suppresses GLUT4 at gene expression level and increases the phosphorylation of PLN. Increased p-PLN is considered to improve relaxation and thereby contractile function by enhancing SERCA activity that promotes Ca^{2+} flux and positive lusitropic and inotropic effects. AC: Adenylyl cyclase. ATP: Adenosine triphosphate. β-AR: β-adrenergic receptor. cAMP: cyclic adenosine monophosphate. CD36: Cluster of differentiation 36. GLUT4: Glucose transporter type 4. mRNA: Messenger ribonucleic acid. NEFA: Non-esterified fatty acids. PDE3B: Phosphodiesterase 3B. PKA: Protein kinase A. PLN: Phospholamban. SERCA: Sarcoendoplasmic reticulum calcium ATPase. SR: Sarcoendoplasmic reticulum.

5 References

Abdullahi, Abdikarim; Samadi, Osai; Auger, Christopher; Kanagalingam, Tharsan; Boehning, Darren; Bi, Sheng; Jeschke, Marc G. (2019): Browning of white adipose tissue after a burn injury promotes hepatic steatosis and dysfunction. In: *Cell death & disease* 10 (12), S. 870. DOI: 10.1038/s41419-019-2103-2.

Abel, E. Dale (2004): Glucose transport in the heart. In: *Frontiers in bioscience : a journal and virtual library* 9, S. 201–215. DOI: 10.2741/1216.

Abel, E. Dale (2021): Insulin signaling in the heart. In: *American journal of physiology. Endocrinology and metabolism* 321 (1), E130-E145. DOI: 10.1152/ajpendo.00158.2021.

Adibi, Peyman; Sadeghi, Masoumeh; Mahsa, Majid; Rozati, Golnaz; Mohseni, Masood (2007): Prediction of coronary atherosclerotic disease with liver transaminase level. In: *Liver international : official journal of the International Association for the Study of the Liver* 27 (7), S. 895–900. DOI: 10.1111/j.1478-3231.2007.01545.x.

Ahima, Rexford S.; Lazar, Mitchell A. (2008): Adipokines and the peripheral and neural control of energy balance. In: *Molecular endocrinology (Baltimore, Md.)* 22 (5), S. 1023–1031. DOI: 10.1210/me.2007-0529.

Armbruster, Blaine N.; Li, Xiang; Pausch, Mark H.; Herlitze, Stefan; Roth, Bryan L. (2007): Evolving the lock to fit the key to create a family of G protein-coupled receptors potently activated by an inert ligand. In: *Proceedings of the National Academy of Sciences of the United States of America* 104 (12), S. 5163–5168. DOI: 10.1073/pnas.0700293104.

Arner, Peter; Langin, Dominique (2014): Lipolysis in lipid turnover, cancer cachexia, and obesity-induced insulin resistance. In: *Trends in endocrinology and metabolism: TEM* 25 (5), S. 255–262. DOI: 10.1016/j.tem.2014.03.002.

Arslan, Fatih; Kleijn, Dominique P. de; Pasterkamp, Gerard (2011): Innate immune signaling in cardiac ischemia. In: *Nature reviews. Cardiology* 8 (5), S. 292–300. DOI: 10.1038/nrcardio.2011.38.

Assimacopoulos-Jeannet, F.; Brichard, S.; Rencurel, F.; Cusin, I.; Jeanrenaud, B. (1995): In vivo effects of hyperinsulinemia on lipogenic enzymes and glucose transporter expression in rat liver and adipose tissues. In: *Metabolism: clinical and experimental* 44 (2), S. 228–233. DOI: 10.1016/0026-0495(95)90270-8.

Baars, Theodor; Neumann, Ursula; Jinawy, Mona; Hendricks, Stefanie; Sowa, Jan-Peter; Kälsch, Julia et al. (2016): In Acute Myocardial Infarction Liver Parameters Are Associated With Stenosis Diameter. In: *Medicine* 95 (6), e2807. DOI: 10.1097/MD.0000000000002807.

Badoer, Emilio; Kosari, Samin; Stebbing, Martin J. (2015): Resistin, an Adipokine with Non-Generalized Actions on Sympathetic Nerve Activity. In: *Frontiers in physiology* 6, S. 321. DOI: 10.3389/fphys.2015.00321.

Bargut, Thereza Cristina Lonzetti; Aguila, Marcia Barbosa; Mandarim-de-Lacerda, Carlos Alberto (2016): Brown adipose tissue: Updates in cellular and molecular biology. In: *Tissue & cell* 48 (5), S. 452–460. DOI: 10.1016/j.tice.2016.08.001.

Bargut, Thereza Cristina Lonzetti; Souza-Mello, Vanessa; Aguila, Marcia Barbosa; Mandarim-de-Lacerda, Carlos Alberto (2017): Browning of white adipose tissue: lessons from experimental models. In: *Hormone molecular biology and clinical investigation* 31 (1). DOI: 10.1515/hmbci-2016-0051.

Barnes, K. M.; Miner, J. L. (2009): Role of resistin in insulin sensitivity in rodents and humans. In: *Current protein & peptide science* 10 (1), S. 96–107. DOI: 10.2174/138920309787315239.

Barquissau, V.; Beuzelin, D.; Pisani, D. F.; Beranger, G. E.; Mairal, A.; Montagner, A. et al. (2016): White-to-brite conversion in human adipocytes promotes metabolic reprogramming towards fatty acid anabolic and catabolic pathways. In: *Molecular metabolism* 5 (5), S. 352–365. DOI: 10.1016/j.molmet.2016.03.002.

Bartelt, Alexander; Weigelt, Clara; Cherradi, M. Lisa; Niemeier, Andreas; Tödter, Klaus; Heeren, Joerg; Scheja, Ludger (2013): Effects of adipocyte lipoprotein lipase on de novo lipogenesis and white adipose tissue browning. In: *Biochimica et biophysica acta* 1831 (5), S. 934–942. DOI: 10.1016/j.bbalip.2012.11.011.

Bates, Rhiannon; Huang, Wei; Cao, Lei (2020): Adipose Tissue: An Emerging Target for Adeno-associated Viral Vectors. In: *Molecular therapy. Methods & clinical development* 19, S. 236–249. DOI: 10.1016/j.omtm.2020.09.009.

Bertero, Edoardo; Maack, Christoph (2018): Metabolic remodelling in heart failure. In: *Nature reviews. Cardiology* 15 (8), S. 457–470. DOI: 10.1038/s41569-018-0044-6.

Betts, J. Gordon; Desaix, Peter; Johnson, Eddie; Johnson, Jody E.; Korol, Oksana; Kruse, Dean et al. (2013-): Anatomy & physiology. Houston, Texas: OpenStax College, Rice University.

Betz, Matthias J.; Enerbäck, Sven (2015): Human Brown Adipose Tissue: What We Have Learned So Far. In: *Diabetes* 64 (7), S. 2352–2360. DOI: 10.2337/db15-0146.

Bokarewa, Maria; Nagaev, Ivan; Dahlberg, Leif; Smith, Ulf; Tarkowski, Andrej (2005): Resistin, an adipokine with potent proinflammatory properties. In: *Journal of immunology (Baltimore, Md. : 1950)* 174 (9), S. 5789–5795. DOI: 10.4049/jimmunol.174.9.5789.

Boufenzer, Amir; Lemarié, Jérémie; Simon, Tabassome; Derive, Marc; Bouazza, Youcef; Tran, Nguyen et al. (2015): TREM-1 Mediates Inflammatory Injury and Cardiac Remodeling Following Myocardial Infarction. In: *Circulation research* 116 (11), S. 1772–1782. DOI: 10.1161/CIRCRESAHA.116.305628.

Bourlier, V.; Zakaroff-Girard, A.; Miranville, A.; Barros, S. de; Maumus, M.; Sengenes, C. et al. (2008): Remodeling phenotype of human subcutaneous adipose tissue macrophages. In: *Circulation* 117 (6), S. 806–815. DOI: 10.1161/CIRCULATIONAHA.107.724096.

Brink, J.; Sherman, M. B.; Berriman, J.; Chiu, W. (1998): Evaluation of charging on macromolecules in electron cryomicroscopy. In: *Ultramicroscopy* 72 (1-2), S. 41–52. DOI: 10.1016/s0304-3991(97)00126-5.

Chait, Alan; Hartigh, Laura J. den (2020): Adipose Tissue Distribution, Inflammation and Its Metabolic Consequences, Including Diabetes and Cardiovascular Disease. In: *Frontiers in cardiovascular medicine* 7, S. 22. DOI: 10.3389/fcvm.2020.00022.

Chang, W. H.; Lin, S. K.; Lane, H. Y.; Wei, F. C.; Hu, W. H.; Lam, Y. W.; Jann, M. W. (1998): Reversible metabolism of clozapine and clozapine N-oxide in schizophrenic patients. In: *Progress in neuro-psychopharmacology & biological psychiatry* 22 (5), S. 723–739. DOI: 10.1016/s0278-5846(98)00035-9.

Chao, L.; Marcus-Samuels, B.; Mason, M. M.; Moitra, J.; Vinson, C.; Arioglu, E. et al. (2000): Adipose tissue is required for the antidiabetic, but not for the hypolipidemic, effect of thiazolidinediones. In: *J. Clin. Invest.* 106 (10), S. 1221–1228. DOI: 10.1172/JCI11245.

Cheong, Lai Yee; Xu, Aimin (2021): Intercellular and inter-organ crosstalk in browning of white adipose tissue: molecular mechanism and therapeutic complications. In: *Journal of molecular cell biology* 13 (7), S. 466–479. DOI: 10.1093/jmcb/mjab038.

Cinti, Saverio (2012): The adipose organ at a glance. In: *Disease models & mechanisms* 5 (5), S. 588–594. DOI: 10.1242/dmm.009662.

Clifford, G. M.; Londos, C.; Kraemer, F. B.; Vernon, R. G.; Yeaman, S. J. (2000): Translocation of hormone-sensitive lipase and perilipin upon lipolytic stimulation of rat adipocytes. In: *The Journal of biological chemistry* 275 (7), S. 5011–5015. DOI: 10.1074/jbc.275.7.5011.

Codoñer-Franch, Pilar; Alonso-Iglesias, Eulalia (2015): Resistin: insulin resistance to malignancy. In: *Clinica chimica acta; international journal of clinical chemistry* 438, S. 46–54. DOI: 10.1016/j.cca.2014.07.043.

Cohen, Paul; Levy, Julia D.; Zhang, Yingying; Frontini, Andrea; Kolodin, Dmitriy P.; Svensson, Katrin J. et al. (2014): Ablation of PRDM16 and beige adipose causes metabolic dysfunction and a subcutaneous to visceral fat switch. In: *Cell* 156 (1-2), S. 304–316. DOI: 10.1016/j.cell.2013.12.021.

Cypess, Aaron M.; Weiner, Lauren S.; Roberts-Toler, Carla; Franquet Elía, Elisa; Kessler, Skyler H.; Kahn, Peter A. et al. (2015): Activation of human brown adipose tissue by a β3-adrenergic receptor agonist. In: *Cell metabolism* 21 (1), S. 33–38. DOI: 10.1016/j.cmet.2014.12.009.

D'Souza, Kenneth; Nzirorera, Carine; Kienesberger, Petra C. (2016): Lipid metabolism and signaling in cardiac lipotoxicity. In: *Biochimica et biophysica acta* 1861 (10), S. 1513–1524. DOI: 10.1016/j.bbalip.2016.02.016.

Duncan, Robin E.; Ahmadian, Maryam; Jaworski, Kathy; Sarkadi-Nagy, Eszter; Sul, Hei Sook (2007): Regulation of lipolysis in adipocytes. In: *Annual review of nutrition* 27, S. 79–101. DOI: 10.1146/annurev.nutr.27.061406.093734.

Dunn, G. D.; Hayes, P.; Breen, K. J.; Schenker, S. (1973): The liver in congestive heart failure: a review. In: *The American journal of the medical sciences* 265 (3), S. 174–189. DOI: 10.1097/00000441-197303000-00001.

Durak-Nalbantić, Azra; Džubur, Alen; Dilić, Mirza; Pozderac, Zana; Mujanović-Narančić, Alma; Kulić, Mehmed et al. (2012): Brain natriuretic peptide release in acute myocardial infarction. In: *Bosnian journal of basic medical sciences* 12 (3), S. 164–168. DOI: 10.17305/bjbms.2012.2470.

Egan, J. J.; Greenberg, A. S.; Chang, M. K.; Wek, S. A.; Moos, M. C.; Londos, C. (1992): Mechanism of hormone-stimulated lipolysis in adipocytes: translocation of hormone-sensitive lipase to the lipid storage droplet. In: *Proceedings of the National Academy of Sciences of the United States of America* 89 (18), S. 8537–8541. DOI: 10.1073/pnas.89.18.8537.

Eltzschig, Holger K.; Eckle, Tobias (2011): Ischemia and reperfusion--from mechanism to translation. In: *Nature medicine* 17 (11), S. 1391–1401. DOI: 10.1038/nm.2507.

Emde, B.; Heinen, A.; Gödecke, A.; Bottermann, K. (2014): Wheat germ agglutinin staining as a suitable method for detection and quantification of fibrosis in cardiac tissue after myocardial infarction. In: *European journal of histochemistry : EJH* 58 (4), S. 2448. DOI: 10.4081/ejh.2014.2448.

Enerbäck, S.; Jacobsson, A.; Simpson, E. M.; Guerra, C.; Yamashita, H.; Harper, M. E.; Kozak, L. P. (1997): Mice lacking mitochondrial uncoupling protein are cold-sensitive but not obese. In: *Nature* 387 (6628), S. 90–94. DOI: 10.1038/387090a0.

Essop, M. Faadiel; Opie, Lionel H. (2020): The acute coronary syndrome revisited: effects and therapeutic modulation of excess metabolic fuel supply. In: *Cardiovascular Journal of Africa* 31 (3), S. 159–161.

Fajas, L.; Schoonjans, K.; Gelman, L.; Kim, J. B.; Najib, J.; Martin, G. et al. (1999): Regulation of peroxisome proliferator-activated receptor gamma expression by adipocyte differentiation and determination factor 1/sterol regulatory element binding protein 1: implications for adipocyte differentiation and metabolism. In: *Molecular and Cellular Biology* 19 (8), S. 5495–5503. DOI: 10.1128/MCB.19.8.5495.

Fang, Han; Judd, Robert L. (2018): Adiponectin Regulation and Function. In: *Comprehensive Physiology* 8 (3), S. 1031–1063. DOI: 10.1002/cphy.c170046.

Fantuzzi, Giamila; Mazzone, Theodore (2007): Adipose Tissue and Adipokines in Health and Disease. Totowa, NJ: Humana Press.

Farooqi, I. Sadaf; O'Rahilly, Stephen (2014): 20 years of leptin: human disorders of leptin action. In: *The Journal of endocrinology* 223 (1), T63-70. DOI: 10.1530/JOE-14-0480.

Farrell, Martilias S.; Roth, Bryan L. (2013): Pharmacosynthetics: Reimagining the pharmacogenetic approach. In: *Brain research* 1511, S. 6–20. DOI: 10.1016/j.brainres.2012.09.043.

Feldmann, Helena M.; Golozoubova, Valeria; Cannon, Barbara; Nedergaard, Jan (2009): UCP1 ablation induces obesity and abolishes diet-induced thermogenesis in mice exempt from thermal stress by living at thermoneutrality. In: *Cell metabolism* 9 (2), S. 203–209. DOI: 10.1016/j.cmet.2008.12.014.

Fischer, Kyle B.; Collins, Hannah K.; Callaway, Edward M. (2019): Sources of off-target expression from recombinase-dependent AAV vectors and mitigation with cross-over insensitive ATG-out vectors. In: *Proceedings of the National Academy of Sciences of the United States of America* 116 (52), S. 27001–27010. DOI: 10.1073/pnas.1915974116.

Florea, Viorel G.; Cohn, Jay N. (2014): The autonomic nervous system and heart failure. In: *Circulation research* 114 (11), S. 1815–1826. DOI: 10.1161/CIRCRESAHA.114.302589#.

Frangogiannis, N. G.; Michael, L. H.; Entman, M. L. (2000): Myofibroblasts in reperfused myocardial infarcts express the embryonic form of smooth muscle myosin heavy chain (SMemb). In: *Cardiovascular research* 48 (1), S. 89–100. DOI: 10.1016/s0008-6363(00)00158-9.

Frangogiannis, Nikolaos G. (2014): The inflammatory response in myocardial injury, repair, and remodelling. In: *Nature reviews. Cardiology* 11 (5), S. 255–265. DOI: 10.1038/nrcardio.2014.28.

Frayn, K. N.; Karpe, F.; Fielding, B. A.; Macdonald, I. A.; Coppack, S. W. (2003): Integrative physiology of human adipose tissue. In: *International journal of obesity and related metabolic disorders : journal of the International Association for the Study of Obesity* 27 (8), S. 875–888. DOI: 10.1038/sj.ijo.0802326.

Friedman, Jeffrey (2016): The long road to leptin. In: *The Journal of clinical investigation* 126 (12), S. 4727–4734. DOI: 10.1172/JCI91578.

Fu, Yuchang; Luo, Nanlan; Klein, Richard L.; Garvey, W. Timothy (2005): Adiponectin promotes adipocyte differentiation, insulin sensitivity, and lipid accumulation. In: *Journal of lipid research* 46 (7), S. 1369–1379. DOI: 10.1194/jlr.M400373-JLR200.

Fujimaki, S.; Kanda, T.; Fujita, K.; Tamura, J.; Kobayashi, I. (2001): The significance of measuring plasma leptin in acute myocardial infarction. In: *The Journal of international medical research* 29 (2), S. 108–113. DOI: 10.1177/147323000102900207.

Gastaldelli, Amalia; Miyazaki, Yoshinori; Pettiti, Maura; Matsuda, Masafumi; Mahankali, Srihanth; Santini, Eleonora et al. (2002): Metabolic effects of visceral fat accumulation in

type 2 diabetes. In: *The Journal of clinical endocrinology and metabolism* 87 (11), S. 5098–5103. DOI: 10.1210/jc.2002-020696.

Goyal, Abhinav; Daneshpajouhnejad, Parnaz; Hashmi, Muhammad F.; Bashir, Khalid (2023): StatPearls. Acute Kidney Injury. Treasure Island (FL).

Grabner, Gernot F.; Xie, Hao; Schweiger, Martina; Zechner, Rudolf (2021): Lipolysis: cellular mechanisms for lipid mobilization from fat stores. In: *Nature metabolism* 3 (11), S. 1445–1465. DOI: 10.1038/s42255-021-00493-6.

Granneman, James G.; Moore, Hsiao-Ping H.; Granneman, Rachel L.; Greenberg, Andrew S.; Obin, Martin S.; Zhu, Zhengxian (2007): Analysis of lipolytic protein trafficking and interactions in adipocytes. In: *The Journal of biological chemistry* 282 (8), S. 5726–5735. DOI: 10.1074/jbc.M610580200.

Grogan, Alyssa; Lucero, Emilio Y.; Jiang, Haoran; Rockman, Howard A. (2023): Pathophysiology and pharmacology of G protein-coupled receptors in the heart. In: *Cardiovascular research* 119 (5), S. 1117–1129. DOI: 10.1093/cvr/cvac171.

Gruzdeva, Olga; Uchasova, Evgenya; Belik, Ekaterina; Dyleva, Yulia; Shurygina, Ekaterina; Barbarash, Olga (2014): Lipid, adipokine and ghrelin levels in myocardial infarction patients with insulin resistance. In: *BMC cardiovascular disorders* 14, S. 7. DOI: 10.1186/1471-2261-14-7.

Gualillo, Oreste; González-Juanatey, José Ramón; Lago, Francisca (2007): The emerging role of adipokines as mediators of cardiovascular function: physiologic and clinical perspectives. In: *Trends in cardiovascular medicine* 17 (8), S. 275–283. DOI: 10.1016/j.tcm.2007.09.005.

Guettier, Jean-Marc; Gautam, Dinesh; Scarselli, Marco; Ruiz de Azua, Inigo; Li, Jian Hua; Rosemond, Erica et al. (2009): A chemical-genetic approach to study G protein regulation of beta cell function in vivo. In: *Proceedings of the National Academy of Sciences of the United States of America* 106 (45), S. 19197–19202. DOI: 10.1073/pnas.0906593106.

Guo, M.; Li, C.; Lei, Y.; Xu, S.; Zhao, D.; Lu, X-Y (2017): Role of the adipose PPARγ-adiponectin axis in susceptibility to stress and depression/anxiety-related behaviors. In: *Molecular psychiatry* 22 (7), S. 1056–1068. DOI: 10.1038/mp.2016.225.

Gustafson, Birgit; Smith, Ulf (2015): Regulation of white adipogenesis and its relation to ectopic fat accumulation and cardiovascular risk. In: *Atherosclerosis* 241 (1), S. 27–35. DOI: 10.1016/j.atherosclerosis.2015.04.812.

Haan, J. J. de; Smeets, M. B.; Pasterkamp, G.; Arslan, F. (2013): Danger signals in the initiation of the inflammatory response after myocardial infarction. In: *Mediators of inflammation* 2013, S. 206039. DOI: 10.1155/2013/206039.

Hagemann, Dirk; Xiao, Rui-Ping (2002): Dual site phospholamban phosphorylation and its physiological relevance in the heart. In: *Trends in cardiovascular medicine* 12 (2), S. 51–56. DOI: 10.1016/S1050-1738(01)00145-1.

Han, Chang Yeop; Subramanian, Savitha; Chan, Christina K.; Omer, Mohamed; Chiba, Tsuyoshi; Wight, Thomas N.; Chait, Alan (2007): Adipocyte-derived serum amyloid A3 and hyaluronan play a role in monocyte recruitment and adhesion. In: *Diabetes* 56 (9), S. 2260–2273. DOI: 10.2337/db07-0218.

Hanson, Madelyn S.; Stephenson, Alan H.; Bowles, Elizabeth A.; Sprague, Randy S. (2010): Insulin inhibits human erythrocyte cAMP accumulation and ATP release: role of phosphodiesterase 3 and phosphoinositide 3-kinase. In: *Experimental biology and medicine (Maywood, N.J.)* 235 (2), S. 256–262. DOI: 10.1258/ebm.2009.009206.

Harman-Boehm, Ilana; Blüher, Matthias; Redel, Henry; Sion-Vardy, Netta; Ovadia, Shira; Avinoach, Eliezer et al. (2007): Macrophage infiltration into omental versus subcutaneous fat across different populations: effect of regional adiposity and the comorbidities of obesity. In: *The Journal of clinical endocrinology and metabolism* 92 (6), S. 2240–2247. DOI: 10.1210/jc.2006-1811.

Harms, Matthew J.; Ishibashi, Jeff; Wang, Wenshan; Lim, Hee-Woong; Goyama, Susumu; Sato, Tomohiko et al. (2014): Prdm16 is required for the maintenance of brown adipocyte identity and function in adult mice. In: *Cell metabolism* 19 (4), S. 593–604. DOI: 10.1016/j.cmet.2014.03.007.

Hasenfuss, G.; Reinecke, H.; Studer, R.; Meyer, M.; Pieske, B.; Holtz, J. et al. (1994): Relation between myocardial function and expression of sarcoplasmic reticulum Ca(2+)-ATPase in failing and nonfailing human myocardium. In: *Circulation research* 75 (3), S. 434–442. DOI: 10.1161/01.res.75.3.434.

Heinen, Andre; Raupach, Annika; Behmenburg, Friederike; Hölscher, Nina; Flögel, Ulrich; Kelm, Malte et al. (2018): Echocardiographic Analysis of Cardiac Function after Infarction in Mice: Validation of Single-Plane Long-Axis View Measurements and the Bi-Plane Simpson Method. In: *Ultrasound in medicine & biology* 44 (7), S. 1544–1555. DOI: 10.1016/j.ultrasmedbio.2018.03.020.

Hondares, Elayne; Rosell, Meritxell; Díaz-Delfín, Julieta; Olmos, Yolanda; Monsalve, Maria; Iglesias, Roser et al. (2011): Peroxisome proliferator-activated receptor α (PPARα) induces PPARγ coactivator 1α (PGC-1α) gene expression and contributes to thermogenic activation of brown fat: involvement of PRDM16. In: *The Journal of biological chemistry* 286 (50), S. 43112–43122. DOI: 10.1074/jbc.M111.252775.

Horton, J. D.; Shimomura, I. (1999): Sterol regulatory element-binding proteins: activators of cholesterol and fatty acid biosynthesis. In: *Current opinion in lipidology* 10 (2), S. 143–150. DOI: 10.1097/00041433-199904000-00008.

Iwaki, Masanori; Matsuda, Morihiro; Maeda, Norikazu; Funahashi, Tohru; Matsuzawa, Yuji; Makishima, Makoto; Shimomura, Iichiro (2003): Induction of adiponectin, a fat-derived antidiabetic and antiatherogenic factor, by nuclear receptors. In: *Diabetes* 52 (7), S. 1655–1663. DOI: 10.2337/diabetes.52.7.1655.

Jamaluddin, Md S.; Weakley, Sarah M.; Yao, Qizhi; Chen, Changyi (2012): Resistin: functional roles and therapeutic considerations for cardiovascular disease. In: *British journal of pharmacology* 165 (3), S. 622–632. DOI: 10.1111/j.1476-5381.2011.01369.x.

Jenča, Dominik; Melenovský, Vojtěch; Stehlik, Josef; Staněk, Vladimír; Kettner, Jiří; Kautzner, Josef et al. (2021): Heart failure after myocardial infarction: incidence and predictors. In: *ESC heart failure* 8 (1), S. 222–237. DOI: 10.1002/ehf2.13144.

Jocken, Johan W. E.; Blaak, Ellen E. (2008): Catecholamine-induced lipolysis in adipose tissue and skeletal muscle in obesity. In: *Physiology & behavior* 94 (2), S. 219–230. DOI: 10.1016/j.physbeh.2008.01.002.

Kajimura, Shingo; Seale, Patrick; Tomaru, Takuya; Erdjument-Bromage, Hediye; Cooper, Marcus P.; Ruas, Jorge L. et al. (2008): Regulation of the brown and white fat gene programs through a PRDM16/CtBP transcriptional complex. In: *Genes & development* 22 (10), S. 1397–1409. DOI: 10.1101/gad.1666108.

Kakuma, T.; Lee, Y.; Higa, M.; Wang, Z. w.; Pan, W.; Shimomura, I.; Unger, R. H. (2000): Leptin, troglitazone, and the expression of sterol regulatory element binding proteins in liver and pancreatic islets. In: *Proceedings of the National Academy of Sciences of the United States of America* 97 (15), S. 8536–8541. DOI: 10.1073/pnas.97.15.8536.

Kallunki, Tuula; Barisic, Marin; Jäättelä, Marja; Liu, Bin (2019): How to Choose the Right Inducible Gene Expression System for Mammalian Studies? In: *Cells* 8 (8). DOI: 10.3390/cells8080796.

Kaur, Supreet; Auger, Christopher; Barayan, Dalia; Shah, Priyal; Matveev, Anna; Knuth, Carly M. et al. (2021): Adipose-specific ATGL ablation reduces burn injury-induced metabolic derangements in mice. In: *Clinical and translational medicine* 11 (6), e417. DOI: 10.1002/ctm2.417.

Keane, Thomas M.; Goodstadt, Leo; Danecek, Petr; White, Michael A.; Wong, Kim; Yalcin, Binnaz et al. (2011): Mouse genomic variation and its effect on phenotypes and gene regulation. In: *Nature* 477 (7364), S. 289–294. DOI: 10.1038/nature10413.

Kersten, S. (2001): Mechanisms of nutritional and hormonal regulation of lipogenesis. In: *EMBO reports* 2 (4), S. 282–286. DOI: 10.1093/embo-reports/kve071.

Khafaji, Hadi A. R. Hadi; Bener, Abdul Bari; Rizk, Nasser M.; Al Suwaidi, Jassim (2012): Elevated serum leptin levels in patients with acute myocardial infarction; correlation with coronary angiographic and echocardiographic findings. In: *BMC research notes* 5, S. 262. DOI: 10.1186/1756-0500-5-262.

Kissebah, A. H.; Vydelingum, N.; Murray, R.; Evans, D. J.; Hartz, A. J.; Kalkhoff, R. K.; Adams, P. W. (1982): Relation of body fat distribution to metabolic complications of obesity. In: *The Journal of clinical endocrinology and metabolism* 54 (2), S. 254–260. DOI: 10.1210/jcem-54-2-254.

Kitamura, Tadahiro; Kitamura, Yukari; Kuroda, Shoji; Hino, Yasuhisa; Ando, Miwa; Kotani, Ko et al. (1999): Insulin-Induced Phosphorylation and Activation of Cyclic Nucleotide Phosphodiesterase 3B by the Serine-Threonine Kinase Akt. In: *Molecular and Cellular Biology* 19 (9), S. 6286–6296.

Kojima, S.; Funahashi, T.; Sakamoto, T.; Miyamoto, S.; Soejima, H.; Hokamaki, J. et al. (2003): The variation of plasma concentrations of a novel, adipocyte derived protein,

adiponectin, in patients with acute myocardial infarction. In: *Heart (British Cardiac Society)* 89 (6), S. 667. DOI: 10.1136/heart.89.6.667.

Korah, Tarek E.; Ibrahim, Hesham H.; Badr, Eman A. E.; ElShafie, Maathir K. (2011): Serum resistin in acute myocardial infarction patients with and without diabetes mellitus. In: *Postgraduate medical journal* 87 (1029), S. 463–467. DOI: 10.1136/pgmj.2010.113571.

Kubo, S. H.; Walter, B. A.; John, D. H.; Clark, M.; Cody, R. J. (1987): Liver function abnormalities in chronic heart failure. Influence of systemic hemodynamics. In: *Archives of internal medicine* 147 (7), S. 1227–1230.

Kwok, Kelvin H. M.; Lam, Karen S. L.; Xu, Aimin (2016): Heterogeneity of white adipose tissue: molecular basis and clinical implications. In: *Experimental & molecular medicine* 48 (3), e215. DOI: 10.1038/emm.2016.5.

Lane, M. D.; Flores-Riveros, J. R.; Hresko, R. C.; Kaestner, K. H.; Liao, K.; Janicot, M. et al. (1990): Insulin-receptor tyrosine kinase and glucose transport. In: *Diabetes care* 13 (6), S. 565–575. DOI: 10.2337/diacare.13.6.565.

Lavin, Thomas K.; Jin, Lei; Lea, Nicholas E.; Wickersham, Ian R. (2020): Monosynaptic Tracing Success Depends Critically on Helper Virus Concentrations. In: *Frontiers in synaptic neuroscience* 12, S. 6. DOI: 10.3389/fnsyn.2020.00006.

Lewis, Eldrin F.; Moye, Lemuel A.; Rouleau, Jean L.; Sacks, Frank M.; Arnold, J. Malcolm O.; Warnica, J. Wayne et al. (2003): Predictors of late development of heart failure in stable survivors of myocardial infarction: the CARE study. In: *Journal of the American College of Cardiology* 42 (8), S. 1446–1453. DOI: 10.1016/s0735-1097(03)01057-x.

Li, Pingping; Lu, Min; Nguyen, M. T. Audrey; Bae, Eun Ju; Chapman, Justin; Feng, Daorong et al. (2010): Functional heterogeneity of CD11c-positive adipose tissue macrophages in diet-induced obese mice. In: *The Journal of biological chemistry* 285 (20), S. 15333–15345. DOI: 10.1074/jbc.M110.100263.

Liu, Dianxin; Ceddia, Ryan P.; Collins, Sheila (2018): Cardiac natriuretic peptides promote adipose 'browning' through mTOR complex-1. In: *Molecular metabolism* 9, S. 192–198. DOI: 10.1016/j.molmet.2017.12.017.

Liu, Jian; Divoux, Adeline; Sun, Jiusong; Zhang, Jie; Clément, Karine; Glickman, Jonathan N. et al. (2009): Genetic deficiency and pharmacological stabilization of mast cells reduce

diet-induced obesity and diabetes in mice. In: *Nature medicine* 15 (8), S. 940–945. DOI: 10.1038/nm.1994.

Longchamp, Alban; Tao, Ming; Bartelt, Alexander; Ding, Kui; Lynch, Lydia; Hine, Christopher et al. (2016): Surgical injury induces local and distant adipose tissue browning. In: *Adipocyte* 5 (2), S. 163–174. DOI: 10.1080/21623945.2015.1111971.

Lumeng, Carey N.; Bodzin, Jennifer L.; Saltiel, Alan R. (2007): Obesity induces a phenotypic switch in adipose tissue macrophage polarization. In: *J. Clin. Invest.* 117 (1), S. 175–184. DOI: 10.1172/JCI29881.

Luong, Quyen; Lee, Kevin Y. (2018): The Heterogeneity of White Adipose Tissue. In: Leszek Szablewski (Hg.): Adipose Tissue: InTech.

Lymperopoulos, Anastasios; Rengo, Giuseppe; Koch, Walter J. (2013a): Adrenergic nervous system in heart failure: pathophysiology and therapy. In: *Circulation research* 113 (6), S. 739–753. DOI: 10.1161/CIRCRESAHA.113.300308.

Lymperopoulos, Anastasios; Rengo, Giuseppe; Koch, Walter J. (2013b): Adrenergic nervous system in heart failure: pathophysiology and therapy. In: *Circulation research* 113 (6), S. 739–753. DOI: 10.1161/CIRCRESAHA.113.300308.

Malfacini, Davide; Pfeifer, Alexander (2023): GPCR in Adipose Tissue Function-Focus on Lipolysis. In: *Biomedicines* 11 (2). DOI: 10.3390/biomedicines11020588.

Mangmool, Supachoke; Denkaew, Tananat; Phosri, Sarawuth; Pinthong, Darawan; Parichatikanond, Warisara; Shimauchi, Tsukasa; Nishida, Motohiro (2016a): Sustained βAR Stimulation Mediates Cardiac Insulin Resistance in a PKA-Dependent Manner. In: *Molecular endocrinology (Baltimore, Md.)* 30 (1), S. 118–132. DOI: 10.1210/me.2015-1201.

Mangmool, Supachoke; Denkaew, Tananat; Phosri, Sarawuth; Pinthong, Darawan; Parichatikanond, Warisara; Shimauchi, Tsukasa; Nishida, Motohiro (2016b): Sustained βAR Stimulation Mediates Cardiac Insulin Resistance in a PKA-Dependent Manner. In: *Molecular endocrinology (Baltimore, Md.)* 30 (1), S. 118–132. DOI: 10.1210/me.2015-1201.

Masterson, Larry R.; Yu, Tao; Shi, Lei; Wang, Yi; Gustavsson, Martin; Mueller, Michael M.; Veglia, Gianluigi (2011): cAMP-dependent protein kinase A selects the excited state of the membrane substrate phospholamban. In: *Journal of molecular biology* 412 (2), S. 155–164. DOI: 10.1016/j.jmb.2011.06.041.

Matsubara, Toshiya; Mita, Ayako; Minami, Kohtaro; Hosooka, Tetsuya; Kitazawa, Sohei; Takahashi, Kenichi et al. (2012): PGRN is a key adipokine mediating high fat diet-induced insulin resistance and obesity through IL-6 in adipose tissue. In: *Cell metabolism* 15 (1), S. 38–50. DOI: 10.1016/j.cmet.2011.12.002.

Matsuzawa, Yuji; Funahashi, Tohru; Nakamura, Tadashi (2011): The concept of metabolic syndrome: contribution of visceral fat accumulation and its molecular mechanism. In: *Journal of atherosclerosis and thrombosis* 18 (8), S. 629–639. DOI: 10.5551/jat.7922.

Milan, Gabriella; Granzotto, Marnie; Scarda, Alessandro; Calcagno, Alessandra; Pagano, Claudio; Federspil, Giovanni; Vettor, Roberto (2002): Resistin and adiponectin expression in visceral fat of obese rats: effect of weight loss. In: *Obesity research* 10 (11), S. 1095–1103. DOI: 10.1038/oby.2002.149.

Mirbolooki, M. Reza; Upadhyay, Sanjeev Kumar; Constantinescu, Cristian C.; Pan, Min-Liang; Mukherjee, Jogeshwar (2014): Adrenergic pathway activation enhances brown adipose tissue metabolism: a ^{18}FFDG PET/CT study in mice. In: *Nuclear medicine and biology* 41 (1), S. 10–16. DOI: 10.1016/j.nucmedbio.2013.08.009.

Møller, Søren; Bernardi, Mauro (2013): Interactions of the heart and the liver. In: *European heart journal* 34 (36), S. 2804–2811. DOI: 10.1093/eurheartj/eht246.

Morris, David L.; Singer, Kanakadurga; Lumeng, Carey N. (2011): Adipose tissue macrophages: phenotypic plasticity and diversity in lean and obese states. In: *Current opinion in clinical nutrition and metabolic care* 14 (4), S. 341–346. DOI: 10.1097/MCO.0b013e328347970b.

Mottillo, Emilio P.; Granneman, James G. (2011a): Intracellular fatty acids suppress β-adrenergic induction of PKA-targeted gene expression in white adipocytes. In: *American journal of physiology. Endocrinology and metabolism* 301 (1), E122-31. DOI: 10.1152/ajpendo.00039.2011.

Mottillo, Emilio P.; Granneman, James G. (2011b): Intracellular fatty acids suppress β-adrenergic induction of PKA-targeted gene expression in white adipocytes. In: *American journal of physiology. Endocrinology and metabolism* 301 (1), E122-31. DOI: 10.1152/ajpendo.00039.2011.

Mottillo, Emilio P.; Shen, Xiang Jun; Granneman, James G. (2007): Role of hormone-sensitive lipase in beta-adrenergic remodeling of white adipose tissue. In: *American journal*

of physiology. Endocrinology and metabolism 293 (5), E1188-97. DOI: 10.1152/ajpendo.00051.2007.

Murano, I.; Barbatelli, G.; Parisani, V.; Latini, C.; Muzzonigro, G.; Castellucci, M.; Cinti, S. (2008): Dead adipocytes, detected as crown-like structures, are prevalent in visceral fat depots of genetically obese mice. In: *Journal of lipid research* 49 (7), S. 1562–1568. DOI: 10.1194/jlr.M800019-JLR200.

Nakae, J.; Accili, D. (1999): The mechanism of insulin action. In: *Journal of pediatric endocrinology & metabolism : JPEM* 12 Suppl 3, S. 721–731.

Nguyen, Andrew; Guo, James; Banyard, Derek A.; Fadavi, Darya; Toranto, Jason D.; Wirth, Garrett A. et al. (2016): Stromal vascular fraction: A regenerative reality? Part 1: Current concepts and review of the literature. In: *Journal of plastic, reconstructive & aesthetic surgery : JPRAS* 69 (2), S. 170–179. DOI: 10.1016/j.bjps.2015.10.015.

Nguyen, Thi Mong Diep (2020): Adiponectin: Role in Physiology and Pathophysiology. In: *International journal of preventive medicine* 11, S. 136. DOI: 10.4103/ijpvm.IJPVM_193_20.

Oliver, Michael F. (2014): Fatty acids and recovery during first hours of acute myocardial ischemia. In: *The American journal of cardiology* 113 (2), S. 285–286. DOI: 10.1016/j.amjcard.2013.10.005.

Ort, Tatiana; Arjona, Anibal A.; MacDougall, John R.; Nelson, Pam J.; Rothenberg, Mark E.; Wu, Frank et al. (2005): Recombinant human FIZZ3/resistin stimulates lipolysis in cultured human adipocytes, mouse adipose explants, and normal mice. In: *Endocrinology* 146 (5), S. 2200–2209. DOI: 10.1210/en.2004-1421.

Osanai, Yasuyuki; Xing, Yao Lulu; Kobayashi, Kenta; Homman-Ludiye, Jihane; Cooray, Amali; Poh, Jasmine et al. (2022): 5′ transgenes drive leaky expression of 3′ transgenes in inducible bicistronic vectors.

Parajuli, Nirmal; Takahara, Shingo; Matsumura, Nobutoshi; Kim, Ty T.; Ferdaoussi, Mourad; Migglautsch, Anna K. et al. (2018): Atglistatin ameliorates functional decline in heart failure via adipocyte-specific inhibition of adipose triglyceride lipase. In: *American journal of physiology. Heart and circulatory physiology* 315 (4), H879-H884. DOI: 10.1152/ajpheart.00308.2018.

Pekgor, Selma; Duran, Cevdet; Berberoglu, Ufuk; Eryilmaz, Mehmet Ali (2019): The Role of Visceral Adiposity Index Levels in Predicting the Presence of Metabolic Syndrome and Insulin Resistance in Overweight and Obese Patients. In: *Metabolic syndrome and related disorders* 17 (5), S. 296–302. DOI: 10.1089/met.2019.0005.

Pellegrinelli, Vanessa; Carobbio, Stefania; Vidal-Puig, Antonio (2016): Adipose tissue plasticity: how fat depots respond differently to pathophysiological cues. In: *Diabetologia* 59 (6), S. 1075–1088. DOI: 10.1007/s00125-016-3933-4.

Perman, Jeanna C.; Boström, Pontus; Lindbom, Malin; Lidberg, Ulf; StÅhlman, Marcus; Hägg, Daniel et al. (2011): The VLDL receptor promotes lipotoxicity and increases mortality in mice following an acute myocardial infarction. In: *The Journal of clinical investigation* 121 (7), S. 2625–2640. DOI: 10.1172/JCI43068.

Petrovic, Natasa; Walden, Tomas B.; Shabalina, Irina G.; Timmons, James A.; Cannon, Barbara; Nedergaard, Jan (2010): Chronic peroxisome proliferator-activated receptor gamma (PPARgamma) activation of epididymally derived white adipocyte cultures reveals a population of thermogenically competent, UCP1-containing adipocytes molecularly distinct from classic brown adipocytes. In: *The Journal of biological chemistry* 285 (10), S. 7153–7164. DOI: 10.1074/jbc.M109.053942.

Piantadosi, Claude A.; Suliman, Hagir B. (2006): Mitochondrial transcription factor A induction by redox activation of nuclear respiratory factor 1. In: *The Journal of biological chemistry* 281 (1), S. 324–333. DOI: 10.1074/jbc.M508805200.

Pischon, Tobias; Girman, Cynthia J.; Hotamisligil, Gokhan S.; Rifai, Nader; Hu, Frank B.; Rimm, Eric B. (2004): Plasma adiponectin levels and risk of myocardial infarction in men. In: *JAMA* 291 (14), S. 1730–1737. DOI: 10.1001/jama.291.14.1730.

Poetsch, Mareike S.; Strano, Anna; Guan, Kaomei (2020): Role of Leptin in Cardiovascular Diseases. In: *Frontiers in endocrinology* 11, S. 354. DOI: 10.3389/fendo.2020.00354.

Pond, C. M. (1992): An evolutionary and functional view of mammalian adipose tissue. In: *The Proceedings of the Nutrition Society* 51 (3), S. 367–377. DOI: 10.1079/PNS19920050.

Prabhu, Sumanth D.; Frangogiannis, Nikolaos G. (2016): The Biological Basis for Cardiac Repair After Myocardial Infarction: From Inflammation to Fibrosis. In: *Circulation research* 119 (1), S. 91–112. DOI: 10.1161/CIRCRESAHA.116.303577.

Rajala, Michael W.; Lin, Ying; Ranalletta, Mollie; Yang, Xiao Man; Qian, Hao; Gingerich, Ron et al. (2002): Cell type-specific expression and coregulation of murine resistin and resistin-like molecule-alpha in adipose tissue. In: *Molecular endocrinology (Baltimore, Md.)* 16 (8), S. 1920–1930. DOI: 10.1210/me.2002-0048.

Rajala, Michael W.; Qi, Yong; Patel, Hiral R.; Takahashi, Nobuhiko; Banerjee, Ronadip; Pajvani, Utpal B. et al. (2004): Regulation of resistin expression and circulating levels in obesity, diabetes, and fasting. In: *Diabetes* 53 (7), S. 1671–1679. DOI: 10.2337/diabetes.53.7.1671.

RANDLE, P. J.; GARLAND, P. B.; HALES, C. N.; NEWSHOLME, E. A. (1963): The glucose fatty-acid cycle. Its role in insulin sensitivity and the metabolic disturbances of diabetes mellitus. In: *Lancet (London, England)* 1 (7285), S. 785–789. DOI: 10.1016/s0140-6736(63)91500-9.

Robidoux, Jacques; Cao, Wenhong; Quan, Hui; Daniel, Kiefer W.; Moukdar, Fatiha; Bai, Xu et al. (2005): Selective activation of mitogen-activated protein (MAP) kinase kinase 3 and p38alpha MAP kinase is essential for cyclic AMP-dependent UCP1 expression in adipocytes. In: *Molecular and Cellular Biology* 25 (13), S. 5466–5479. DOI: 10.1128/MCB.25.13.5466-5479.2005.

Rogan, Sarah C.; Roth, Bryan L. (2011): Remote control of neuronal signaling. In: *Pharmacological reviews* 63 (2), S. 291–315. DOI: 10.1124/pr.110.003020.

Sackmann-Sala, Lucila; Berryman, Darlene E.; Munn, Rachel D.; Lubbers, Ellen R.; Kopchick, John J. (2012): Heterogeneity among white adipose tissue depots in male C57BL/6J mice. In: *Obesity (Silver Spring, Md.)* 20 (1), S. 101–111. DOI: 10.1038/oby.2011.235.

Saely, Christoph H.; Vonbank, Alexander; Rein, Philipp; Woess, Magdalena; Beer, Stefan; Aczel, Stefan et al. (2008): Alanine aminotransferase and gamma-glutamyl transferase are associated with the metabolic syndrome but not with angiographically determined coronary atherosclerosis. In: *Clinica chimica acta; international journal of clinical chemistry* 397 (1-2), S. 82–86. DOI: 10.1016/j.cca.2008.07.024.

Salatzki, Janek; Foryst-Ludwig, Anna; Bentele, Kajetan; Blumrich, Annelie; Smeir, Elia; Ban, Zsofia et al. (2018): Adipose tissue ATGL modifies the cardiac lipidome in pressure-overload-induced left ventricular failure. In: *PLoS genetics* 14 (1), e1007171. DOI: 10.1371/journal.pgen.1007171.

Saleh, Moussa; Ambrose, John A. (2018): Understanding myocardial infarction. In: *F1000Research* 7. DOI: 10.12688/f1000research.15096.1.

Santiago, Jon-Jon; Dangerfield, Aran L.; Rattan, Sunil G.; Bathe, Krista L.; Cunnington, Ryan H.; Raizman, Joshua E. et al. (2010): Cardiac fibroblast to myofibroblast differentiation in vivo and in vitro: expression of focal adhesion components in neonatal and adult rat ventricular myofibroblasts. In: *Developmental dynamics : an official publication of the American Association of Anatomists* 239 (6), S. 1573–1584. DOI: 10.1002/dvdy.22280.

Saternos, Hannah C.; Almarghalani, Daniyah A.; Gibson, Hayley M.; Meqdad, Mahmood A.; Antypas, Raymond B.; Lingireddy, Ajay; AbouAlaiwi, Wissam A. (2018): Distribution and function of the muscarinic receptor subtypes in the cardiovascular system. In: *Physiological genomics* 50 (1), S. 1–9. DOI: 10.1152/physiolgenomics.00062.2017.

Savage, D. B.; Sewter, C. P.; Klenk, E. S.; Segal, D. G.; Vidal-Puig, A.; Considine, R. V.; O'Rahilly, S. (2001): Resistin / Fizz3 expression in relation to obesity and peroxisome proliferator-activated receptor-gamma action in humans. In: *Diabetes* 50 (10), S. 2199–2202. DOI: 10.2337/diabetes.50.10.2199.

Scheel, Anna K.; Espelage, Lena; Chadt, Alexandra (2022): Many Ways to Rome: Exercise, Cold Exposure and Diet-Do They All Affect BAT Activation and WAT Browning in the Same Manner? In: *International journal of molecular sciences* 23 (9). DOI: 10.3390/ijms23094759.

Scherer, P. E.; Williams, S.; Fogliano, M.; Baldini, G.; Lodish, H. F. (1995): A novel serum protein similar to C1q, produced exclusively in adipocytes. In: *The Journal of biological chemistry* 270 (45), S. 26746–26749. DOI: 10.1074/jbc.270.45.26746.

Schoettl, Theresa; Fischer, Ingrid P.; Ussar, Siegfried (2018): Heterogeneity of adipose tissue in development and metabolic function. In: *The Journal of experimental biology* 221 (Pt Suppl 1). DOI: 10.1242/jeb.162958.

Schreiber, Renate; Xie, Hao; Schweiger, Martina (2019): Of mice and men: The physiological role of adipose triglyceride lipase (ATGL). In: *Biochimica et biophysica acta. Molecular and cell biology of lipids* 1864 (6), S. 880–899. DOI: 10.1016/j.bbalip.2018.10.008.

Schweiger, Martina; Eichmann, Thomas O.; Taschler, Ulrike; Zimmermann, Robert; Zechner, Rudolf; Lass, Achim (2014): Measurement of lipolysis. In: *Methods in enzymology* 538, S. 171–193. DOI: 10.1016/B978-0-12-800280-3.00010-4.

Seale, Patrick; Bjork, Bryan; Yang, Wenli; Kajimura, Shingo; Chin, Sherry; Kuang, Shihuan et al. (2008): PRDM16 controls a brown fat/skeletal muscle switch. In: *Nature* 454 (7207), S. 961–967. DOI: 10.1038/nature07182.

Seale, Patrick; Kajimura, Shingo; Yang, Wenli; Chin, Sherry; Rohas, Lindsay M.; Uldry, Marc et al. (2007): Transcriptional control of brown fat determination by PRDM16. In: *Cell metabolism* 6 (1), S. 38–54. DOI: 10.1016/j.cmet.2007.06.001.

Sengenès, C.; Berlan, M.; Glisezinski, I. de; Lafontan, M.; Galitzky, J. (2000): Natriuretic peptides: a new lipolytic pathway in human adipocytes. In: *FASEB journal : official publication of the Federation of American Societies for Experimental Biology* 14 (10), S. 1345–1351.

Shabalina, Irina G.; Petrovic, Natasa; Jong, Jasper M. A. de; Kalinovich, Anastasia V.; Cannon, Barbara; Nedergaard, Jan (2013): UCP1 in brite/beige adipose tissue mitochondria is functionally thermogenic. In: *Cell reports* 5 (5), S. 1196–1203. DOI: 10.1016/j.celrep.2013.10.044.

Shibata, Rei; Sato, Kaori; Pimentel, David R.; Takemura, Yukihiro; Kihara, Shinji; Ohashi, Koji et al. (2005): Adiponectin protects against myocardial ischemia-reperfusion injury through AMPK- and COX-2-dependent mechanisms. In: *Nature medicine* 11 (10), S. 1096–1103. DOI: 10.1038/nm1295.

Shimizu, Ippei; Yoshida, Yohko; Katsuno, Taro; Tateno, Kaoru; Okada, Sho; Moriya, Junji et al. (2012): p53-induced adipose tissue inflammation is critically involved in the development of insulin resistance in heart failure. In: *Cell metabolism* 15 (1), S. 51–64. DOI: 10.1016/j.cmet.2011.12.006.

Shimomura, I.; Hammer, R. E.; Richardson, J. A.; Ikemoto, S.; Bashmakov, Y.; Goldstein, J. L.; Brown, M. S. (1998): Insulin resistance and diabetes mellitus in transgenic mice expressing nuclear SREBP-1c in adipose tissue: model for congenital generalized lipodystrophy. In: *Genes & development* 12 (20), S. 3182–3194. DOI: 10.1101/gad.12.20.3182.

Silswal, Nirupama; Singh, Anil K.; Aruna, Battu; Mukhopadhyay, Sangita; Ghosh, Sudip; Ehtesham, Nasreen Z. (2005): Human resistin stimulates the pro-inflammatory cytokines TNF-alpha and IL-12 in macrophages by NF-kappaB-dependent pathway. In: *Biochemical and biophysical research communications* 334 (4), S. 1092–1101. DOI: 10.1016/j.bbrc.2005.06.202.

Skurk, Carsten; Izumiya, Yasuhiro; Maatz, Henrike; Razeghi, Peter; Shiojima, Ichiro; Sandri, Marco et al. (2005): The FOXO3a transcription factor regulates cardiac myocyte size downstream of AKT signaling. In: *The Journal of biological chemistry* 280 (21), S. 20814–20823. DOI: 10.1074/jbc.M500528200.

Smeir, Elia; Kintscher, Ulrich; Foryst-Ludwig, Anna (2021): Adipose tissue-heart crosstalk as a novel target for treatment of cardiometabolic diseases. In: *Current opinion in pharmacology* 60, S. 249–254. DOI: 10.1016/j.coph.2021.07.017.

Soehnlein, Oliver; Lindbom, Lennart (2010): Phagocyte partnership during the onset and resolution of inflammation. In: *Nature reviews. Immunology* 10 (6), S. 427–439. DOI: 10.1038/nri2779.

Soukas, A.; Cohen, P.; Socci, N. D.; Friedman, J. M. (2000): Leptin-specific patterns of gene expression in white adipose tissue. In: *Genes & development* 14 (8), S. 963–980.

Swett, C. (1975): Outpatient phenothiazine use and bone marrow depression. A report from the drug epidemiology unit and the Boston collaborative drug surveillance program. In: *Archives of general psychiatry* 32 (11), S. 1416–1418. DOI: 10.1001/archpsyc.1975.01760290084010.

Takahara, Shingo; Ferdaoussi, Mourad; Srnic, Nikola; Maayah, Zaid H.; Soni, Shubham; Migglautsch, Anna K. et al. (2021): Inhibition of ATGL in adipose tissue ameliorates isoproterenol-induced cardiac remodeling by reducing adipose tissue inflammation. In: *American journal of physiology. Heart and circulatory physiology* 320 (1), H432-H446. DOI: 10.1152/ajpheart.00737.2020.

Takahashi, Toshiyuki; Tang, Tong; Lai, N. Chin; Roth, David M.; Rebolledo, Brian; Saito, Miho et al. (2006): Increased cardiac adenylyl cyclase expression is associated with increased survival after myocardial infarction. In: *Circulation* 114 (5), S. 388–396. DOI: 10.1161/CIRCULATIONAHA.106.632513.

Taleb, Soraya; Herbin, Olivier; Ait-Oufella, Hafid; Verreth, Wim; Gourdy, Pierre; Barateau, Véronique et al. (2007): Defective leptin/leptin receptor signaling improves regulatory T cell immune response and protects mice from atherosclerosis. In: *Arteriosclerosis, thrombosis, and vascular biology* 27 (12), S. 2691–2698. DOI: 10.1161/ATVBAHA.107.149567.

Tani, M.; Neely, J. R. (1989): Role of intracellular Na+ in Ca2+ overload and depressed recovery of ventricular function of reperfused ischemic rat hearts. Possible involvement of H+-Na+ and Na+-Ca2+ exchange. In: *Circulation research* 65 (4), S. 1045–1056. DOI: 10.1161/01.res.65.4.1045.

Thiele, Arne; Luettges, Katja; Ritter, Daniel; Beyhoff, Niklas; Smeir, Elia; Grune, Jana et al. (2022): Pharmacological inhibition of adipose tissue adipose triglyceride lipase by Atglistatin prevents catecholamine-induced myocardial damage. In: *Cardiovascular research* 118 (11), S. 2488–2505. DOI: 10.1093/cvr/cvab182.

Thompson, Karen J.; Khajehali, Elham; Bradley, Sophie J.; Navarrete, Jovana S.; Huang, Xi Ping; Slocum, Samuel et al. (2018): DREADD Agonist 21 Is an Effective Agonist for Muscarinic-Based DREADDs in Vitro and in Vivo. In: *ACS pharmacology & translational science* 1 (1), S. 61–72. DOI: 10.1021/acsptsci.8b00012.

Thor, Doreen (2022): G protein-coupled receptors as regulators of pancreatic islet functionality. In: *Biochimica et biophysica acta. Molecular cell research* 1869 (5), S. 119235. DOI: 10.1016/j.bbamcr.2022.119235.

Timmers, Leo; Pasterkamp, Gerard; Hoog, Vince C. de; Arslan, Fatih; Appelman, Yolande; Kleijn, Dominique P. V. de (2012): The innate immune response in reperfused myocardium. In: *Cardiovascular research* 94 (2), S. 276–283. DOI: 10.1093/cvr/cvs018.

Tomankova, Hana; Valuskova, Paulina; Varejkova, Eva; Rotkova, Jana; Benes, Jan; Myslivecek, Jaromir (2015): The M2 muscarinic receptors are essential for signaling in the heart left ventricle during restraint stress in mice. In: *Stress (Amsterdam, Netherlands)* 18 (2), S. 208–220. DOI: 10.3109/10253890.2015.1007345.

Torres, Mercedes; Moayedi, Siamak (2007): Evaluation of the acutely dyspneic elderly patient. In: *Clinics in geriatric medicine* 23 (2), 307-25, vi. DOI: 10.1016/j.cger.2007.01.007.

Tran, Thien T.; Kahn, C. Ronald (2010): Transplantation of adipose tissue and stem cells: role in metabolism and disease. In: *Nature reviews. Endocrinology* 6 (4), S. 195–213. DOI: 10.1038/nrendo.2010.20.

Turner, Neil A.; Porter, Karen E. (2013): Function and fate of myofibroblasts after myocardial infarction. In: *Fibrogenesis & tissue repair* 6 (1), S. 5. DOI: 10.1186/1755-1536-6-5.

Ukkola, Olavi; Santaniemi, Merja (2002): Adiponectin: a link between excess adiposity and associated comorbidities? In: *Journal of molecular medicine (Berlin, Germany)* 80 (11), S. 696–702. DOI: 10.1007/s00109-002-0378-7.

Valori, C.; Thomas, M.; Shillingford, J. (1967): Free noradrenaline and adrenaline excretion in relation to clinical syndromes following myocardial infarction. In: *The American journal of cardiology* 20 (5), S. 605–617. DOI: 10.1016/0002-9149(67)90001-x.

Varcoe, R.; Halliday, D.; Carson, E. R.; Richards, P.; Tavill, A. S. (1975): Efficiency of utilization of urea nitrogen for albumin synthesis by chronically uraemic and normal man. In: *Clinical science and molecular medicine* 48 (5), S. 379–390. DOI: 10.1042/cs0480379.

VAUGHAN, M.; BERGER, J. E.; STEINBERG, D. (1964): HORMONE-SENSITIVE LIPASE AND MONOGLYCERIDE LIPASE ACTIVITIES IN ADIPOSE TISSUE. In: *The Journal of biological chemistry* 239, S. 401–409.

Vidal-Puig, A. J.; Considine, R. V.; Jimenez-Liñan, M.; Werman, A.; Pories, W. J.; Caro, J. F.; Flier, J. S. (1997): Peroxisome proliferator-activated receptor gene expression in human tissues. Effects of obesity, weight loss, and regulation by insulin and glucocorticoids. In: *J. Clin. Invest.* 99 (10), S. 2416–2422. DOI: 10.1172/JCI119424.

Wang, Cong; Pei, Yuan-Yuan; Ma, Yun-Hui; Ma, Xiao-Lu; Liu, Zhi-Wei; Zhu, Ji-Hong; Li, Chun-Sheng (2019): Risk factors for acute kidney injury in patients with acute myocardial infarction. In: *Chinese medical journal* 132 (14), S. 1660–1665. DOI: 10.1097/CM9.0000000000000293.

Wang, H.; Han, H.; Zhang, L.; Shi, H.; Schram, G.; Nattel, S.; Wang, Z. (2001): Expression of multiple subtypes of muscarinic receptors and cellular distribution in the human heart. In: *Molecular pharmacology* 59 (5), S. 1029–1036. DOI: 10.1124/mol.59.5.1029.

Wang, Hong; Eckel, Robert H. (2009): Lipoprotein lipase: from gene to obesity. In: *American journal of physiology. Endocrinology and metabolism* 297 (2), E271-88. DOI: 10.1152/ajpendo.90920.2008.

Wang, Luzhou; Zabri, Heba; Gorressen, Simone; Semmler, Dominik; Hundhausen, Christian; Fischer, Jens W.; Bottermann, Katharina (2022): Cardiac ischemia modulates

white adipose tissue in a depot-specific manner. In: *Frontiers in physiology* 13, S. 1036945. DOI: 10.3389/fphys.2022.1036945.

Weber, Bahar Zehra Camurdanoglu; Arabaci, Dilsad H.; Kir, Serkan (2022): Metabolic Reprogramming in Adipose Tissue During Cancer Cachexia. In: *Frontiers in oncology* 12, S. 848394. DOI: 10.3389/fonc.2022.848394.

Wedellová, Z.; Dietrich, J.; Siklová-Vítková, M.; Kološtová, K.; Kováčiková, M.; Dušková, M. et al. (2011): Adiponectin inhibits spontaneous and catecholamine-induced lipolysis in human adipocytes of non-obese subjects through AMPK-dependent mechanisms. In: *Physiological research* 60 (1), S. 139–148. DOI: 10.33549/physiolres.931863.

Wehrens, Xander H. T.; Lehnart, Stephan E.; Huang, Fannie; Vest, John A.; Reiken, Steven R.; Mohler, Peter J. et al. (2003): FKBP12.6 deficiency and defective calcium release channel (ryanodine receptor) function linked to exercise-induced sudden cardiac death. In: *Cell* 113 (7), S. 829–840. DOI: 10.1016/s0092-8674(03)00434-3.

Weikert, Cornelia; Westphal, Sabine; Berger, Klaus; Dierkes, Jutta; Möhlig, Matthias; Spranger, Joachim et al. (2008): Plasma resistin levels and risk of myocardial infarction and ischemic stroke. In: *The Journal of clinical endocrinology and metabolism* 93 (7), S. 2647–2653. DOI: 10.1210/jc.2007-2735.

Weiner, D. M.; Meltzer, H. Y.; Veinbergs, I.; Donohue, E. M.; Spalding, T. A.; Smith, T. T. et al. (2004): The role of M1 muscarinic receptor agonism of N-desmethylclozapine in the unique clinical effects of clozapine. In: *Psychopharmacology* 177 (1-2), S. 207–216. DOI: 10.1007/s00213-004-1940-5.

Weisberg, Stuart P.; McCann, Daniel; Desai, Manisha; Rosenbaum, Michael; Leibel, Rudolph L.; Ferrante, Anthony W. (2003): Obesity is associated with macrophage accumulation in adipose tissue. In: *J. Clin. Invest.* 112 (12), S. 1796–1808. DOI: 10.1172/JCI200319246.

Wellen, Kathryn E.; Hotamisligil, Gokhan S. (2003): Obesity-induced inflammatory changes in adipose tissue. In: *J. Clin. Invest.* 112 (12), S. 1785–1788. DOI: 10.1172/JCI20514.

Winer, Daniel A.; Winer, Shawn; Shen, Lei; Wadia, Persis P.; Yantha, Jason; Paltser, Geoffrey et al. (2011): B cells promote insulin resistance through modulation of T cells and

production of pathogenic IgG antibodies. In: *Nature medicine* 17 (5), S. 610–617. DOI: 10.1038/nm.2353.

Winer, Shawn; Chan, Yin; Paltser, Geoffrey; Truong, Dorothy; Tsui, Hubert; Bahrami, Jasmine et al. (2009): Normalization of obesity-associated insulin resistance through immunotherapy. In: *Nature medicine* 15 (8), S. 921–929. DOI: 10.1038/nm.2001.

Wu, Jun; Boström, Pontus; Sparks, Lauren M.; Ye, Li; Choi, Jang Hyun; Giang, An-Hoa et al. (2012): Beige adipocytes are a distinct type of thermogenic fat cell in mouse and human. In: *Cell* 150 (2), S. 366–376. DOI: 10.1016/j.cell.2012.05.016.

Xu, Haiyan; Barnes, Glenn T.; Yang, Qing; Tan, Guo; Yang, Daseng; Chou, Chieh J. et al. (2003): Chronic inflammation in fat plays a crucial role in the development of obesity-related insulin resistance. In: *J. Clin. Invest.* 112 (12), S. 1821–1830. DOI: 10.1172/JCI200319451.

Yan, Xiaoxiang; Anzai, Atsushi; Katsumata, Yoshinori; Matsuhashi, Tomohiro; Ito, Kentaro; Endo, Jin et al. (2013): Temporal dynamics of cardiac immune cell accumulation following acute myocardial infarction. In: *Journal of molecular and cellular cardiology* 62, S. 24–35. DOI: 10.1016/j.yjmcc.2013.04.023.

Yang, Haihua; Yang, Linghai (2016): Targeting cAMP/PKA pathway for glycemic control and type 2 diabetes therapy. In: *Journal of molecular endocrinology* 57 (2), R93-R108. DOI: 10.1530/JME-15-0316.

Yeop Han, Chang; Kargi, Atil Y.; Omer, Mohamed; Chan, Christina K.; Wabitsch, Martin; O'Brien, Kevin D. et al. (2010): Differential effect of saturated and unsaturated free fatty acids on the generation of monocyte adhesion and chemotactic factors by adipocytes: dissociation of adipocyte hypertrophy from inflammation. In: *Diabetes* 59 (2), S. 386–396. DOI: 10.2337/db09-0925.

Young, Stephen G.; Zechner, Rudolf (2013): Biochemistry and pathophysiology of intravascular and intracellular lipolysis. In: *Genes & development* 27 (5), S. 459–484. DOI: 10.1101/gad.209296.112.

Yu, Jing; Zhu, Jiabing; Deng, Jian; Shen, Jing; Du, Fukuan; Wu, Xu et al. (2022): Dopamine receptor D1 signaling stimulates lipolysis and browning of white adipocytes. In: *Biochemical and biophysical research communications* 588, S. 83–89. DOI: 10.1016/j.bbrc.2021.12.040.

Yue, Tian-li; Bao, Weike; Jucker, Beat M.; Gu, Juan-li; Romanic, Anne M.; Brown, Peter J. et al. (2003): Activation of peroxisome proliferator-activated receptor-alpha protects the heart from ischemia/reperfusion injury. In: *Circulation* 108 (19), S. 2393–2399. DOI: 10.1161/01.CIR.0000093187.42015.6C.

Zahorska-Markiewicz, B. (2006): Metabolic effects associated with adipose tissue distribution. In: *Advances in medical sciences* 51, S. 111–114.

Zhang, Mingzhi; Hu, Tian; Zhang, Shaoyan; Zhou, Li (2015): Associations of Different Adipose Tissue Depots with Insulin Resistance: A Systematic Review and Meta-analysis of Observational Studies. In: *Scientific reports* 5, S. 18495. DOI: 10.1038/srep18495.

Zhang, Wenliang; Mottillo, Emilio P.; Zhao, Jiawei; Gartung, Allison; VanHecke, Garrett C.; Lee, Jen-Fu et al. (2014a): Adipocyte lipolysis-stimulated interleukin-6 production requires sphingosine kinase 1 activity. In: *The Journal of biological chemistry* 289 (46), S. 32178–32185. DOI: 10.1074/jbc.M114.601096.

Zhang, Xiaodong; Xie, Xitao; Heckmann, Bradlee L.; Saarinen, Alicia M.; Czyzyk, Traci A.; Liu, Jun (2014b): Targeted disruption of G0/G1 switch gene 2 enhances adipose lipolysis, alters hepatic energy balance, and alleviates high-fat diet-induced liver steatosis. In: *Diabetes* 63 (3), S. 934–946. DOI: 10.2337/db13-1422.

Zhang, Y.; Proenca, R.; Maffei, M.; Barone, M.; Leopold, L.; Friedman, J. M. (1994): Positional cloning of the mouse obese gene and its human homologue. In: *Nature* 372 (6505), S. 425–432. DOI: 10.1038/372425a0.

Zhu, Hu; Aryal, Dipendra K.; Olsen, Reid H. J.; Urban, Daniel J.; Swearingen, Amanda; Forbes, Stacy et al. (2016a): Cre-dependent DREADD (Designer Receptors Exclusively Activated by Designer Drugs) mice. In: *Genesis (New York, N.Y. : 2000)* 54 (8), S. 439–446. DOI: 10.1002/dvg.22949.

Zhu, Hu; Aryal, Dipendra K.; Olsen, Reid H. J.; Urban, Daniel J.; Swearingen, Amanda; Forbes, Stacy et al. (2016b): Cre-dependent DREADD (Designer Receptors Exclusively Activated by Designer Drugs) mice. In: *Genesis (New York, N.Y. : 2000)* 54 (8), S. 439–446. DOI: 10.1002/dvg.22949.

Zimmermann, Robert; Strauss, Juliane G.; Haemmerle, Guenter; Schoiswohl, Gabriele; Birner-Gruenberger, Ruth; Riederer, Monika et al. (2004): Fat mobilization in adipose tissue

is promoted by adipose triglyceride lipase. In: *Science (New York, N.Y.)* 306 (5700), S. 1383–1386. DOI: 10.1126/science.1100747.

Acknowledgements

The past three and a half years must be the most unforgettable journey of my life. Therefore, first I do want to appreciate Prof. Dr. Jens. W Fischer and Dr. med. Katharina Bottermann for providing the nice opportunity to finish my doctoral thesis in the institute of Pharmacology of University Hospital Düsseldorf, thank you so much for always giving me good advice and guidance. Second, I would like to appreciate Prof. Dr. Martina Krüger for being my second referent. Thank you for always giving me lots of professional suggestions and kind encourages.

I want to thank to the people from German Diabetes Center (DDZ) to offer the help to collect nice multiplex analysis data and support my thesis.

My special thanks are given to my supervisor Dr. med. Katharina Bottermann. Thank you so much for the kind encourage, good advice and inspirations, and huge supports to let me finish my PhD time. Thank you for the warm cares and concerns not only at work, but also in life. The past PhD time was really a special period for me, there were many special moments and experiences, either good or bad, thanks for always understanding, trusting and standing behind.

Besides, I want to appreciate my colleague and friend Sara Metry, it was really a lucky and unforgettable experience to be with you in the same office for more than three years, thanks for the understanding, trust, help and everything. I appreciate to have the chance to learn academically and personally a lot from you. I also want to thank to my closest working partner and friend Heba Zabri, thanks for having the chance to work with you together and grow up together, I hope we can both become who we want to be.

Additionally, I want to give my thanks to Dr. Micheal Krybus, Dr. Christian Hundhausen and Dr. Florian Funk, Petra Pieres and all the other colleagues. I feel grateful for having the chance to work with you all and being a member of this big love-full family.

Finally, I want to thank to my families, my husband, mom, parents in law, and my dad, who left this world at the beginning of my PhD, but his love is always an encourage and support to help me to accomplish. Thank you, I achieve my dream, I achieve the dream as well for you all.